Defining the Key Residues in PCNA - Protein Interactions

Alice J Kroker
B.Sc. (Honours)

A thesis submitted to the University of Adelaide, South Australia in fulfilment of the requirements for the degree of Master of Philosophy (Sciences)

Department of Molecular & Cellular Biology
School of Biological Sciences University of Adelaide
South Australia

July, 2017

Table of Contents

Abstract

Proliferating cell nuclear antigen (PCNA), also known as processivity factor or sliding clamp, is a trimeric, ring-shaped protein that tethers proteins to DNA in cellular processes including DNA replication, DNA repair and cell cycle control. PCNA interacts with proteins through a PCNA interacting protein (PIP)-box, an 8 amino acid consensus sequence. Different PCNA binding partners bind to PCNA with different affinity, predicted to be a consequence of differences in their PIP-box sequence. Of all biological PIP-boxes p21 has the highest known affinity for PCNA, allowing for the binding of p21 to PCNA to inhibit DNA replication and cell growth. PCNA is used as a marker for cell proliferation and is overexpressed in cancer. As it is at a bottleneck in DNA replication, PCNA is an appealing target for inhibition as an anti-cancer therapeutic.

A human PCNA-p21 peptide structure has been previously solved (PDB:1AXC) and has given insight into how the PIP-box binds to PCNA and the residues of the PIP-box that form particular interactions with PCNA. This line of research was continued through structure solution and binding affinity studies of human PCNA in complex with a mutated p21 peptide, p21Tyr151Phe. This showed that the single amino acid mutation within the PIP-box resulted in a 3-fold decrease in binding affinity. Structurally, this is likely explained by the loss of water-mediated hydrogen bonding to PCNA with mutation from tyrosine to phenylalanine, thus the conclusion that the hydroxyl group of Tyr151 in the p21 PIP-box acts as a tether.

As key proteins in DNA replication, sliding clamps have been investigated as potential drug targets for the treatment of cancer and bacterial infections. Fungal infections are another pathology that might be treated with PCNA inhibition. The research presented here is the first crystal structure of PCNA from the fungal pathogen *Aspergillus fumigatus*. This structure surprisingly had greater similarity to human PCNA than the other previously solved fungal PCNA molecules. Binding affinity experiments demonstrated that AfumPCNA interacts with the human p21 PIP-box motif, supporting the hypothesis that AfumPCNA interacts with binding proteins in a way similar to the human system, rather than the

different/alternate prokaryotic system. This was then further investigated using molecular dynamics simulations to understand the interactions.

This thesis will be presented as a combination of a publication and an accepted manuscript, both articles being included as separate chapters, each with their own references. A third article is included as an appendix, of additional structural biology research that was undertaken on a separate protein. A beginning introductory chapter and a concluding discussion chapter, with a combined reference list at the end, will provide the background of the research and detail how the project fits together.

Declaration

I certify that this work contains no material which has been accepted for the award of any other degree or diploma in my name, in any university or other tertiary institution and, to the best of my knowledge and belief, contains no material previously published or written by another person, except where due reference has been made in the text. In addition, I certify that no part of this work will, in the future, be used in a submission in my name, for any other degree or diploma in any university or other tertiary institution without the prior approval of the University of Adelaide and where applicable, any partner institution responsible for the joint-award of this degree.

I give consent to this copy of my thesis when deposited in the University Library, being made available for loan and photocopying, subject to the provisions of the Copyright Act 1968.

I acknowledge that copyright of published works contained within this thesis resides with the copyright holder(s) of those works.

I also give permission for the digital version of my thesis to be made available on the web, via the University's digital research repository, the Library Search and also through web search engines, unless permission has been granted by the University to restrict access for a period of time.

I acknowledge the support I have received for my research through the provision of an Australian Government Research Training Program Scholarship.

.....	3/7/17 .....
Alice Kroker	Date

Acknowledgements

There have been many people that have had an impact on the life-changing experience and period of my life that has been my postgraduate research.

Thank you to all those that stuck with me and supported me through the medical challenges, who constantly reminded me that me and my health are the most important things, who valued me for me and not just because of my study. Things did not go as we thought they would, but the experience has taught me more than I could have ever dreamed.

To John Bruning, thank you for your passion and support, for caring about me and not just my work.

To Andrew Marshall, thank you for your friendship and comradery, for our afternoon teas, for helping me to look at the bigger picture of life, for the laughs, for the chats, for the sharing, for still being there for me whether I was in the lab or not, thank you so so much.

To the 6pm community at Westbourne Park Uniting Church, thank you for showing an interest in my work and at least attempting to understand even though I could have been speaking in another language, for all the friendships you've offered, for knowing when not to ask about the writing, for accepting my research as part of me but seeing beyond it and seeing me as more than just what I was doing, for showing me why and how I matter.

And to my parents, Steve and Janet Kroker, thank you mum and dad for supporting me no matter what and for reminding me about what's important in life. After my honours I thanked you "for encouraging me to go with my heart and to not put things off, because life is too short and you never know what might happen in the future". Even though we were once again reminded that we don't know what the future will hold you are still encouraging me to go with my heart. I know that I'm loved, and that you will never stop supporting me.

Abbreviations

Ab	antibody
AfumPCNA	*Aspergillus fumigatus* PCNA
APIM	AlkB homologue 2 PCNA-interacting motif
ASU	asymmetric unit
BER	base excision repair
caPCNA	cancer-associated PCNA
CDK	cyclin-dependent kinase
csPCNA	cancer-specific PCNA
DEAE	diethylaminoethyl
DNA	deoxyribonucleic acid
DTT	dithiothreitol
EDTA	ethylenediaminetetraacetic acid
FEN1	flap endonuclease 1
HPLC	high-pressure liquid chromatography
HR	homologous recombination
IDCL	interdomain connector loop
ITC	isothermal titration calorimetry
kDa	kilodalton
Lig1	DNA ligase 1
LM	linear motif
MMR	mismatch repair
mRNA	messenger ribonucleic acid
NER	nucleotide excision repair
NHEJ	nonhomologous end joining
PCNA	proliferating cell nuclear antigen
PCNA-I1	PCNA-inhibitor 1
PDB	Protein Data Bank
PIM	percent identity matrix
PIP	PCNA-interacting protein
rmsd	root-mean-square deviation
RNA	ribonucleic acid
SLE	systemic lupus erythematous
T2AA	T2 amino alcohol
T3	3,3',5-triiodothyronine
TLS	translesion synthesis

Chapter 1: Introduction

1.1 Function of PCNA/role in cell cycle

Proliferating cell nuclear antigen (PCNA), also known as a processivity factor or sliding clamp, is a trimeric, ring-shaped protein that tethers proteins to DNA in cellular processes including DNA replication, DNA repair and cell cycle control (De Biasio & Blanco 2013). It was initially identified following the isolation of autoantibodies to PCNA from the sera of patients with systemic lupus erythematous (SLE), specifically from tissues with proliferating cells, such as the thyroid, spleen and lymph node tissue samples (Miyachi, Fritzler & Tan 1978). Around the same time a polypeptide of the same size (molecular weight of 36kDa) was also identified and proposed as a marker of cell proliferation (Bravo et al. 1981). It was later determined that the two proteins were the same and the name originally given by Miyachi *et al* was chosen for continued use (Mathews 1984).

PCNA on its own has no intrinsic enzymatic activity but, through its topological interaction with DNA, is able to control and coordinate the access of proteins to DNA, particularly at the DNA replication fork; PCNA functions by fully encircling DNA and freely sliding along (Krishna et al. 1994). Within the cell, the primary roles of PCNA are in DNA replication, DNA repair and cell cycle control (Moldovan, Pfander & Jentsch 2007). PCNA is often referred to as a 'tool belt' to describe its ability to interact with numerous and varied proteins (De Biasio & Blanco 2013; Freudenthal et al. 2010). These proteins are also changeable, allowing for the 'belt' to hold different 'tools' depending on its current role within the cell. Each PCNA ring contains three PCNA-interacting protein binding sites, allowing for the binding of up to three such proteins at one time (Gulbis et al. 1996). PCNA is sometimes also referred to as a processivity factor to describe its role in DNA replication, where it increases the processivity of DNA polymerases δ and is required for non-dissociative DNA replication (Krishna et al. 1994).

The cell cycle consists of four key phases, G1, S, G2 and mitosis (Schorpp et al. 2016). DNA synthesis (S phase) occurs between the two growth phases G1 and G2, and is then followed by the segregation of duplicated sister chromosomes in mitosis (M phase). PCNA is present in the cell throughout the cell cycle, but is synthesised mainly during the S phase, which is subsequently when PCNA levels

are highest (Schafer 1998). There is little to no expression of PCNA during G1 but, with a half-life of ~20 hours *in vivo,* PCNA is still present in the G0 and G1 cell cycle phases of daughter cells.

1.2 Evolutionary conservation

PCNA is a member of the sliding-clamp family of proteins that are found across all three domains of life, in eukaryotes, archaea and bacteria (Jeruzalmi, O'Donnell & Kuriyan 2002) (Maga & Hubscher 2003). Despite a lack of sequence homology between them (Krishna et al. 1994) all sliding clamps share a pseudo six-fold symmetry from six structurally similar domains (Maga & Hubscher 2003; Matsumiya, Ishino & Morikawa 2001), and have a high level of structural conservation (Jeruzalmi, O'Donnell & Kuriyan 2002) (Figure 1).

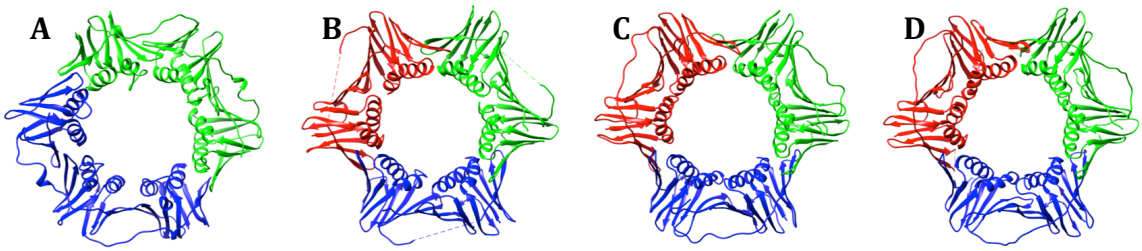

Figure 1: The structure of sliding clamps is evolutionarily conserved. Despite a lack of sequence homology all sliding clamps exhibit the same ring-shaped structure with β-sheets assembled on the outside, α-helices lining the inner surface and pseudo six-fold symmetry. A: *Escherichia coli* β-sliding clamp (PDB:1MMI). B: *Pyrococcus furiosus* (archae) PCNA (PDB:1GE8). C: *Saccharomyces cerevisiae* (yeast) PCNA (PDB:1PLQ). D: Human PCNA (PDB:1AXC). B-D are shown with subunits coloured separately in red, blue and green, while the separate subunits of the dimeric β-sliding clamp (A) are coloured blue and green.

In prokaryotes the sliding clamp exists as a homodimeric β-clamp (Kong et al. 1992). This β-subunit forms part of the Pol III holoenzyme, which is involved in DNA replication, and is responsible for conferring processivity to the rest of the enzyme.

In archaea and eukaryotes the sliding clamp is trimeric (Krishna et al. 1994; Matsumiya, Ishino & Morikawa 2001; Shamoo & Steitz 1999). Archael PCNA can

be either homo- or heterotrimeric in state depending on the phylum (Chia, Cann & Olsen 2010). In eukaryotes a single PCNA subunit is generally transcribed. An example of an exception to this is *Arabidopsis thaliana*, which transcribes two different PCNA subunits that differ by only eight amino acids and can function as both homo- and heterotrimers (Strzalka et al. 2009). (Note - where the sequence of PCNA from *A. thaliana* is referred to in this thesis the PCNA1 sequence is used.)

Given the high level of sequence homology between various eukaryotes (Jeruzalmi, O'Donnell & Kuriyan 2002), particularly in the residues of PCNA that are predicted to be important for trimerisation and the PCNA-PIP-box interaction, it is anticipated that mutations capable of preventing or altering interaction with binding partners, whilst still retaining the ability to undergo normal DNA replication, are unlikely. In support of this there has only been one example in the literature of a clinical mutation in human PCNA, found in just four individuals from an Ohio Amish community (Baple et al. 2014). A homozygous hypomorphic mutation in PCNA (Ser228Ile) was found to be causative for a phenotype that was reminiscent of other disorders where nucleotide excision repair (NER) is impaired. Whilst Ser228 doesn't appear to directly interact with PCNA-interacting proteins (Ser228 isn't part of the interdomain connector loop or one of the nearby residues) mutation to isoleucine showed impaired binding of the mutant PCNA with Fen1, Lig1 and XPG, all PCNA-interacting proteins involved in NER. Interestingly, the mutation did not appear to have an impact on DNA replication. The high level of structural conservation and the lack of observed mutations within PCNA supports the significance of PCNA within the cell and its role in the cell cycle. It also suggests that sliding clamps could make good drug targets that are unlikely to respond to selection pressure and become drug-resistant.

1.3 Sliding clamp structure

Human PCNA is homotrimeric, with its three subunits assembled in a head-to-tail manner (Gulbis et al. 1996) (Figure 2), and each subunit consisting of two similarly folded domains (Figure 3). The N-terminal domain has been defined as residues 1-117 and the C-terminal domain as residues 135-261. The interdomain

connector loop (IDCL) (residues 118-134) connects the two domains. Each subunit has nine β-strands and two α-helices. The α-helices assemble on the inner surface of the clamp and contain lysine and arginine residues, allowing the inner surface of the clamp to interact with the negative phosphate backbone of DNA, despite the overall negative charge of the protein (Dieckman, Freudenthal & Washington 2012). The β-strands assemble into β-sheets on the outside of the ring and are involved in both intersubunit and interdomain β-sheets. The ring structure also has a defined front and back face; the front face contains the IDCL and is the site of protein-protein interactions, and the back face is the site of post-translational modifications (Jonsson, Hindges & Hubscher 1998).

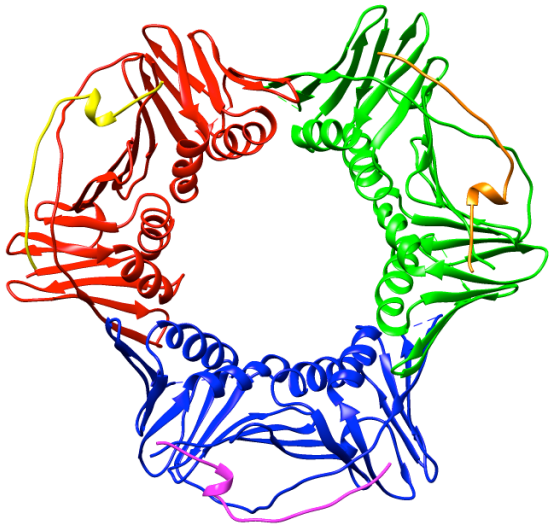

Figure 2: PCNA-p21 ribbon structure (PDB:1AXC). Human PCNA is a homotrimer. The three subunits are shown coloured separately in red, green or blue. A 22 amino acid peptide containing the p21 PIP-box binds with a stoichiometry of one peptide per subunit. The three peptides that are bound to the trimer are shown coloured yellow, orange or purple.

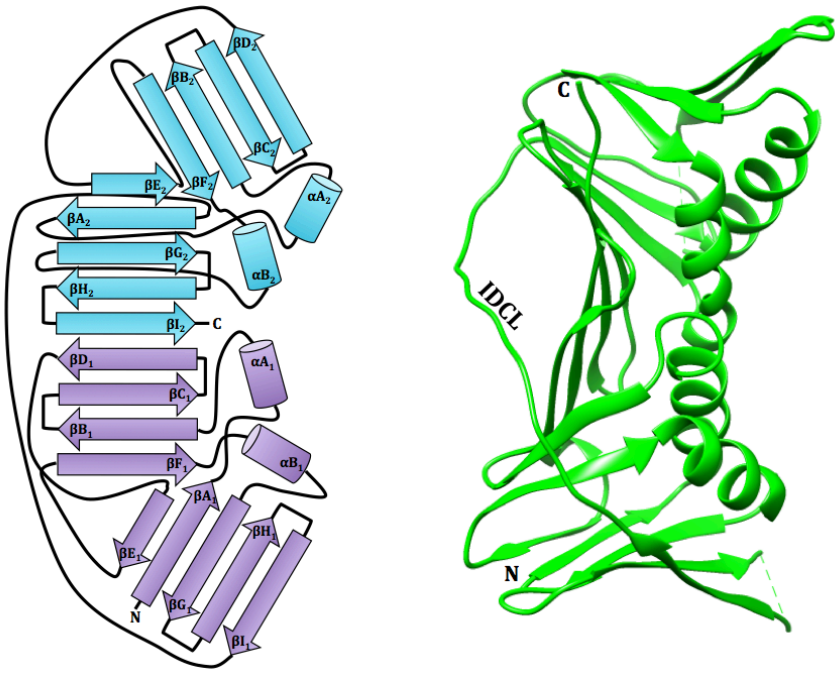

Figure 3: Structure of proliferating cell nuclear antigen (PCNA). (A) Schematic diagram of the arrangement of α-helices and β-strands in a PCNA monomer. (B) Ribbon structure of a human PCNA monomer (PDB:1AXC) (Gulbis et al. 1996; Krishna et al. 1994). Each subunit of PCNA contains two domains connected by an interdomain connector loop (IDCL), and each domain contains two α-helices and nine β-strands.

The first structure solved of a sliding clamp was of the β-clamp from *E. coli* (Kong et al. 1992). The bacterial β-clamp is a part of the *E. coli* DNA polymerase III holoenzyme, a complex of at least ten different protein subunits; the β-subunit is important for enabling non-dissociative and highly processive DNA replication (O'Donnell et al. 1992). The X-ray crystal structure revealed a highly symmetrical, dimeric structure (Kong et al. 1992). The dimers assembled in a head-to-tail manner to form a ring-shape, with six β-sheets on the outside and twelve α-helices lining the inner surface. The high level of symmetry was a consequence of the subunits each having three domains of identical topology, with the βαβββ motif repeated twelve times to form the complete ring. This had not been predicted prior to solving the structure because of the lack of sequence homology between the separate domains. Based on this structure of a bacterial sliding clamp and comparison of differences in the sequence length of the *E. coli* β-clamp compared to PCNA from humans and *S. cerevisiae* (the eukaryotic

sequence was about 2/3rds the size of the bacterial sequence) it was proposed that the eukaryotic sliding clamp might be composed of three subunits with two domains each, instead of the bacterial arrangement of two subunits with three domains each.

The first structure solved of eukaryotic PCNA was from *S. cerevisiae* (Krishna et al. 1994). This structure revealed that the predictions made by Kong et al. (1992) were indeed correct, that the structure of the eukaryotic sliding clamp was a trimeric ring, with each subunit containing two topologically identical domains. Like the bacterial β-clamp, the yeast sliding clamp still consists of six β-sheets and twelve α-helices, and the βαββββ motif is again present, however there is an additional short β-strand present between the two motifs in each subunit. The most significant difference between the two sliding clamps is the trimerization versus dimerization state.

The first structure of human PCNA solved was in complex with a p21 protein; it was also the first structure of a eukaryotic sliding clamp in complex with a binding partner (Gulbis et al. 1996). The sliding clamps from human and *S. cerevisiae* share 35% sequence identity and have a highly similar structure, as expected.

There are currently 23 structures of human PCNA in the Protein Data Bank (PDB) that have been solved using X-ray crystallography (as of 14/2/17) (Table 1). There have been more than 100 structures of sliding clamps solved using X-ray crystallography, particularly from prokaryotes and yeast, with few from higher order eukaryotes (Table 2).

Table 1: Human PCNA crystal structures deposited in the Protein Data Bank.

PDB ID	Pub. Year	Structure Title	Description of Protein Crystallized	Reference
1AXC	1996	Human PCNA	PCNA complexed with 22 amino acid p21 peptide	Gulbis et al. (1996)
1U76	2004	Crystal structure of hPCNA bound to residues 452-466 of the DNA polymerase δ p66 subunit	PCNA complexed with 15 amino acid p66 peptide	Bruning and Shamoo (2004)
1U7B	2004	Crystal structure of hPCNA bound to residues 331-350 of the flap endonuclease-1 (FEN1)	PCNA complexed with 20 amino acid FEN1 peptide	
1UL1	2005	Crystal structure of the human FEN1-PCNA complex	PCNA complexed with full length FEN1	Sakurai et al. (2005)
1VYJ	2005	PCNA PL peptide complex	PCNA complexed with 16 amino acid Pogo-ligase peptide	Kontopidis et al. (2005)
1VYM	2005	Native human PCNA monoclinic	Apo PCNA	
1W60	2005	Native human PCNA trigonal	Apo PCNA	
2ZVK	2009	Crystal structure of PCNA in complex with DNA polymerase eta fragment	PCNA complexed with 21 amino acid DNA pol η peptide	Hishiki et al. (2009)
2ZVL	2009	Crystal structure of PCNA in complex with DNA polymerase kappa fragment	PCNA complexed with 14 amino acid DNA pol κ peptide	
2ZVM	2009	Crystal structure of PCNA in complex with DNA polymerase iota fragment	PCNA complexed with 23 amino acid DNA pol ι peptide	
3P87	2011	Structure of human PCNA bound to RNaseH2B PIP box peptide	PCNA complexed with 23 amino acid RNase peptide	Bubeck et al. (2011)
3TBL	2012	Structure of Mono-ubiquitinated PCNA: Implications for DNA Polymerase Switching and Okazaki Fragment Maturation	Ubiquitinated PCNA	Zhang et al. (2012)
3VKX	2012	Structure of PCNA	PCNA and T3	Punchihewa et al. (2012)
3WGW	2014	Structure of PCNA bound to a small molecule inhibitor	PCNA and T2 amino acid (T2AA)	Inoue et al. (2014)
4D2G	2015	Crystal structure of human PCNA in complex with p15 peptide	PCNA complexed with 21 amino acid p15 peptide	De Biasio et al. (2015)
4RJF	2015	Structure of PCNA in complex with p21 mutant peptide	PCNA complexed with 22 amino acid p21Y151F peptide	Kroker and Bruning (2015)
4ZTD	2015	Crystal Structure of Human PCNA in complex with a TRAIP peptide	PCNA complexed with 12 amino acid TRAIP peptide	Hoffmann et al. (2016)
5E0T	2016	Human PCNA mutant - S228I	Apo PCNA with S228I mutation	Duffy, Hilbert and Kelch (2015)
5E0U	2016	Human PCNA variant (S228I) complexed with p21 at 1.9 Angstroms	PCNA with S228I mutation complexed with 23 amino acid p21 peptide	
5E0V	2016	Human PCNA variant (S228I) complexed with FEN1 at 2.1 Angstroms	PCNA with S228I mutation complexed with 16 amino acid FEN1 peptide	
5IY4	2016	Crystal structure of human PCNA in complex with the PIP box of DVC1	PCNA complexed with 16 amino acid DVC1 peptide	Wang, Y, Xu and Jiang (2016)

5L7C	2017	Structural basis of human clamp sliding on DNA	PCNA and DNA	De March et al. (2017)
5MOM	2017	Crystal structure of PCNA encoding the hypomorphic mutation S228I	Apo PCNA with S228I mutation	Wilson et al. (2017)

Table 2: Examples of organisms from which the structure of their sliding clamp has been solved by X-ray crystallography.

bacteriophage	Enterobacteria phage RB69
	Enterobacteria phage T4 sensu lato
bacteria	*Bacillus subtilis*
	Escherichia coli
	Helicobacter pylori
	Mycobacterium smegmatis
	Mycobacterium tuberculosis
	Pseudomonas aeruginosa
	Streptococcus pyogenes
virus	Human herpesvirus 1
	Human herpesvirus 5
archaea	*Archaeoglobus fulgidus*
	Haloferax volcanii
	Pyrococcus furiosus
	Sulfolobus solfataricus
	Sulfolobus tokodaii
	Thermococcus kodakarensis
eukaryote	*Arabidopsis thaliana*
	Drosophila melanogaster
	Entamoeba histolytica
	Homo sapiens
	Leishmania donovani
	Litopenaeus vannamei
	Saccharomyces cerevisiae

1.4 PIP-boxes

PCNA acts as a scaffold for proteins to interact with DNA. Many of the proteins that interact with PCNA do so through a PCNA-interacting protein (PIP)-box. The PIP-box was first defined by Warbrick et al. (1995), following a yeast two-hybrid screen to identify the regions of each protein involved in the PCNA-p21 interaction. This screen allowed the critical region for the interaction to be narrowed down to the C-terminus of p21. To pinpoint the exact region of the C-terminus of p21 important for the PCNA-p21 interaction a series of overlapping

peptides were tested for their ability to bind to PCNA. One particular 20 amino acid peptide, ^{141}KRRQTSMTDFYHSKRRLIFS^{160}, showed the greatest specificity for PCNA. This peptide showed significantly greater binding to PCNA compared to a peptide missing the first four amino acids (KRRQ), suggesting that all or part of the fragment KRRQ is important for binding. The identified peptide was also capable of blocking SV40 DNA replication.

Warbrick et al. (1995) also performed alanine scanning along the length of the identified 20 amino acid peptide, and the mutant peptides were tested for both PCNA binding efficiency and ability to inhibit SV40 DNA replication. In general, there was a correlation between decreased PCNA binding and loss of DNA replication inhibition. From these experiments it was identified that mutation of M147 and F150 to alanine caused the most significant decrease in PCNA binding, followed by Q144, D149 and Y151, and that the ability to inhibit DNA replication was most significantly affected by mutation of Q144, M147 and Y151 to alanine. Based on this, Warbrick *et al* proposed that drugs based on this peptide (either as a derivative or mimetic) could have therapeutic uses in down-regulating DNA replication in tumour cells.

From these experiments the PIP-box was defined as an eight amino acid sequence, with the consensus Qxx[M/L/I]xx[F/Y][F/Y], where x is any amino acid (Warbrick 1998). Most commonly the PIP-box is found at the C-terminus of the PCNA-interacting protein, but can also be located at the N-terminus or middle of the protein. Despite there being several ways that proteins interact with PCNA, such as the AlkB homologue 2 PCNA-interacting motif (APIM) (Gilljam et al. 2009), the most common is through this PIP-box sequence.

Sequence predictions have identified almost 200 human proteins that match the consensus sequence Qxx[M/L/I]xx[F/H/D][F/Y] (Gilljam et al. 2009). To date, only a small portion of these interactions have been demonstrated experimentally. Many other PIP-boxes (consensus sequence Qxx[M/L/I]xx[F/Y][F/Y] (Warbrick et al. 1995)) have been experimentally supported in the literature, which were possibly not identified by the sequence prediction due to the divergence of the sequence chosen by Gilljam et al. (2009) from the consensus.

1.5 PIP-box structures

In both bacterial and eukaryotic sliding clamps a hydrophobic pocket on the side of the ring acts as the binding pocket for short peptide sequences (Wolff et al. 2011). This is observed in all sliding clamps despite significant differences in both the pockets and the binding peptide sequence between bacteria and eukaryotes. The first eukaryotic crystal structure solved that showed this interaction between PCNA and a binding partner was of human PCNA in complex with a p21 peptide containing its PIP-box sequence (PDB:1AXC). One 22 amino acid long PIP-box-containing peptide was observed to bind per PCNA subunit, with a total of three peptides binding around the outside of one trimer (Gulbis et al. 1996). There were three main regions of PCNA that the peptide was identified to make contacts with (Figures 4 and 5). The N-terminus of the peptide bound near the C-terminus of PCNA. The C-terminus of the peptide (HSKRRLIFS) formed an anti-parallel β-sheet with the N-terminal end of the IDCL of PCNA, and was also bound near the N-terminus of PCNA. Thirdly, residues 146-151 (SMTDFY) of the p21 peptide formed a 3_{10} helix that aided to position three key residues of the PIP-box, M147, F150 and Y151 (Warbrick et al. 1995), within a hydrophobic pocket that was formed by the IDCL and C-terminus of PCNA (Gulbis et al. 1996).

Crystallization of further PCNA-PIP-box complexes has continued, with a total of 11 structures of different PIP-box peptides in complex with PCNA having been solved by X-ray crystallography to date (14/2/17) (Table 3). All PIP-box peptides form the same characteristic structure upon PCNA binding that was observed for the p21 peptide (Figure 6). The characteristic 3_{10} helix is the most significant similarity between all of the structures, emphasising the importance of this structural element for positioning and inserting the conserved residues of the PIP-box (positions 4, 7 and 8) into the hydrophobic pocket of PCNA (Kroker & Bruning 2015). The differences that are observed in the interaction between PCNA and the N- and C-termini of the peptides in the crystal structures are most likely a consequence of differences in the length of the peptides, as well as the specific nature of the residues outside of the PIP-box. It is proposed that differences in the residues outside of the PIP-box may explain some of the

differences that are seen in the binding affinity of different PCNA-interacting proteins for PCNA (Bruning & Shamoo 2004).

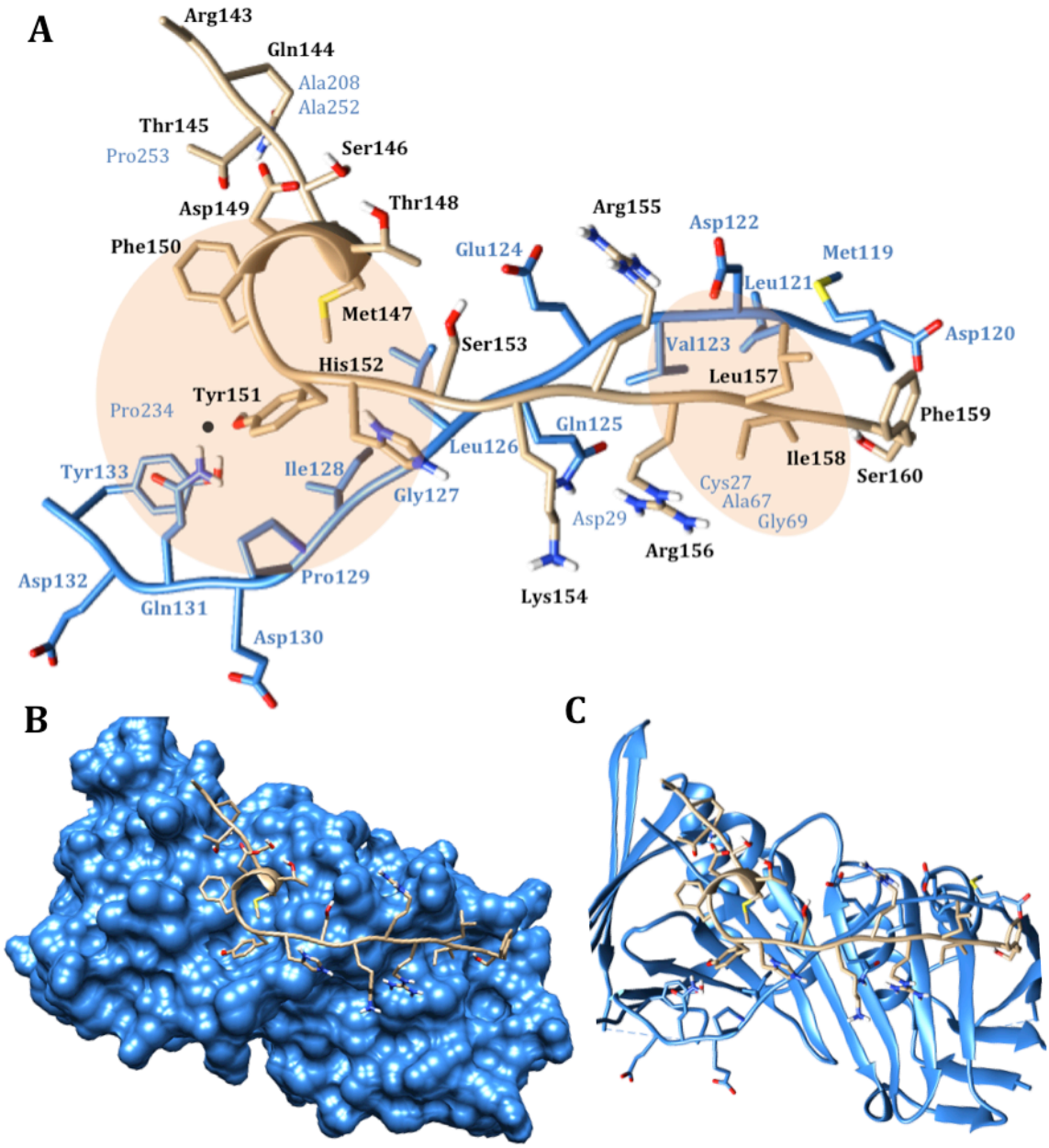

Figure 4: Diagrams of the PCNA-p21 complex (1AXC). A: p21 peptide (orange) and the PCNA IDCL (blue). p21 peptide residues are labeled in black bold type, PCNA IDCL residues are labeled in blue bold type, other key PCNA residues are in blue normal type. The orange regions represent hydrophobic pockets on the surface of PCNA that residues of the p21 peptide interact with. B: PCNA monomer space-filled with a p21 peptide ribbon structure. C: PCNA-p21 complex ribbon structure. Residues of the p21 peptide and PCNA IDCL are shown.

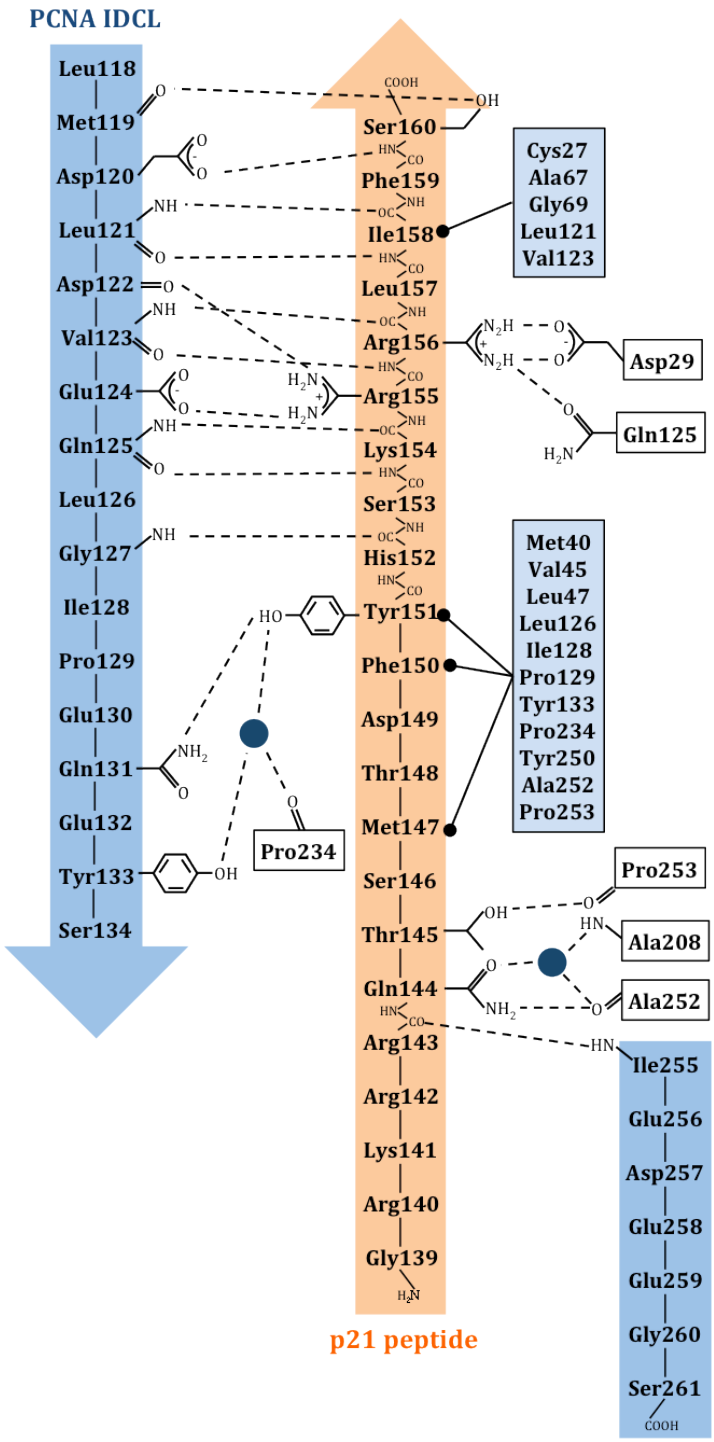

Figure 5: Schematic of the interactions between PCNA and p21 peptide identified in the crystal structure PDB:1AXC. The p21 peptide is shown in the orange arrow. The PCNA IDCL is shown in the blue arrow on the left, and the C-terminal region of PCNA in the blue box on the lower right. The two hydrophobic pockets on the surface of PCNA are shown in separate pale blue boxes, and other key PCNA residues that interact with the p21 peptide are shown in white boxes. The blue circles represent water molecules involved in water-mediated interactions. Adapted from Gulbis et al. (1996).

Table 3: List of PIP-box peptides crystallized in complex with human PCNA. As of 14/2/17. Conserved residues are highlighted.

Protein	Peptide sequence	PDB code
p21	GRKRRQTSMTDFYHSKRRLIFS	1AXC
p21Y151F	GRKRRQTSMTDFFHSKRRLIFS	4RJF
p66 (pol δ)	KANRQVSITGFFQRK	1U76
FEN1	SRQGSTQGRLDDFFKVTGSL	1U7B
Pogo-ligase	SAVLQKKITDYFHPKK	1VYJ
DNA pol η	CKRPRPEGMQTLESFFKPLTH	2ZVK
DNA pol κ	PKHTLDIFFKPLTH	2ZVL
DNA pol ι	ALNTAKKGLIDYYLMPSLSTTSR	2ZVM
RNase H2B	DKSGMKSIDTFFGVKNKKKIGKV	3P87
p15	APVCVRPTPKWQKGIGEFFAA	4D2G
TRAIP	AFQAKLDTFLWS	4ZTD
DVC1	SNSHQNVLSNYFPRVS	5IY4

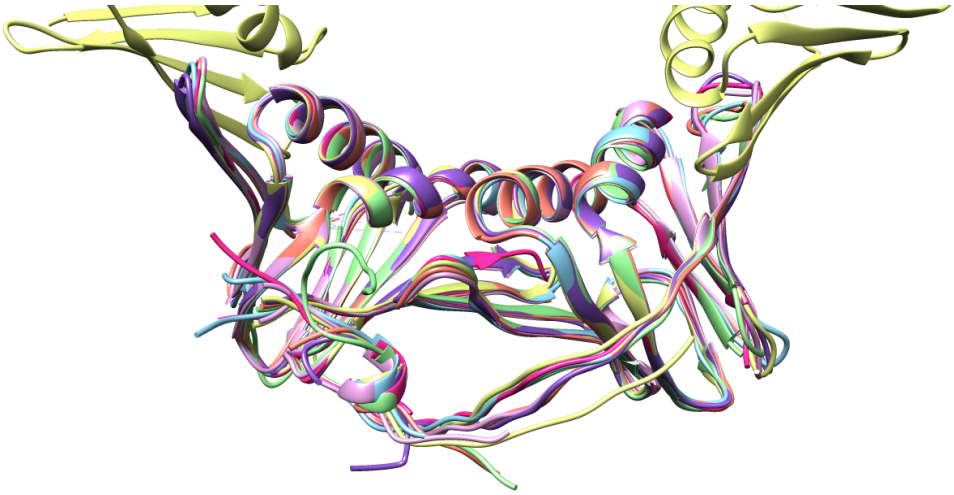

Figure 6: Structure of PIP-box peptides crystallized in complex with human PCNA. All peptides form very similar interactions and structures with PCNA, in particular the characteristic 3_{10} helix. p21 (PDB:1AXC) (yellow), p66 (PDB:1U76) (blue), FEN1 (PDB:1U7B) (pale pink), RNase H2B (PDB:3P87) (bright pink) and DNA polymerases η (PDB:2ZVK) (green), κ (PDB:2ZVL) (orange) and ι (PDB:2ZVM) (purple).

1.6 Bacterial binding motif

In contrast to the eukaryotic PCNA, the bacterial sliding clamp is a dimer and, as such, only has two binding sites for interacting proteins, one per subunit (Yin, Wang, et al. 2014). Each binding site consists of two subsites linked by a shallow channel region and, like the eukaryotic system, binds to short, intrinsically disordered peptide sequences (Yin, Whittell, et al. 2014). The consensus linear motif (LM) sequence in bacteria is QLx_1Lx_2F/L, where S/D is preferred at x_1, and x_2 may be absent. This LM consensus sequence is conserved among all bacterial species (both Gram-positive and Gram-negative), as are the key residues within the sliding clamp that form the binding pocket (Yin, Wang, et al. 2014). The residues within subsite I are particularly highly conserved, and this site has been referred to as an 'anchor site' and acts as the first point of contact in inhibitor binding. An 'anchor-based' sequential manner of binding has been proposed for LMs to the sliding clamp, where key, more highly conserved residues in the interacting protein first bind in the more highly conserved subsite I, followed by binding in subsite II, such that the residues that bind first act as anchors (Yin et al. 2015). The bacterial inhibitors of sliding clamps that have been identified so far bind within the 'anchor site' subsite I, an example being the non-steroidal anti-inflammatory drugs (NSAIDs) (Yin, Wang, et al. 2014). It is proposed that targeting 'anchor sites' in protein-protein interactions is an effective strategy for inhibitor design and that binding partners in other biological systems (such as the PIP-boxes that bind eukaryotic PCNA) may also have key 'anchor' residues that drive binding and could be targeted (Yin et al. 2015). This strategy first requires a more thorough understanding of the mechanism of motif binding, determination of whether sequential binding occurs, and identification of the key anchor residues and sites.

Like the recognition of many other peptide motifs, including the linear motif that interacts with the bacterial sliding clamp, there are both specific and promiscuous binding characteristics in the PCNA-PIP-box interaction (Yin et al. 2013). Promiscuity is a consequence of the fact that PCNA acts as a 'binding hub' or 'tool belt' and interacts with multiple different binding partners (PIP-boxes). This requires a certain level of structural plasticity in the protein, and results in a wide range of binding affinities of the binding partners (Bruning & Shamoo 2004;

De Biasio et al. 2012; Kroker & Bruning 2015; Zheleva et al. 2000). The specificity is seen in the conserved residues of the binding motif; these residues are significant for binding and a decrease or loss of binding affinity is observed following mutation or deletion (Warbrick et al. 1995).

1.7 PCNA in cancer

A major characteristic of cancer is an increased rate of replication, resulting from the deregulation of normal growth and cell cycle control (Hanahan & Weinberg 2000, 2011). Therefore, any proteins involved in replication could be ideal targets for anti-cancer therapeutics. PCNA is necessary for DNA replication and repair, placing it at a bottleneck in cell replication and making it a particularly appealing target for anticancer drugs (Wolff et al. 2011).

PCNA has long been used as a marker of cell proliferation (Stoimenov & Helleday 2009). In cancer cells PCNA has been observed to be increased 5-6 fold (Naryzhny & Lee 2007), in-line with the higher rate of replication that occurs with the deregulation of cell proliferation (Hanahan & Weinberg 2000). p21 expression is also often downregulated in cancer, leading to decreased PCNA inhibition and cell cycle halting, and is associated with a poorer prognosis (Abbas & Dutta 2009). It is also of note that there are no examples in the literature of PCNA mutations either in cancer cells or causative of cancer. This is another reason that makes PCNA an appealing target for treating cancer.

It has been proposed that there is a form of PCNA specific to cancer cells (Bechtel et al. 1998). Two isoforms of PCNA, an acidic form and a basic form, were identified using 2D PAGE in cancer cell lines. Only the basic form, not the acidic form, was detectable in non-malignant cell lines. cDNA sequence analysis showed that all cell lines had the same PCNA nucleotide sequence so it was proposed that the difference in isoforms was due to an altered posttranslational modification. The acidic form of PCNA that was only present in the cancer cell lines and absent in primary tissue samples was termed ‘cancer-specific PCNA’ (csPCNA) (Hoelz et al. 2006) or ‘cancer-associated PCNA’ (caPCNA) (Malkas et al. 2006). It was proposed that the posttranslational modification on csPCNA was

methyl esterification on one or more of 15 specific glutamic or aspartic acid residues in PCNA (Hoelz et al. 2006) (Figure 7).

MF**E**ARLVQGS ILKKVLEALK DLINEACWDI SSSGVNLQSM
DSSHVSLVQL TLRSEGFDTY RCDRNLAMGV NLTSMSKILK
CAGN**E**DIITL RA**ED**NADTLA LVF**E**APNQ**E**K VSDY**E**MK*LM**D***
*LDVEQLGIPE QEYS*CVVKMP SG**E**FARICRD LSHIGDAVVI
SCAKDGVKFS ASG**E**LGNGNI KLSQTSNV**D**K EEEAVTIEMN
EPVQLTFALR YLNFFTKATP LSSTVTLSMS ADVPLVV**E**YK
IADMGHLKYY LAPKI**E**DE**E**G S

Figure 7: Protein sequence of PCNA. Glutamic and aspartic acid residues that could be subject to posttranslational modification and undergo methyl esterification are in **bold**. The residues that correspond to the synthetic peptide used to develop the cancer-associated PCNA antibody are underlined (Hoelz et al. 2006). Residues of the IDCL are in *italics* (Gulbis et al. 1996).

An antibody has been developed that is specific for cancer-associated PCNA (caPCNA) but does not bind to or recognise non-malignant PCNA (nmPCNA) (Malkas et al. 2006). This antibody was prepared using a synthetic peptide fragment of PCNA, residues 123-140, corresponding to part of the IDCL of PCNA (residues 118-134) (Gulbis et al. 1996). The caPCNA-specific antigenic site identified using this antibody was the basis of the development of a cell permeable peptide that was shown to selectively inhibit neuroblastoma cell growth (Gu et al. 2014).

It is not widely accepted that there is a cancer-associated form of PCNA, but rather that the difference between cancer and non-malignant cells is simply the level of PCNA present; PCNA can be present at levels 5-6 fold higher in cancer cells than in normal cells (Naryzhny & Lee 2007). It has been proposed that the 'cancer-specific' nature of the caPCNAab was not the result of a difference in the PCNA epitope, but more likely could be contributed to the fact that the caPCNAab appeared to have lower affinity or titer compared to commercial antibodies, and therefore was more reactive in cancer cells with higher levels of PCNA. It is of

note to mention that the posttranslational modifications proposed to be unique to caPCNA were not identified within the region used as the peptide fragment for caPCNAab development. This raises concerns about the accuracy of the conclusions drawn by Bechtel et al. (1998), Hoelz et al. (2006) and Malkas et al. (2006), and appears to support the conclusions drawn by Naryzhny and Lee (2007), that there is in fact no cancer-specific form of PCNA, at least not the form that had been previously proposed.

The two different forms of PCNA that are accepted to exist, and are present in all cells, are chromatin-bound (involved in replication) and chromatin-unbound (Zhao et al. 2011), also described as detergent soluble and insoluble (Cayrol, Knibiehler & Ducommun 1998). The detergent soluble (chromatin-unbound) population exists for the majority of the cell cycle, but becomes insoluble (chromatin-bound) when PCNA is associated with replication machinery during DNA synthesis (S phase) or when involved in DNA repair following DNA damage. These two populations of PCNA have also been observed within the cell as diffuse localisation of PCNA (particularly during G1 and G2 phases) and then as discrete foci during the S phase (Schorpp et al. 2016).

1.8 PCNA inhibitors

Several groups have demonstrated that inhibition of human PCNA through different mechanisms can inhibit cell growth (Table 4). Several sets of high-throughput screening employing small molecule compound libraries have uncovered novel compounds that inhibit PCNA through two main mechanisms. Small molecule inhibitors were identified that bind between PCNA subunits, blocking clamp loading onto DNA (Tan et al. 2012). Another similar screen identified 3,3'5-triiodothyronine (T3) as an inhibitor of PCNA (Punchihewa et al. 2012). T3 is a thyroid hormone unsuitable to be used clinically as a PCNA inhibitor because of its endocrine function, but the T3 derivative T2 amino acid (T2AA) was identified as still maintaining PCNA inhibitory function but without thyroid activity. Both T3 and T2AA bind in a hydrophobic pocket on PCNA created between the IDCL and the C-terminus of PCNA, the same region where the PIP-box binds (Inoue et al. 2014; Punchihewa et al. 2012). T2AA was shown to be capable of reducing cell proliferation when used in addition to cisplatin, a

DNA-damaging chemotherapeutic agent (Actis et al. 2013). Crystal structures have been published of PCNA in complex with both T3 (PDB:3VKX) and T2AA (PDB:3WGW).

Table 4: Examples in the literature of human PCNA inhibitors. Not included are several other methods of inhibiting PCNA to inhibit cell growth (eg. through APIM, an alternate PCNA-binding motif) (Wang, SC 2014).

Name	Type	Mechanism
p21 peptide (Warbrick et al. 1995)	peptide	•inhibits interaction of PIP-box proteins with PCNA •based on p21 PIP-box (residues 139-160) •GRKRRQTSMTDFYHSKRRLIFS
Antp-ELP-p21 peptide (Massodi, Bidwell & Raucher 2005)	cell-penetrating peptide	•inhibits interaction of PIP-box proteins with PCNA •based on p21 PIP-box (residues 139-160) •RQIKIWFQNRRMKWKK-MSK$(VPGXG)_{120}$WP-WPGSGGRKRRQTSMTDFYHSKRRLIFSKRKP
$p21^{WT}$-Antp (Cayrol, Knibiehler & Ducommun 1998)	cell-penetrating peptide	•inhibits interaction of PIP-box proteins with PCNA •based on p21 PIP-box (residues 141-160) •KRRQTSMTDFYHSKRRLIFSRQIKIWFQNRRMKWKK
R9-caPep (Gu et al. 2014)	cell-penetrating peptide	•inhibits interaction of PCNA with PIP-box proteins •based on PCNA IDCL sequence (residues 126-133) •$R_DR_DR_DR_DR_DR_DR_DR_DR_D$CCLGIPEQEY
PCNA-I1 (Dillehay, Lu & Dong 2014; Tan et al. 2012)	small molecule	•locks trimerization state, inhibiting loading onto DNA •binds at PCNA subunit interface
T3 and T2AA (Actis et al. 2013; Inoue et al. 2014; Punchihewa et al. 2012)	small molecule	•inhibits interaction of PIP-box proteins with PCNA •binds in PIP-box binding site

In silico analysis has suggested that PCNA-PIP interactions may not have been fully optimized during evolution to be high affinity, something that could be exploited in the design of PCNA inhibitors (Fridman et al. 2013). It is likely that interactions are not fully optimized because a range of affinities is important for the function of the interactions. This raises the potential for the design of peptide mimetics that are fully optimized for high affinity. Such molecules would be ideally suited as drugs to compete with and inhibit PCNA-PIP-box interactions (Kroker & Bruning 2015; Warbrick et al. 1995).

PCNA inhibition has also been observed to be less toxic to non-malignant cells compared to cancer cells. The PCNA inhibitor PCNA-I1 is capable of inhibiting cell growth, independent of the tissue of origin, with less toxicity to non-malignant cells compared to cancer cells (Tan et al. 2012). It was proposed that the

difference in potency is due to the increased demands of PCNA in cancer cells, where there is a greater dependence on PCNA to deal with higher levels of DNA instability. This supports the notion that a PCNA inhibitor could be particularly effective clinically if used in combination with a DNA-damaging agent such as cisplatin (Inoue et al. 2014). An agent (such as a PCNA inhibitor) capable of sensitizing specifically cancer cells to chemotherapeutics would mean lower chemotherapy doses would be required, in turn lowering the risk of drug resistance and side effects (Lingeman, Hickey & Malkas 2014). The small molecule inhibitor PCNA-I1 has also been tested in a LNCaP xenograft mouse model of prostate cancer (Dillehay, Lu & Dong 2014). Intravenous treatment with PCNA-I1 significantly inhibited tumour growth without significant toxicity to the mouse. There have also been similar observations with a PCNA-based peptide (residues 126-133, corresponding to a fragment of the IDCL) that selectively inhibited the growth of neuroblastoma cells compared to non-malignant cells (Gu et al. 2014).

1.9 Aims of project

The aim of this project was to define the key residues in PCNA-protein interactions. This was approached by two sub-aims. The interaction between human PCNA and a mutant p21 peptide was investigated, in terms of structure and binding affinity. It was then compared to a previous structure of human PCNA in complex with a wild-type p21 peptide (PDB:1AXC) (Gulbis et al. 1996). The structure of fungal PCNA from *A. fumigatus* was also solved, a previously unstudied species. This structure was compared to that of human PCNA, and binding data for the interaction between AfumPCNA and a p21 peptide was also obtained. It is anticipated that understanding more about the structure of various different sliding clamps and how they interact with other proteins will provide an insight into how this system of cell cycle and replication control and coordination occurs, and will then provide the opportunity for exploitation for therapeutic advantage.

The two main chapters in this thesis, chapters 2 and 3, each address one of these sub-aims. Chapter 2 is a paper published in *Biochemistry*, titled 'p21 Exploits Residue Tyr151 as a Tether for High-Affinity PCNA Binding'. This article

looks at the interaction between human PCNA and an altered p21 peptide, to investigate the affect that such a change has on the protein-peptide interaction and the associated binding affinity. The structure of PCNA bound to a 22 amino acid peptide was solved using X-ray crystallography. This structure was then also compared to a previously solved structure of PCNA in complex with an unaltered p21 peptide. Isothermal titration calorimetry data revealed that the Tyr151Phe mutation reduced binding affinity, and highlighted the involvement of a water-mediated hydrogen bond in tethering the p21 PIP-box to PCNA.

Chapter 3 is a manuscript accepted for publication, titled 'Structure of the Sliding Clamp from the Fungal Pathogen *Aspergillus fumigatus* (AfumPCNA) and Interactions with Human p21'. This article looks at the previously unsolved structure of PCNA from *A. fumigatus*, comparing it to the human PCNA as well as other available fungal sliding clamps. AfumPCNA was shown to interact with the PIP-box from human p21 by fluorescence quenching experiments, demonstrating that AfumPCNA interacts with proteins through a conserved PIP-box mechanism. Molecular dynamics simulations were also performed to better understand these interactions.

Chapter 2: p21 Exploits Residue Tyr151 as a Tether for High-Affinity PCNA Binding

Statement of Authorship

Title of Paper	p21 Exploits Residue Tyr151 as a Tether for High-Affinity PCNA Binding
Publication Status	☐ Published
Publication Details	Kroker, A. J.; Bruning, J. B., p21 Exploits Residue Tyr151 as a Tether for High-Affinity PCNA Binding. Biochemistry, 2015.

Principal Author

Name of Principal Author (Candidate)	Alice J Kroker
Contribution to the Paper	Performed protein purification, ITC, protein cocrystallization, and structure solution and helped with manuscript preparation.
Overall percentage (%)	80%
Certification	This paper reports on original research I conducted during the period of my Higher Degree by Research candidature and is not subject to any obligations or contractual agreements with a third party that would constrain its inclusion in this thesis. I am the primary author of this paper.
Signature	Date 27/2/17

Co-Author Contributions

By signing the Statement of Authorship, each author certifies that:

i. the candidate's stated contribution to the publication is accurate (as detailed above);

ii. permission is granted for the candidate in include the publication in the thesis; and

iii. the sum of all co-author contributions is equal to 100% less the candidate's stated contribution.

Name of Co-Author	John B Bruning
Contribution to the Paper	Managed and contributed to structure solution, data collection, and manuscript preparation.
Signature	Date 13/2/2017

BIOCHEMISTRY
including biophysical chemistry & molecular biology

Article

pubs.acs.org/biochemistry

p21 Exploits Residue Tyr151 as a Tether for High-Affinity PCNA Binding

Alice J. Kroker and John B. Bruning*

School of Biological Sciences, University of Adelaide, Adelaide, South Australia 5005, Australia

Supporting Information

ABSTRACT: Proliferating cell nuclear antigen (PCNA, processivity factor, sliding clamp) is a ring-shaped protein that tethers proteins to DNA in processes, including DNA replication, DNA repair, and cell-cycle control. Often used as a marker for cell proliferation, PCNA is overexpressed in cancer cells, making it an appealing pharmaceutical target. PCNA interacts with proteins through a PCNA interacting protein (PIP)-box, an eight-amino acid consensus sequence; different binding partners display a wide range of affinities based on function. Of all biological PIP-boxes, p21 has the highest known affinity for PCNA, allowing for inhibition of DNA replication and cell growth under cellular stress. As p21 is one of the few PIP-box sequences to contain a tyrosine rather than a phenylalanine in the eighth conserved position, we probed the significance of the hydroxyl group at this position using a mutational approach. Here we present the cocrystal structure of PCNA bound to a mutant p21 PIP-box peptide, p21Tyr151Phe, with associated isothermal titration calorimetry data. The p21Tyr151Phe peptide showed a 3-fold difference in affinity, as well as differences in entropy and enthalpy of binding. These differences can be attributed to a loss of hydrogen bonding capacity, as well as structural plasticity in the PCNA interdomain connector loop and the hydrophobic cavity of PCNA to which p21 binds. Thus, the hydroxyl group of Tyr151 in p21 acts as a tethering point for ideal packing and surface recognition of the peptide interface, increasing the binding affinity of p21 for PCNA.

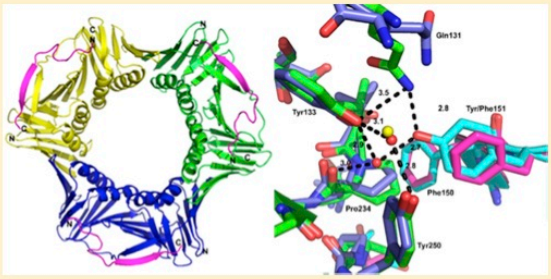

Proliferating cell nuclear antigen (PCNA), also known as the sliding clamp, is a nuclear protein with essential roles in DNA replication, DNA repair, and chromatin formation.[1] The function of PCNA is that of a molecular adaptor, tool belt, or docking platform, to control access to, recruitment to, and affinity of proteins for DNA and the replication fork.[2] PCNA is also a processivity factor, required for processive DNA polymerization by multiple polymerases, including the major replicative polymerase, Pol δ; PCNA increases the affinity of DNA Pol δ for DNA by 64000-fold.[3] In addition, PCNA interacts with a host of other partners, involved in processes such as Okazaki strand resolution, DNA repair, including mismatch repair, nucleotide excision repair, base excision repair, nonhomologous end joining, homologous recombination, and translesion synthesis, DNA modification, and cell-cycle control.[4]

Human PCNA is a ring-shaped, trimeric protein with pseudo 6-fold symmetry. Each subunit contains two similarly folded domains, each containing two α-helices and nine β-strands.[5,6] The α-helices line the center of the ring, while the β-strands form the outer surface of the ring. Within each subunit, the two domains are connected by the interdomain connector loop (IDCL) (residues 119−134), which runs along the outside of the ring.[6] The subunits are arranged in a head-to-tail manner, creating defined front and back faces.[7] The toroid structure allows for PCNA to encircle DNA and interact topologically to slide along it. This is facilitated by the positively charged inner surface, contributed by lysine and arginine residues within the α-helices, allowing for an electrostatic interaction between PCNA and the negatively charged backbone of DNA.[8,9] This overall structure is conserved in all sliding clamps across eukaryotes, prokaryotes, and archaea, despite a lack of sequence homology between different species.

Many of the proteins that interact with PCNA do so through a conserved motif coined the PCNA-interacting protein (PIP)-box.[10] The PIP-box is defined as Qxx[M/L/I]xx[F/Y][F/Y] and is usually, although not always, located in the C-terminal region of its interacting partners.[11] Almost 200 different biological PIP-boxes have been proposed from bioinformatics analysis.[12] Of the handful of PIP-boxes for which binding affinity data are available for the interaction with PCNA, differences in binding affinities have been reported.[3,13,14] Diversity in binding affinity is predicted to be a consequence of differences in the PIP-box consensus sequence and allow for the "tuning" of affinity relative to the role of the PCNA−PIP-box interaction, such that there is a link between binding affinity and protein function.

Of the biological PIP-boxes so far investigated, a key example is the p21 PIP-box. The levels of tumor suppressor protein p21

Received: March 6, 2015
Revised: May 13, 2015

DOI: 10.1021/acs.biochem.5b00241
Biochemistry XXXX, XXX, XXX−XXX

are elevated in response to DNA damage, not only to modulate cell-cycle progression by inhibiting cyclin-dependent kinases but also to interact directly with PCNA and block DNA replication and other processes, allowing DNA repair to occur prior to the resumption of replication.[6,10] This process is competitive, as p21 and Pol δ (p66 subunit) have both been shown through crystallographic studies to bind to the same site on PCNA.[3,6]

The p21 PIP-box has the highest known binding affinity for PCNA and is considered a model for high-affinity PCNA binding.[15] A p21 peptide containing the PIP-box has a 725-fold greater binding affinity for PCNA compared to that of an equivalent FEN1 peptide.[3] A structure of a p21 peptide containing the PIP-box (residues 139−160) has been crystallized in complex with human PCNA [Protein Data Bank (PDB) entry 1AXC].[6] This structure revealed that the PIP-box binding site is located near the IDCL of PCNA. The N-terminus of the peptide containing the PIP-box forms a 3_{10} helix that inserts into a hydrophobic pocket proximal to the IDCL on the surface of PCNA. The C-terminal end of the peptide forms an antiparallel β-sheet with the IDCL.[6] Several other PIP-box peptides have been crystallized in complex with human PCNA and also form the characteristic 3_{10} helix that inserts residues at positions 4, 7, and 8 of the PIP-box into the hydrophobic cavity of PCNA.[3,16,17] It has therefore been hypothesized that the residues at these three positions (4, 7, and 8) could be important for the interaction with PCNA and for tuning the degree of affinity. The PCNA−p21 crystal structure revealed that p21 Tyr151 (position 8 of the PIP-box) is involved in a water-mediated interaction with several PCNA residues.[6] The majority of PIP-boxes contain phenylalanine at this position, lacking the hydroxyl group observed in the p21 PIP-box (Table 1). This has led to the prediction that the Tyr151 residue in p21 could be, at least in part, responsible for the higher binding affinity of p21 for PCNA.

Table 1. Examples of Biological PIP-Box Sequences[a]

Protein	PIP-box
p21	QTSMTDFY
p66 (pol δ)	QVSITGFF
FEN1	QGRLDDFF
DNA pol η	MQTLESFF
DNA pol κ	KHTLDIFF
DNA pol ι	KKGLIDYY
RNase H2B	MKSIDTFF
MCMT	QTTITSHF
MSH3	QAVLSRFF
MSH6	QSTLYSFF
RecQ5	QNLIRHFF
UNG2	QKTLYSFF
WRN	QWKLLRDF
XPG	QLRIDSFF

[a]Conserved positions 1, 4, 7, and 8 that match the consensus sequence are highlighted.[3,6,8,11,16,17]

Misregulation of PCNA is associated with proliferative disorders such as cancer and is commonly used as a marker of cell proliferation.[18,19] PCNA levels have been reported to be 5−6-fold higher in cancer cells than in nonmalignant cells,[20] and the malignancy of several tumors has been directly correlated to PCNA expression levels.[21] Inhibition of PCNA, at the mRNA[21] and protein level,[10] has been shown to inhibit proliferation and cell growth, highlighting the protein as a potential anticancer target. Indeed, peptides and small molecule inhibitors of PCNA have been shown to be capable of selectively inhibiting malignant cell growth, in both cell culture and a mouse model.[15,22−28] Thyroid hormone T3 and its derivative, T2AA, have both been shown to bind to PCNA in the PIP-box binding site, thus inhibiting PIP-box binding. These small molecules were capable of inhibiting DNA replication and repair as well as sensitizing cells to the effects of the chemotherapeutic agent cisplatin.[15,22,26] However, no clinical trials have yet been undertaken with PCNA inhibitors, underscoring the need for a better understanding of the structural mechanism of its interacting partners. Current inhibitors often demonstrate low potency, cell permeability, bioavailability, and possible off-target effects. Peptide mimetics make up an approach to PCNA inhibition that has been suggested;[10] however, no such research has yet been performed.

In this study, we have used X-ray crystallography to determine the structure of PCNA in complex with a p21 peptide in which Tyr151 has been mutated to phenylalanine. This structure and the associated binding affinity calculated using isothermal titration calorimetry (ITC) have provided insight into the importance of residue 151 in the PCNA−p21 interaction. Binding affinity data revealed a 3-fold decrease in binding with the change of tyrosine to phenylalanine corresponding to a binding event that is enthalpically driven but has a reduced entropic term compared to that of wild-type binding. Our crystal structure not only shows the obvious loss of hydrogen bonding capacity compared to that of the wild-type structure but also demonstrates that shifts in the PCNA interdomain connector loop (IDCL) relative to the core structure and the hydrophobic cavity of PCNA to which p21 binds are key determinants of binding. Thus, the hydroxyl group of Tyr151 in p21 acts as a tethering point for ideal packing and surface recognition of the peptide interface, increasing the binding affinity of p21 for PCNA.

EXPERIMENTAL PROCEDURES

Computational Alanine Scanning. Computational alanine scanning was performed using a Robetta algorithm (http://robetta.bakerlab.org/alascansubmit.jsp).[29,30] PDB entry 1AXC was used as the input. $\Delta\Delta G$ was averaged across the three peptide−subunit complexes in the asymmetric unit.

Protein Expression. pET-28a-PCNA, which was cloned previously,[3] was transformed into BL21(DE3) cells. The bacterial culture was grown at 37 °C to an OD_{600} of 0.7 and induced using 0.5 mM IPTG at 16 °C for 16 h. Cells were harvested by centrifugation and cell pellets resuspended in 20 mM Tris (pH 8.0), 20 mM NaCl, 2 mM DTT, and 10% glycerol for ITC or 20 mM Tris (pH 7.5), 20 mM NaCl, 2 mM DTT, and 0.5 mM EDTA (pH 8.0) for crystallization. Resuspended cells were stored at −80 °C until they were purified.

PCNA Purification. Protein for ITC was produced as follows. Cells were lysed using high-pressure disruption

DOI: 10.1021/acs.biochem.5b00241
Biochemistry XXXX, XXX, XXX−XXX

(Microfluidics cell disruptor), and the cell lysate was clarified by centrifugation. The clarified lysate was applied to a 5 mL DEAE Sepharose FF column (GE) and eluted with a linear NaCl gradient (0.1 to 0.5 M). Fractions containing PCNA were pooled and brought up to 1 M ammonium sulfate by the dropwise addition of 4 M ammonium sulfate, loaded onto a 5 mL HiTrap Phenyl FF column (GE), and eluted with a reverse linear gradient (1 to 0 M ammonium sulfate, 500 to 50 mM NaCl). Fractions containing PCNA were pooled and dialyzed overnight to 20 mM Tris (pH 7.5), 0.1 M NaCl, 10% glycerol, 2 mM DTT, and 0.5 mM EDTA. The sample was applied to an ENrich Q 5 × 50 column (Bio-Rad) and eluted with a linear NaCl gradient (0.2 to 0.8 M). Fractions containing PCNA were pooled and dialyzed overnight to 1× PBS for ITC.

Protein for crystallization was produced as follows. Cells were lysed using high-pressure disruption (Microfluidics cell disruptor), and the cell lysate was clarified by centrifugation. The clarified lysate was made up to 1.5 M ammonium sulfate by the dropwise addition of 4 M ammonium sulfate, applied to a HiTrap Phenyl FF column (GE), and eluted with a reverse linear gradient (1.5 to 0 M ammonium sulfate, 20 to 0 mM NaCl). Fractions containing PCNA were pooled and dialyzed to 20 mM Tris (pH 7.5), 20 mM NaCl, and 1 mM DTT. PCNA was applied to a HiTrap Q FF column (GE) and eluted with a linear NaCl gradient (20 to 700 mM). Fractions containing PCNA were pooled and dialyzed to 20 mM Tris (pH 7.5), 50 mM NaCl, and 1 mM DTT, then brought up to 1.5 M ammonium sulfate by the dropwise addition of 4 M ammonium sulfate, applied to a HiTrap Phenyl FF column (GE), and eluted with a reverse linear gradient (1.5 to 0 M ammonium sulfate, 20 to 0 mM NaCl). Fractions containing PCNA were pooled and dialyzed to 20 mM Tris (pH 7.5), 50 mM NaCl, and 1 mM DTT. PCNA was loaded onto a HiPrep 26/60 Sephacryl S-300 HR column (GE) equilibrated in 20 mM Tris (pH 7.5), 50 mM NaCl, and 1 mM DTT. Fractions containing PCNA were pooled and dialyzed to 20 mM Tris (pH 7.5), 10% glycerol, 0.5 mM EDTA, and 2 mM DTT. PCNA was concentrated to 12.6 mg/mL using an Amicon Ultra-15 Centrifugal Filter Unit (10 kDa molecular mass cutoff) and used fresh in crystallization experiments.

Peptide Synthesis. p21Tyr151Phe peptide (^{139}GRKRRQTSMTDFFHSKRRLIFS^{160}) was purchased from GenScript and synthesized at >95% purity by HPLC. Prior to being used in experiments, the lyophilized powder was resuspended in Tris (pH 8.0) and then dialyzed extensively to Tris (pH 7.5).

Isothermal Titration Calorimetry. Both peptide and PCNA solutions were dialyzed using either 500 or 10000 Da molecular mass cutoff dialysis tubing, respectively, to the same stock of PBS for 16 h at 4 °C prior to use in ITC experiments. Binding affinity data were determined using isothermal titration calorimetry (MicroCal iTC-200). PCNA was thermostated at 30 °C in the cell and the p21Tyr151Phe peptide injected stepwise over 20 injections. The initial PCNA concentration was 10 μM, and the initial peptide concentration was 270 μM. Data were fitted and analyzed using Origin 7 (MicroCal).

Crystallization. Cocrystals were produced using a 1:1 molar ratio (PCNA:peptide) at a final complex concentration of 0.44 mM. PCNA−p21Tyr151Phe cocrystals were grown by vapor diffusion in sitting drops at 16 °C; 1 μL of complex was mixed with 1 μL of well solution, containing 0.08 M strontium chloride hexahydrate, 0.02 M magnesium chloride hexahydrate, 0.04 M sodium cacodylate trihydrate (pH 7.0), 20% (v/v) (±)-2-methyl-2,4-pentanediol, and 0.012 M spermine tetrahydrochloride (Natrix G7, Hampton Research). The total volume of the well solution was 75 μL, and crystals were grown in a 96-well Intelliplate (Art Robbins). Hexagonal crystals grew to full size (approximately 250 μm in each dimension) within 1 week.

Data Collection and Processing. A single crystal was harvested without additional cryo-solution and cryo-cooled to 100 K for data collection. Diffraction data were collected at the Braggs Facility (University of Adelaide) using a Rigaku R-AXIS IV^{++} detector at a wavelength of 1.54 Å. Crystal diffraction data that extended to a resolution of 2.0 Å were collected using CrystalClear (Rigaku) and processed using iMosflm and Scala.[31,32] Data processing statistics are listed in Table 2.

Table 2. Crystallographic Data

Data Collection	
wavelength (Å)	1.54
space group	*P*3
unit cell dimensions	a = 142.97 Å, b = 142.97 Å, c = 41.41 Å, α = 90°, β = 90°, γ = 120°
resolution (Å)	41.4−2.0
no. of unique reflections	63391
average redundancy	7.1 (6.4)
completeness (%)	100 (99.9)
R_{merge}	0.051 (0.404)
I/σ	25.0 (3.8)
Refinement	
resolution (Å)	39.272−2.006
no. of protein atoms	7910
no. of water molecules	296
R_{free}	0.189
R_{work}	0.148
root-mean-square deviation	
bonds (Å)	0.002
angles (deg)	0.631
Ramachandran analysis	
no. of outliers	3 (0.3%)
no. favored	765 (95.7%)

Previous attempts to determine the structure involved hexagonal crystals grown in 0.1 M HEPES (pH 7.0) and 3.2 M ammonium sulfate (AmSO4 suite F10, Qiagen), cryo-protected with 20% glycerol, and cryo-cooled to 100 K for data collection. Diffraction data were recorded at the Australian Synchrotron on the MX1 beamline[33,34] to a resolution of 2.4 Å. The apparent space group was $P6_322$. Structures could not be determined because of the presence of twinning as has been reported previously for PCNA[3,6] and so was not pursued further.

Structure Refinement. The PCNA−p21Tyr151Phe crystal structure was determined by molecular replacement using Phaser MR.[35] The previously published PCNA−p21 structure (PDB entry 1AXC) was used as the search model, modified to contain a single PCNA subunit with a p21 peptide bound but missing the residue at position 151 to prevent bias. Three different PCNA subunit−p21Tyr151Phe peptide complexes were present within the asymmetric unit (ASU), with each subunit from a separate trimer. Three trimers were formed when the symmetry operators were applied to the monomers in the ASU, such that each trimer formed contained one subunit

DOI: 10.1021/acs.biochem.5b00241
Biochemistry XXXX, XXX, XXX−XXX

from the ASU and two subunits that were symmetry mates (Figure 1 of the Supporting Information).

The presence of twinning in the crystal structure was identified using phenix.xtriage,[36] with the twin law $-h-kl$ and a near perfect twin fraction of 0.49. The true space group was *P*3, which generated an apparent space group of *P*6. Data, as well as twinning, were refined using phenix.refine and rebuilding performed in Coot.[37] Multiple rounds of refinement in Phenix followed by manual rebuilding in Coot were conducted until *R* factors converged. Molprobity and ADIT 2.0 were used for validation of the structure solution.[38,39] Crystal packing contacts are observed between some of the PCNA subunit−peptide complexes. As such, chains E and F were used for all structural analyses as no crystal contacts were found to interfere with the PCNA−peptide interaction. Likewise, the previous PCNA−p21 structure (PDB entry 1AXC) has several crystal packing contacts that possibly alter the PCNA−peptide interaction, so chains C and D were specifically chosen for comparison with our PCNA−peptide structure because of a lack of these contacts. Final refinement statistics are listed in Table 2.

Accession Number. Atomic coordinates and structure factors have been deposited in the PDB as entry 4RJF.

RESULTS

Energetic and Thermodynamic Analysis of the p21Tyr151Phe−PCNA Complex. While the p21 PIP-box remains the highest-affinity PIP-box for PCNA that has been measured experimentally, the amino acids that contribute most significantly to the p21 binding energy remain largely unexplored. A quantitative model of binding energies was implemented to delineate hot spots along the p21−PCNA interface that contribute most significantly to binding affinity. A computational model developed by Kortemme et al. was used, which is characterized by an all-atom rotamer description of interacting side chains combined with an energy function defined by hydrogen bonding, Lennard-Jones interactions, and solvation interactions;[29,30] this model was used to encompass the packing interactions and electrostatic interactions observed in the wild-type p21−PCNA cocrystal structure while using an implicit solvation model. The previously determined wild-type PCNA−p21 cocrystal structure was used to determine free energies of interaction, with successive alanine substitution at each position along the p21 peptide (PDB entry 1AXC). $\Delta\Delta G$ values ranged from 0.05 to 3.63 kcal mol^{-1} (see Table 3). The greatest $\Delta\Delta G$ determined within the PIP-box was for substitution of Tyr151 with alanine (3.55 kcal mol^{-1}), followed by Gln144, Met147, and Phe150 (3.06, 2.45, and 2.45 kcal mol^{-1}, respectively), which correspond to the conserved residues within the PIP-box. Because p21 is one of the few PIP-box peptides with a tyrosine in the second of the conserved aromatic positions of the PIP-box (rather than phenylalanine), the high value of the $\Delta\Delta G$ term suggests that the hydroxyl group of Tyr151 may be, at least in part, responsible for the high affinity of p21 compared to those of other PIP-box peptides (see Table 1 for a comparison of known PIP-box sequences and Figure 1 for an analysis of the frequency of amino acids at this position).

Given that computational approaches often ignore changes in backbone conformation or effects on the dynamics of interaction interfaces, the thermodynamic parameters and binding affinity of the peptide p21Tyr151Phe (residues 139−160) for PCNA were measured using ITC (the binding isotherm is shown in Figure 2). The Tyr151Phe mutation was engineered to probe the effect of the hydroxyl group of residue 151 on binding affinity, energetics of binding, and thermodynamic properties. This mutant p21-derived peptide was identical in length and composition to previously published p21−PCNA binding species (with the exception of the mutation of Tyr151 to phenylalanine),[3,6] allowing for straightforward comparison to the wild-type PCNA−p21 binding interaction. Fitting of the p21Tyr151Phe peptide binding data gave a stoichiometry of approximately 1:1, consistent with one peptide binding to one subunit or three peptides per trimer. The Gibbs free energy (ΔG), enthalpic (ΔH), and entropic ($T\Delta S$) terms are listed in Table 4. A 3-fold decrease in affinity was demonstrated for the p21Tyr151Phe peptide in comparison to that of the wild-type p21 peptide, corresponding to a shift in K_d from 83 nM for wild-type p21[3] to 250 nM for p21Tyr151Phe. The free energies of binding (ΔG) were similar for both peptides. Wild-type p21 showed binding (ΔH = −29.1 kcal mol^{-1}) 3-fold more enthalpically favorable than that of the Tyr151Phe mutant (−10.2 kcal mol^{-1}). Interestingly, the p21Tyr151Phe peptide showed a 15-fold difference in its entropy of binding compared to that of the wild-type peptide (a $T\Delta S$ value of 1.3 versus 19.3 kcal mol^{-1}). Consistent with previous PIP-box−PCNA interactions, the enthalpic terms are the favorable driving force in the Gibbs free energy equation. As such, the enthalpic term, which is not as favorable for the p21Tyr151Phe peptide, correlates with a decrease in binding affinity. Similarly, the FEN1 and p66 PIP-box peptides have a lower affinity in proportion to their lower enthalpic terms as compared to those of p21.[3] While the entropic term is unfavorable for the Tyr151Phe mutation, it is significantly more favorable than those of all previously reported PIP-box peptides, including the wild-type p21 PIP-box peptide.

Table 3. Energies of Binding Analysis by Amino Acid Residue for the p21−PCNA Complex (PDB entry 1AXC)[a]

residue no.	amino acid	$\Delta\Delta G$ (complex) (kcal mol^{-1})
144	Q	3.06
145	T	0.56
146	S	0.85
147	M	2.45
148	T	1.01
149	D	1.52
150	F	2.45
151	Y	3.55
152	H	0.10
153	S	0.40
154	K	0.05
155	R	1.76
156	R	3.63
157	L	0.34
158	I	1.96
159	F	0.26
160	S	0.98

[a] $\Delta\Delta G$ (complex) averaged across all three peptide−subunit complexes. See Experimental Procedures for experimental details.

Structure Solution and Global Fold of the p21Tyr151-Phe−PCNA Complex. The X-ray crystal structure of PCNA in complex with a mutant p21Tyr151Phe peptide (residues 139−160) was determined to a resolution of 2.0 Å by means of molecular replacement. The structure was determined in space

DOI: 10.1021/acs.biochem.5b00241
Biochemistry XXXX, XXX, XXX−XXX

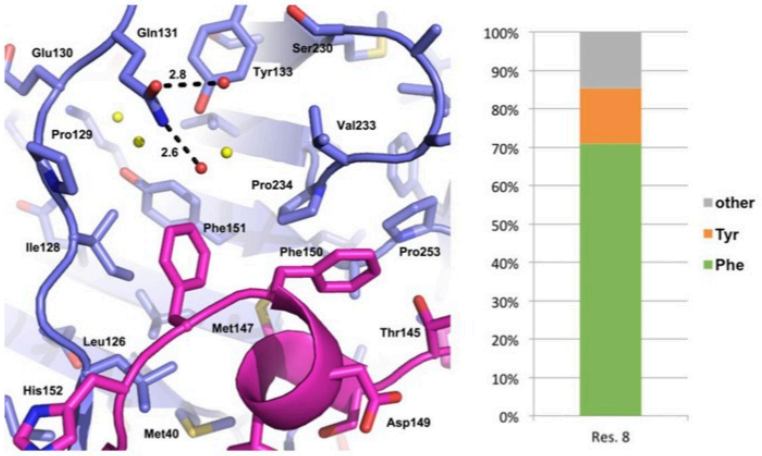

Figure 1. Position 8 of the PIP-box. Ribbon diagram of the p21Tyr151Phe (magenta) binding site on PCNA (blue) with side chains shown as sticks. Water molecules unique to the Tyr151Phe mutant structure are colored red, while others are colored yellow. To see water molecules involved in the bonding of hydrogen to PCNA, see Figure 5C. Chart illustrating the frequency of amino acid type at position 8 of the PIP-box (residue Tyr151 in p21) of all human PIP-boxes described in the literature as interacting with PCNA.[2−4,7,10,11,13,16,43−52]

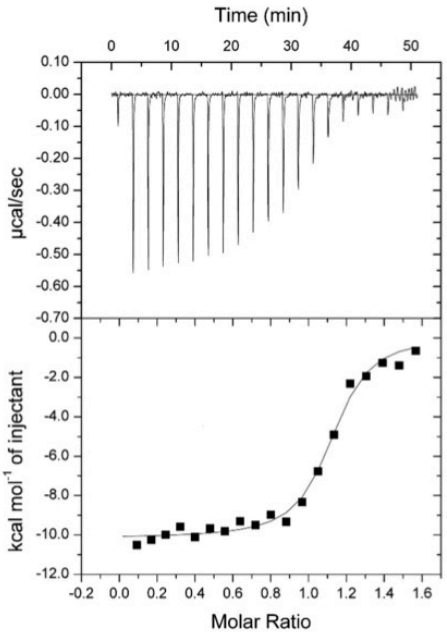

Figure 2. ITC measurements of the binding of the PIP-box-containing peptide p21Tyr151Phe (residues 139−160) to PCNA. Data were fit using a one peptide bound per subunit model. Thermodynamic parameters are listed in Table 4.

Table 4. PCNA Isothermal Titration Calorimetry with p21 and p21Tyr151Phe Peptides

	wild-type p21[3]	p21Tyr151Phe
N (stoichiometry)	1	1.1
K (affinity constant) (M^{-1})	1.21×10^7	4.00×10^6
ΔG (free energy) (kcal mol^{-1})	−9.8	−11.5
ΔH (enthalpy) (kcal mol^{-1})	−29.1	−10.2
ΔS (entropy) (cal mol^{-1} K^{-1})	−63.7	−4.4
$-T\Delta S$ (kcal mol^{-1})	19.3	1.3

group $P3$ with an apparent space group $P6$ due to near perfect twinning (twin fraction of 0.49) with a twinning operator of $-h-kl$. PCNA crystallized with three subunits in the asymmetric unit, with one peptide bound per subunit. The three PCNA subunits were unambiguously modeled from residues 1−255, with poor electron density for the six C-terminal residues as well as two loops (residues 107−108 and 187−190) in two or one of the monomers, respectively; similar regions of disorder have been reported with previously determined PCNA crystal structures.[3,6,15−17,26] Of the peptide, 21, 20, or 18 residues were modeled unambiguously for each of chains B, D, and F, respectively. Ribbon diagrams of the PCNA subunit and trimer are shown in panels A and B of Figure 3, respectively. Reduced model bias difference Fourier maps of the p21Tyr151Phe peptide are shown in Figure 4. X-ray crystal structure processing and refinement statistics are listed in Table 1.

The PCNA structure (Figure 3A) has three subunits that are arranged in a head-to-tail fashion such that the N-terminal and C-terminal regions form subunit−subunit contacts, with the quaternary structure defined as a toroid, as shown in Figure 3B. The three subunits share a high degree of structural similarity with rmsd values between subunits ranging from 0.46 to 1.15 Å (over 253 Cα atoms) and surface area values ranging from 12611 to 12933 Å^2. Each subunit of PCNA contains 4 α-helices and 18 β-strands, with each of the domains in the subunit containing half of the α-helices and β-strands (two and nine, respectively). The PCNA trimer has pseudo 6-fold symmetry.

The p21Tyr151Phe peptide contacts the PCNA surface and shares an overall topology similar to those of previously reported PIP-box structures.[3,6,16,17] The three p21Tyr151Phe peptides share a high degree of structural homology, with rmsd values upon superimposition (over 18 Cα atoms) of 0.3 Å. The surface area of the three p21Tyr151Phe peptides ranges from 2600 to 2827 Å^2 with the area of the interface with PCNA ranging from 1076 to 1142 Å^2 (approximately 40% of the total surface area of the peptide). There are three distinct portions of the peptide: the N-terminal region (residues 139−145), a

DOI: 10.1021/acs.biochem.5b00241
Biochemistry XXXX, XXX, XXX−XXX

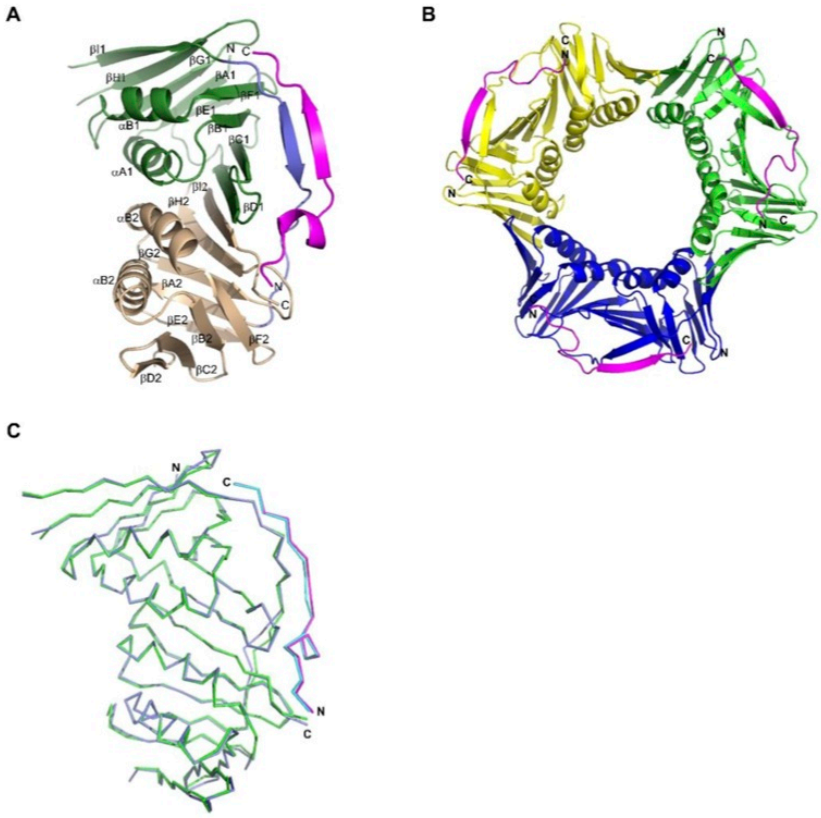

Figure 3. Global fold of the p21Tyr151Phe–PCNA cocrystal structure. (A) Ribbon diagram of the PCNA monomer. Domain 1 is colored green and domain 2 brown. The interdomain connector loop (IDCL) is colored blue. The p21 mutant peptide is colored magenta. (B) Ribbon diagram of the PCNA trimer. Individual subunits of PCNA are denoted by differences in color: yellow, green, and blue. Each p21Tyr151Phe peptide is colored magenta. (C) Wire diagram of the superimposition of the wild-type p21– and p21Tyr151Phe–PCNA cocrystal structures. PCNA is colored green for the wild-type structure (PDB entry 1AXC) and blue for the mutant-bound structure, while the wild-type p21 peptide is colored cyan and the mutant peptide magenta.

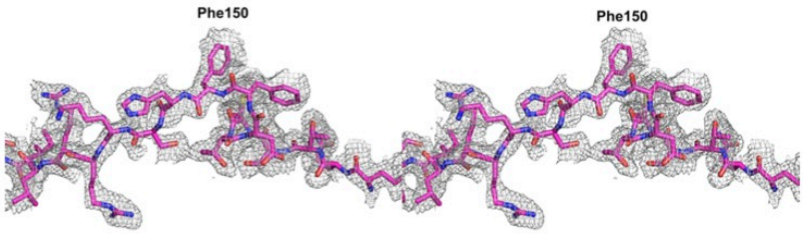

Figure 4. Electron density map of the p21Tyr151Phe peptide. The p21Tyr151Phe peptide is depicted as sticks in magenta with atoms colored by element. The electron density map is a $2F_o - F_c$ omit map contoured at 1σ. The diagram is in wall-eye stereo.

central portion that forms the characteristic 3_{10} helix (residues 146–151), and a C-terminal region (residues 152–160). The N-terminal region makes electrostatic interactions with the C-terminus of PCNA. The 3_{10} helix positions three residues (Ser146, Thr148, and Asp149) such that their side chains extend away from PCNA into the bulk solvent, while three other residues (Met147, Phe150, and Phe151) make contact in a hydrophobic pocket on the PCNA surface created between the IDCL and interdomain β-sheet of PCNA (Figures 5 and 6). The C-terminus of the peptide forms an antiparallel β-sheet with the IDCL of PCNA.

Comparison of Wild-Type p21– and p21Tyr151Phe–PCNA Cocrystal Structures. Both wild-type p21– and p21Tyr151Phe–PCNA cocrystal structures show a high degree of global similarity to the apo form of PCNA (PDB entry 1VYM)[40] upon superimposition, with an rmsd of 0.44 Å over 248 Cα atoms and 0.71 Å over 245 Cα atoms. From this, we deduce that no large-scale structural rearrangements of PCNA are required for or induced by peptide binding. Furthermore,

DOI: 10.1021/acs.biochem.5b00241
Biochemistry XXXX, XXX, XXX–XXX

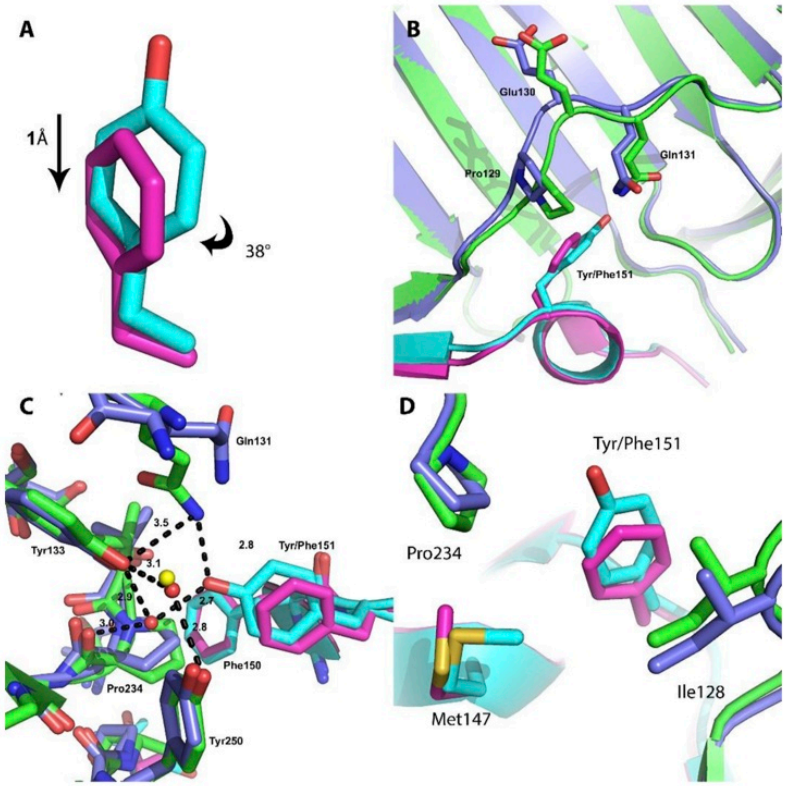

Figure 5. Comparison of the wild-type p21– and p21Tyr151Phe–PCNA cocrystal structures. Ribbon diagrams from a superimposition of PCNA (wild-type p21-bound PCNA and p21Tyr151Phe-bound PCNA), with interacting residues shown as sticks. PCNA bound to wild-type p21 is colored green, wild-type p21 cyan, PCNA bound to p21Tyr151Phe blue, and p21Tyr151Phe peptide magenta. (A) Comparison of the phenylalanine and tyrosine rotamers at position 151. (B) Comparison of the IDCL comprising the p21 binding pocket. (C) Comparison of the water-mediated hydrogen bond network proximal to Tyr151 of p21. Water molecules of the wild-type structure are colored red, while the water molecule in the p21Tyr151Phe-bound structure is colored yellow. For the sake of simplicity, only water molecules interacting with PCNA Tyr133, PCNA Tyr250, and p21 Tyr151 are shown here. (D) Comparison of the hydrophobic contacts at the Tyr151Phe binding site.

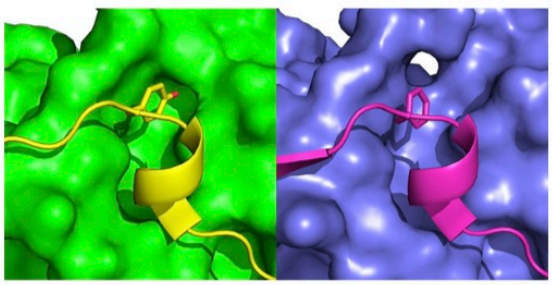

Figure 6. Surface representation of the p21–PCNA binding site. PCNA is depicted as a surface representation, while p21 is shown in ribbons with residue 151 shown as sticks. On the left is the wild-type p21–PCNA structure. PCNA is colored green and p21 yellow. On the right is the p21Tyr151Phe–PCNA structure. PCNA is colored blue and p21Tyr151Phe magenta.

the wild-type p21- and p21Tyr151Phe-bound PCNA structures share a high degree of structural similarity upon being superimposed with an rmsd of 0.43 Å over 248 Cα atoms, implying that differences in affinity and thermodynamic parameters are subtle and localized to the p21–PCNA interface. The superimposition of wild-type and mutant structures is shown in Figure 3C. Superimposition of only the p21 wild-type and Tyr151Phe peptide chains reveals an rmsd value of 0.37 Å over 18 Cα atoms highlighting that both peptides adopt nearly identical topology when bound to PCNA. Calculation of the interface area for the PIP-box region of both peptides (residues 143–152) shows that the p21Tyr151Phe interface area is slightly smaller with a value of 564.4 Å^2 versus 607.3 Å^2 for wild-type p21-bound PCNA, consistent with an extra hydroxyl group for interaction in the wild-type structure and expansion of the cavity size in the mutant structure. Interestingly, the hydrophobic cavity into which residue 151 docks was larger for the mutant structure: 223.6 Å^3 for the p21Tyr151Phe structure compared to 98.9 Å^3 for the wild-type structure, a nearly 2.3-fold expansion in pocket volume (calculated using CASTp[41]). Differences in cavity volume are presented in Figure 6.

Tyr151 of the wild-type p21 peptide participates in not only direct electrostatic interactions but also water-mediated hydrogen bonds, as well as hydrophobic and van der Waals interactions. Wild-type p21 Tyr151 forms a hydrogen bond with Gln131 of the PCNA IDCL (2.8 Å from a lone pair of carbonyl oxygen of the Tyr151 side chain to Nε of the Gln131

DOI: 10.1021/acs.biochem.5b00241
Biochemistry XXXX, XXX, XXX–XXX

side chain) as seen in Figure 5C. In addition to the formation of a hydrogen bond with Tyr151, Gln131 is also found within weak hydrogen bonding distance of Tyr133 of PCNA (3.5 Å from Nε of the Gln151 side chain to the Tyr133 carbonyl oxygen of the side chain). Two water molecules are found in the wild-type p21 structure proximal to Tyr151, both involved in a web of interactions stabilizing the PCNA binding surface. The oxygen atom of the Tyr151 side chain is 2.7 Å from a water molecule, which in turn forms two other hydrogen bonds: 3 Å to the backbone carbonyl of Pro234 and 2.9 Å to the oxygen atom of the Tyr133 side chain, both of PCNA. The second water molecule is not bonded to p21 Tyr151 but rather forms a water-mediated hydrogen bond between the side chain oxygen atoms of PCNA residues Tyr133 (3.1 Å) and Tyr250 (2.8 Å), aiding in the stability of the p21 binding surface. The hydrophobic and van der Waals contacts through Tyr151 of wild-type p21 are responsible for much of the packing of the 3_{10} helix "hydrophobic plug" into the cavity on the PCNA surface, known as the "hydrophobic pocket". These contacts include the side chains of PCNA residues Pro234 and Ile128 as well as Met147 of p21 (Figure 5D).

Mutation of Tyr151 to phenylalanine in the p21 peptide means a loss of both hydrogen bond donor and acceptors on the side chain and results in structural rearrangements in the IDCL, changes in the hydrophobic packing of the 3_{10} helix, and disruption of part of the extensive hydrogen bonding network at the PCNA−p21 interface. The PCNA−p21Tyr151Phe cocrystal structure shows that Phe151, in comparison to Tyr151, is not positioned similarly or as closely to the PCNA surface, with the phenyl ring 1 Å farther from the PCNA surface and the rotamer rotated 38° (Figure 5A). The inability to hydrogen bond results in several structural alterations. PCNA Gln131 no longer forms a hydrogen bond with Phe151, allowing for a shift in the Gln131 side chain of approximately 2 Å away from PCNA and toward the bulk solvent (Figure 5C). This shift in Gln131 position precludes hydrogen bonding to PCNA Tyr133 as occurs in the wild-type structure. As a result, the portion of the IDCL comprising residues 127−131 is not as well tethered to the binding surface of PCNA as in the wild-type structure and is found to be shifted approximately 2 Å from PCNA toward the bulk solvent (Figure 5B). No water-mediated hydrogen bond can be formed between p21 Phe151 and PCNA; however, the PCNA residues Tyr133 and Pro234 that are involved in water-mediated hydrogen bonds with Tyr151 in the wild-type structure are unaffected by the mutation to Phe151 and are found in positions nearly identical to those in the wild-type p21−PCNA cocrystal (Figure 5C). The ability of PCNA residues such as Tyr133 and Tyr250 to maintain the proper conformation for p21 binding is bolstered by the fact that the water-mediated hydrogen bond between the two is also found in the mutant structure; mutation to phenylalanine at position 151 of p21 has no effect on water-mediated hydrogen bonds to residues Tyr133 and Tyr250. The shift in the phenyl ring of Phe151 in the mutant structure away from the PCNA binding surface affects the hydrophobic packing of the 3_{10} helix into the hydrophobic pocket (Figure 5D). The side chains of PCNA residues Pro234 and Ile128 as well as p21 Met147 are not as close to the phenyl ring of p21 Phe151, shifted approximately 1 Å outward from the cavity. This expansion of the cavity results in looser packing and a weaker overall hydrophobic affinity of the p21 peptide for PCNA within the hydrophobic pocket. Interestingly, the lack of an oxygen atom at the terminus of the Phe151 side chain (as is in the wild-type structure), combined with an overall expansion of the pocket, has allowed for the identification of three water molecules not previously reported (Figure 1, left panel). Two are found within hydrogen bonding distance of PCNA Gln131 (2.6 and 2.8 Å), and the last is located in the proximity of where the oxygen atom of the side chain of p21 Tyr151 lies in the wild-type structure (1.6 Å from the oxygen atom of Tyr151 upon superimposition of the structures). None of these water molecules hydrogen bond with p21.

DISCUSSION

While PCNA interacting partners interact with PCNA via the PIP-box consensus sequence, they can display wide variations in binding affinity. For example, the FEN1 PIP-box affinity for PCNA is 725-fold weaker than that of the p21 PIP-box. What is the structural basis for this large difference in affinity among PIP-box peptides? What interactions are critical for optimizing high affinity? These questions have been difficult to answer to date because comparisons have been drawn between only very dissimilar sequences. PIP-box sequences used in structural studies thus far have been too convoluted to dissect the residue by residue impacts on affinity. The limited structural information about the PCNA−PIP-box interaction mechanism is hampering our ability to interpret and explain the hierarchy of binding affinities that exists. To overcome this, we have here chosen a mutational approach that has allowed us to directly probe the significance of Tyr151, a p21 residue previously hypothesized to be critical for high affinity, by means of structure, affinity, and energetic considerations compared to the wild-type p21 sequence. We can now directly measure the significance of Tyr151 in p21 affinity for PCNA and begin to answer the question of which binding epitopes are critical for high-affinity binding to PCNA.

Comparison of the thermodynamic properties of binding revealed differences in binding energetics between the p21 wild-type and Tyr151Phe peptides. All PIP-box peptides measured thus far have shown that negative enthalpic terms are the driving force for the negative Gibbs free energy of binding, including for the p21 wild-type and Tyr151Phe peptides. Comparison of the two enthalpic terms shows that the wild-type peptide (-29 kcal mol^{-1}) is nearly 3 times more favorable in enthalpy (-10 kcal mol^{-1}). Because both peptides have nearly identical overall Gibbs free energies of binding, the decrease in enthalpic favorability is offset in the mutant peptide by a decrease in the value of the entropy term; the p21Tyr151Phe peptide bears a much lower entropic penalty upon binding (-4.4 cal mol^{-1} K^{-1} for the mutant vs -63.7 cal mol^{-1} K^{-1} for the wild type). Because previous studies have shown a loose trend that correlates binding affinity of PIP-boxes with the negativity of Gibbs free energy, it is not surprising that the binding affinity of the mutant, while decreased, is not majorly reduced (K_d of 250 nM vs K_d of 82.6 nM) as the Gibbs free energies of binding are quite similar for both. However, tyrosine instead of phenylalanine at this position imparts an advantage in binding affinity, albeit only a modest advantage (approximately 3-fold).

The hydroxyl group of p21 Tyr151 forms a structural tethering point to PCNA, which can explain an effect on not only affinity but also the packing of the 3_{10} helix, entropic considerations in binding, and effects on enthalpy. The hydroxyl group of Tyr151 forms a tether to PCNA through hydrogen bonding to Gln131 (2.8 Å) as well as water-mediated (2.7 Å to the water molecule) hydrogen bonding to Tyr133 and

DOI: 10.1021/acs.biochem.5b00241
Biochemistry XXXX, XXX, XXX−XXX

Pro234 (Figure 5C). The immediate effect of this tether is that the aromatic ring is pulled deeper into the binding cavity of PCNA; this depth is >1 Å as measured by comparison of the p21 mutant and wild-type structures (Figure 5A). The lack of a hydrogen bonding network in the p21Tyr151Phe structure is the most likely explanation for the decrease in the favorable enthalpy of binding as compared to the wild-type binding mode. The Tyr151 tether has the effect of creating tighter packing as seen by comparison to the mutant structure in which the IDCL (residues 127−131) is packing nearly 2 Å farther away, as well as the hydrophobic contacts, including PCNA residues Ile128 and Pro234 and p21 residue Met147, which are nearly 1 Å farther away (Figures 5D and 6). This is also highlighted by the 43 $Å^2$ difference in interaction surface area between the mutant and wild type. We hypothesize that these structural rearrangements required to facilitate the tighter packing in the wild-type structure are the reason for the higher entropic penalty of binding as compared to that of the p21Tyr151Phe structure. Interestingly, water-mediated hydrogen bonding that is independent of p21 Tyr151 is retained in the p21Tyr151Phe structure between PCNA residues Tyr250 and Tyr133, with these residues found in identical positions in both structures. This infers that this portion of the binding pocket is not affected by hydrogen bonding to p21 and that the water molecule helps form the binding pocket independently and potentially prior to binding.

While it is obvious that removal of the hydroxyl group from Tyr151 of p21 would likely affect the binding affinity and the enthalpic contribution to binding, it is surprising that the reduction in affinity is only 3-fold when other PIP-box sequences bearing a phenylalanine at this position have markedly reduced binding affinities compared to those of p21, reduced by several hundred-fold. The structural rearrangements of both the IDCL and residues of the hydrophobic pocket were not predicted and suggest that high-affinity binding relies, in part, on an entropic penalty of binding that can be overcome by the overall enthalpic nature of the binding mechanism. The significance of this mutation from tyrosine to phenylalanine and the observations made is that at the eighth position of the PIP-box the majority of biological PIP-boxes identified have phenylalanine (which lacks the ability to be tethered) rather than tyrosine (capable of being tethered) (Figure 1, right panel). Of the handful of biological PIP-boxes that do have tyrosine, p21 is the only PIP-box for which there are binding affinity data currently available, so this study is the first time that the significance of tyrosine at this position of the PIP-box has truly been shown. Identifying the determinants of high-affinity PCNA binding lends itself to a mutagenesis approach, so that the significance of differences in the PIP-box can be determined residue by residue. As a tyrosine residue at position 8 of the PIP-box is relatively unique to p21, it is anticipated that differences in the frequency of residues at other conserved sites of the consensus PIP-box will provide hints about critical residues that contribute to high-affinity binding. The determinants of the high affinity of p21 over other PCNA-interacting proteins are likely to be multiple and will require more experiments to decipher completely.

The affinity and structure of a small number of PIP-box peptides that contain Phe in the second conserved aromatic position have been previously studied. These include the p66 PIP-box (K_d = 15.6 μM), the FEN1 PIP-box (K_d = 60 μM), and the nonphysiological PIP-box, the PL peptide (K_d = 100 nM).[3,40] These results, coupled with our mutational results, demonstrate that affinity can largely be modulated by alteration of residues outside of the second conserved aromatic position. The structural mechanism of the differential affinity of these Phe-containing PIP-boxes has been difficult to determine because of the degeneracy of the PIP-box sequence, especially the residues of the 3_{10} helix. The structures containing Phe in the second aromatic residue of the PIP-box bound to human PCNA can be seen in Figure 7. Superimposition of the mutant

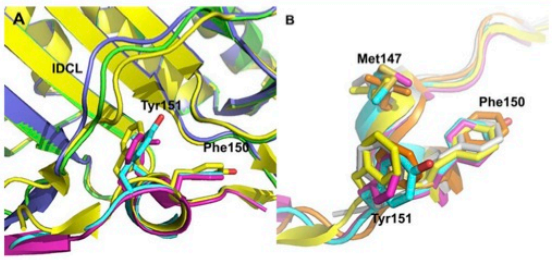

Figure 7. Comparison of PIP-box peptides bound to human PCNA that contain Phe at PIP-box conserved residue 8. Crystal structures were superimposed, and colors represent the following: yellow, PL peptide−PCNA complex (PDB entry 1VYJ); blue, PCNA from the Tyr151Phe complex (PDB entry 4RJF); magenta, p21Tyr151Phe peptide from the Tyr151Phe complex (PDB entry 4RJF); green, PCNA from the wild-type p21 complex (PDB entry 1AXC); cyan, p21 peptide in the wild-type p21−PCNA complex (PDB entry 1AXC); orange, FEN1−PCNA complex (PDB entry 1U7B); and gray, p66−PCNA complex (PDB entry 1U76). (A) Superimposition of PCNA in complex with the p21 wild-type peptide, the Tyr151Phe peptide, and the PL peptide to demonstrate the effect on the IDCL. (B) Superimposition of the 3_{10} helix of PIP-box peptides FEN1, p66, p21, PL peptide, and p21Tyr151Phe.

p21Y151F structure with the PL PIP-box peptide and wild-type p21 peptide structures reveals that the IDCL in the PL peptide structure is drawn closer to the 3_{10} helix by approximately 1.6 Å (as compared to that of wild-type p21), which is in contrast to the p21Tyr151Phe peptide structure, where the IDCL is shifted nearly 2 Å from the 3_{10} helix toward the bulk solvent (Figure 7A). The PL peptide contains a Tyr rather than a Phe in the first conserved aromatic residue of the PIP-box, contains an Ile rather than a Met in the fourth conserved position of the PIP-box, and has several different residues in the variable regions of the PIP-box as compared to p21; these differences may account for the differential packing of the IDCL and the residues of the hydrophobic pocket in the PL structure. Superimposition of the peptides containing Phe at the second conserved aromatic residue of the PIP-box (Figure 7B) shows that the side chains and position of the 3_{10} helix backbone atoms adopt quite variable conformations; however, the conformations of these side chains are most similar to those of the Tyr151Phe mutant structure (Figure 5). From this, we conclude that our mutational approach has allowed us to most accurately (in contrast to comparison to the FEN1, p66, and PL peptide structures) deduce the effect of the Tyr151 residue on affinity and structure. Furthermore, residues other than Tyr151 that pack in the hydrophobic pocket of PCNA such as p21 residues Met147 and Phe150, as well as residues in the variable positions of the PIP-box (positions 2, 3, 5, and 6), likely make strong contributions to PIP-box affinity for PCNA through packing interactions and positioning of the 3_{10} helix.

DOI: 10.1021/acs.biochem.5b00241
Biochemistry XXXX, XXX, XXX−XXX

PCNA−PIP-box interactions may not have been fully optimized during evolution to be high-affinity[42] to ensure the ability of the "tools" to be changed on the "belt" while still maintaining the hierarchy of binding. Our results have revealed that the tyrosine at the last position of the PIP-box makes a contribution to the high affinity of p21 for PCNA. As such, a small molecule or peptide mimetic inhibitor would aim to include or even further encourage this interaction, such as by providing a hydroxyl group for involvement in the interaction, or even extending the residue side chain to replace the water molecule, such that the interaction is then direct rather than water-mediated.

■ ASSOCIATED CONTENT

Supporting Information

Supplemental Figures 1 and 2. The Supporting Information is available free of charge on the ACS Publications website at DOI: 10.1021/acs.biochem.5b00241.

■ AUTHOR INFORMATION

Corresponding Author

*School of Biological Sciences, University of Adelaide, Adelaide, South Australia, Australia. E-mail: john.bruning@adelaide.edu.au. Telephone: +61 (08) 8313-5218. Fax: +61 (08) 8313-4362.

Author Contributions

A.J.K. performed protein purification, ITC, protein cocrystallization, and structure solution and helped with manuscript preparation. J.B.B. managed and contributed to structure solution, data collection, and manuscript preparation.

Funding

Synchrotron funding was provided by Australian Synchrotron Grant AS133/MXCAP/6919.

Notes

The authors declare no competing financial interest.

■ ACKNOWLEDGMENTS

We acknowledge the support of the Bragg's Facility for our home source data collection and the Australian Synchrotron for help with data collection and detwinning. This research was undertaken on the MX1 beamline at the Australian Synchrotron, Victoria, Australia.

■ ABBREVIATIONS

ASU, asymmetric unit; DEAE, diethylaminoethyl; DTT, dithiothreitol; EDTA, ethylenediaminetetraacetic acid; FEN1, flap endonuclease 1; HPLC, high-pressure liquid chromatography; IDCL, interdomain connector loop; ITC, isothermal titration calorimetry; mRNA, messenger ribonucleic acid; PCNA, proliferating cell nuclear antigen; PIP-box, PCNA-interacting protein-box; rmsd, root-mean-square deviation.

■ REFERENCES

(1) Moldovan, G. L., Pfander, B., and Jentsch, S. (2007) PCNA, the maestro of the replication fork. *Cell 129* (4), 665−679.

(2) Mailand, N., Gibbs-Seymour, I., and Bekker-Jensen, S. (2013) Regulation of PCNA-protein interactions for genome stability. *Nat. Rev. Mol. Cell Biol. 14* (5), 269−282.

(3) Bruning, J. B., and Shamoo, Y. (2004) Structural and thermodynamic analysis of human PCNA with peptides derived from DNA polymerase-δ p66 subunit and flap endonuclease-1. *Structure 12* (12), 2209−2219.

(4) De Biasio, A., and Blanco, F. J. (2013) Proliferating cell nuclear antigen structure and interactions: Too many partners for one dancer? *Adv. Protein Chem. Struct. Biol. 91*, 1−36.

(5) Krishna, T. S., Kong, X. P., Gary, S., Burgers, P. M., and Kuriyan, J. (1994) Crystal structure of the eukaryotic DNA polymerase processivity factor PCNA. *Cell 79* (7), 1233−1243.

(6) Gulbis, J. M., Kelman, Z., Hurwitz, J., O'Donnell, M., and Kuriyan, J. (1996) Structure of the C-terminal region of p21(WAF1/CIP1) complexed with human PCNA. *Cell 87* (2), 297−306.

(7) Maga, G., and Hubscher, U. (2003) Proliferating cell nuclear antigen (PCNA): A dancer with many partners. *J. Cell Sci. 116* (Part 15), 3051−3060.

(8) Dieckman, L. M., Freudenthal, B. D., and Washington, M. T. (2012) PCNA Structure and Function: Insights from Structures of PCNA Complexes and Post-translationally Modified PCNA. *Subcell. Biochem. 62*, 281−299.

(9) Georgescu, R. E., Kim, S. S., Yurieva, O., Kuriyan, J., Kong, X. P., and O'Donnell, M. (2008) Structure of a sliding clamp on DNA. *Cell 132* (1), 43−54.

(10) Warbrick, E., Lane, D. P., Glover, D. M., and Cox, L. S. (1995) A small peptide inhibitor of DNA replication defines the site of interaction between the cyclin-dependent kinase inhibitor p21WAF1 and proliferating cell nuclear antigen. *Curr. Biol. 5* (3), 275−282.

(11) Warbrick, E. (1998) PCNA binding through a conserved motif. *BioEssays 20* (3), 195−199.

(12) Gilljam, K. M., Feyzi, E., Aas, P. A., Sousa, M. M., Muller, R., Vagbo, C. B., Catterall, T. C., Liabakk, N. B., Slupphaug, G., Drablos, F., Krokan, H. E., and Otterlei, M. (2009) Identification of a novel, widespread, and functionally important PCNA-binding motif. *J. Cell Biol. 186* (5), 645−654.

(13) De Biasio, A., Campos-Olivas, R., Sanchez, R., Lopez-Alonso, J. P., Pantoja-Uceda, D., Merino, N., Villate, M., Martin-Garcia, J. M., Castillo, F., Luque, I., and Blanco, F. J. (2012) Proliferating cell nuclear antigen (PCNA) interactions in solution studied by NMR. *PLoS One 7* (11), e48390.

(14) Zheleva, D. I., Zhelev, N. Z., Fischer, P. M., Duff, S. V., Warbrick, E., Blake, D. G., and Lane, D. P. (2000) A quantitative study of the in vitro binding of the C-terminal domain of p21 to PCNA: Affinity, stoichiometry, and thermodynamics. *Biochemistry 39* (25), 7388−7397.

(15) Punchihewa, C., Inoue, A., Hishiki, A., Fujikawa, Y., Connelly, M., Evison, B., Shao, Y., Heath, R., Kuraoka, I., Rodrigues, P., Hashimoto, H., Kawanishi, M., Sato, M., Yagi, T., and Fujii, N. (2012) Identification of small molecule proliferating cell nuclear antigen (PCNA) inhibitor that disrupts interactions with PIP-box proteins and inhibits DNA replication. *J. Biol. Chem. 287* (17), 14289−14300.

(16) Hishiki, A., Hashimoto, H., Hanafusa, T., Kamei, K., Ohashi, E., Shimizu, T., Ohmori, H., and Sato, M. (2009) Structural basis for novel interactions between human translesion synthesis polymerases and proliferating cell nuclear antigen. *J. Biol. Chem. 284* (16), 10552−10560.

(17) Bubeck, D., Reijns, M. A., Graham, S. C., Astell, K. R., Jones, E. Y., and Jackson, A. P. (2011) PCNA directs type 2 RNase H activity on DNA replication and repair substrates. *Nucleic Acids Res. 39* (9), 3652−3666.

(18) Miyachi, K., Fritzler, M. J., and Tan, E. M. (1978) Autoantibody to a nuclear antigen in proliferating cells. *J. Immunol. 121* (6), 2228−2234.

(19) Bravo, R., Fey, S. J., Bellatin, J., Larsen, P. M., Arevalo, J., and Celis, J. E. (1981) Identification of a nuclear and of a cytoplasmic polypeptide whose relative proportions are sensitive to changes in the rate of cell proliferation. *Exp. Cell Res. 136* (2), 311−319.

(20) Naryzhny, S. N., and Lee, H. (2007) Characterization of proliferating cell nuclear antigen (PCNA) isoforms in normal and cancer cells: There is no cancer-associated form of PCNA. *FEBS Lett. 581* (25), 4917−4920.

(21) Sakakura, C., Hagiwara, A., Tsujimoto, H., Ozaki, K., Sakakibara, T., Oyama, T., Ogaki, M., and Takahashi, T. (1994) Inhibition of gastric cancer cell proliferation by antisense oligonucleotides targeting

DOI: 10.1021/acs.biochem.5b00241
Biochemistry XXXX, XXX, XXX−XXX

the messenger RNA encoding proliferating cell nuclear antigen. *Br. J. Cancer 70* (6), 1060−1066.
(22) Actis, M., Inoue, A., Evison, B., Perry, S., Punchihewa, C., and Fujii, N. (2013) Small molecule inhibitors of PCNA/PIP-box interaction suppress translesion DNA synthesis. *Bioorg. Med. Chem. 21*, 1972−1977.
(23) Cayrol, C., Knibiehler, M., and Ducommun, B. (1998) p21 binding to PCNA causes G1 and G2 cell cycle arrest in p53-deficient cells. *Oncogene 16* (3), 311−320.
(24) Dillehay, K. L., Lu, S., and Dong, Z. (2014) Anti-tumor effects of a novel small molecule targeting PCNA chromatin association in prostate cancer. *Mol. Cancer Ther.*, 2817−2826.
(25) Gu, L., Smith, S., Li, C., Hickey, R. J., Stark, J. M., Fields, G. B., Lang, W. H., Sandoval, J. A., and Malkas, L. H. (2014) A PCNA-Derived Cell Permeable Peptide Selectively Inhibits Neuroblastoma Cell Growth. *PLoS One 9* (4), e94773.
(26) Inoue, A., Kikuchi, S., Hishiki, A., Shao, Y., Heath, R., Evison, B. J., Actis, M., Canman, C. E., Hashimoto, H., and Fujii, N. (2014) A Small Molecule Inhibitor of Monoubiquitinated Proliferating Cell Nuclear Antigen (PCNA) Inhibits Repair of Interstrand DNA Cross-link, Enhances DNA Double Strand Break, and Sensitizes Cancer Cells to Cisplatin. *J. Biol. Chem. 289* (10), 7109−7120.
(27) Massodi, I., Bidwell, G. L., III, and Raucher, D. (2005) Evaluation of cell penetrating peptides fused to elastin-like polypeptide for drug delivery. *J. Controlled Release 108* (2−3), 396−408.
(28) Tan, Z., Wortman, M., Dillehay, K. L., Seibel, W. L., Evelyn, C. R., Smith, S. J., Malkas, L. H., Zheng, Y., Lu, S., and Dong, Z. (2012) Small-molecule targeting of proliferating cell nuclear antigen chromatin association inhibits tumor cell growth. *Mol. Pharmacol. 81* (6), 811−819.
(29) Kortemme, T., and Baker, D. (2002) A simple physical model for binding energy hot spots in protein-protein complexes. *Proc. Natl. Acad. Sci. U.S.A. 99* (22), 14116−14121.
(30) Kortemme, T., Kim, D. E., and Baker, D. (2004) Computational alanine scanning of protein-protein interfaces. *Sci. STKE 2004* (219), 1−8.
(31) Leslie, A. G., and Powell, H. R. (2007) Processing Diffraction Data with Mosflm. In *Evolving Methods for Macromolecular Crystallography*, Vol. 245, pp 41−51, Springer, Berlin.
(32) Winn, M. D., Ballard, C. C., Cowtan, K. D., Dodson, E. J., Emsley, P., Evans, P. R., Keegan, R. M., Krissinel, E. B., Leslie, A. G., McCoy, A., McNicholas, S. J., Murshudov, G. N., Pannu, N. S., Potterton, E. A., Powell, H. R., Read, R. J., Vagin, A., and Wilson, K. S. (2011) Overview of the CCP4 suite and current developments. *Acta Crystallogr. D67* (Part 4), 235−242.
(33) Cowieson, N. P., Aragao, D., Clift, M., Ericsson, D. J., Gee, C., Harrop, S. J., Mudie, N., Panjikar, S., Price, J. R., Riboldi-Tunnicliffe, A., Williamson, R., and Caradoc-Davies, T. (2015) MX1: A bending-magnet crystallography beamline serving both chemical and macromolecular crystallography communities at the Australian Synchrotron. *J. Synchrotron Radiat. 22* (Part 1), 187−190.
(34) McPhillips, T. M., McPhillips, S. E., Chiu, H. J., Cohen, A. E., Deacon, A. M., Ellis, P. J., Garman, E., Gonzalez, A., Sauter, N. K., Phizackerley, R. P., Soltis, S. M., and Kuhn, P. (2002) Blu-Ice and the Distributed Control System: Software for data acquisition and instrument control at macromolecular crystallography beamlines. *J. Synchrotron Radiat. 9* (Part 6), 401−406.
(35) McCoy, A. J., Grosse-Kunstleve, R. W., Adams, P. D., Winn, M. D., Storoni, L. C., and Read, R. J. (2007) Phaser crystallographic software. *J. Appl. Crystallogr. 40* (Part 4), 658−674.
(36) Adams, P. D., Afonine, P. V., Bunkoczi, G., Chen, V. B., Davis, I. W., Echols, N., Headd, J. J., Hung, L. W., Kapral, G. J., Grosse-Kunstleve, R. W., McCoy, A. J., Moriarty, N. W., Oeffner, R., Read, R. J., Richardson, D. C., Richardson, J. S., Terwilliger, T. C., and Zwart, P. H. (2010) PHENIX: A comprehensive Python-based system for macromolecular structure solution. *Acta Crystallogr. D66* (Part 2), 213−221.
(37) Emsley, P., Lohkamp, B., Scott, W. G., and Cowtan, K. (2010) Features and development of Coot. *Acta Crystallogr. D66* (Part 4), 486−501.
(38) Chen, V. B., Arendall, W. B., III, Headd, J. J., Keedy, D. A., Immormino, R. M., Kapral, G. J., Murray, L. W., Richardson, J. S., and Richardson, D. C. (2010) MolProbity: All-atom structure validation for macromolecular crystallography. *Acta Crystallogr. D66* (Part 1), 12−21.
(39) Davis, I. W., Leaver-Fay, A., Chen, V. B., Block, J. N., Kapral, G. J., Wang, X., Murray, L. W., Arendall, W. B., Snoeyink, J., Richardson, J. S., and Richardson, D. C. (2007) MolProbity: All-atom contacts and structure validation for proteins and nucleic acids. *Nucleic Acids Res. 35* (Web Server Issue), W375−W383.
(40) Kontopidis, G., Wu, S. Y., Zheleva, D. I., Taylor, P., McInnes, C., Lane, D. P., Fischer, P. M., and Walkinshaw, M. D. (2005) Structural and biochemical studies of human proliferating cell nuclear antigen complexes provide a rationale for cyclin association and inhibitor design. *Proc. Natl. Acad. Sci. U.S.A. 102* (6), 1871−1876.
(41) Dundas, J., Ouyang, Z., Tseng, J., Binkowski, A., Turpaz, Y., and Liang, J. (2006) CASTp: Computed atlas of surface topography of proteins with structural and topographical mapping of functionally annotated residues. *Nucleic Acids Res. 34* (Web ServerIssue), W116−W118.
(42) Fridman, Y., Gur, E., Fleishman, S. J., and Aharoni, A. (2013) Computational protein design suggests that human PCNA-partner interactions are not optimized for affinity. *Proteins 81* (2), 341−348.
(43) Kanagaraj, R., Saydam, N., Garcia, P. L., Zheng, L., and Janscak, P. (2006) Human RECQ5β helicase promotes strand exchange on synthetic DNA structures resembling a stalled replication fork. *Nucleic Acids Res. 34* (18), 5217−5231.
(44) Hamajima, N., Johmura, Y., Suzuki, S., Nakanishi, M., and Saitoh, S. (2013) Increased Protein Stability of CDKN1C Causes a Gain-of-Function Phenotype in Patients with IMAGe Syndrome. *PLoS One 8* (9), e75137.
(45) Cazzalini, O., Perucca, P., Mocchi, R., Sommatis, S., Prosperi, E., and Stivala, L. A. (2014) DDB2 association with PCNA is required for its degradation after UV-induced DNA damage. *Cell Cycle 13* (2), 240−248.
(46) Chen, X., Paudyal, S. C., Chin, R. I., and You, Z. (2013) PCNA promotes processive DNA end resection by Exo1. *Nucleic Acids Res. 41*, 9325−9338.
(47) Howlett, N. G., Harney, J. A., Rego, M. A., Kolling, F. W. t., and Glover, T. W. (2009) Functional interaction between the Fanconi Anemia D2 protein and proliferating cell nuclear antigen (PCNA) via a conserved putative PCNA interaction motif. *J. Biol. Chem. 284* (42), 28935−28942.
(48) Bacquin, A., Pouvelle, C., Siaud, N., Perderiset, M., Salome-Desnoulez, S., Tellier-Lebegue, C., Lopez, B., Charbonnier, J. B., and Kannouche, P. L. (2013) The helicase FBH1 is tightly regulated by PCNA via CRL4(Cdt2)-mediated proteolysis in human cells. *Nucleic Acids Res. 41* (13), 6501−6513.
(49) Parker, A., Gu, Y., Mahoney, W., Lee, S. H., Singh, K. K., and Lu, A. L. (2001) Human homolog of the MutY repair protein (hMYH) physically interacts with proteins involved in long patch DNA base excision repair. *J. Biol. Chem. 276* (8), 5547−5555.
(50) Banks, D., Wu, M., Higa, L. A., Gavrilova, N., Quan, J., Ye, T., Kobayashi, R., Sun, H., and Zhang, H. (2006) L2DTL/CDT2 and PCNA interact with p53 and regulate p53 polyubiquitination and protein stability through MDM2 and CUL4A/DDB1 complexes. *Cell Cycle 5* (15), 1719−1729.
(51) Shibata, E., Dar, A., and Dutta, A. (2014) CRL4Cdt2 E3 Ubiquitin Ligase and PCNA Cooperate to Degrade Thymine DNA Glycosylase in S-phase. *J. Biol. Chem. 289*, 23056−23064.
(52) Park, J. M., Yang, S. W., Yu, K. R., Ka, S. H., Lee, S. W., Seol, J. H., Jeon, Y. J., and Chung, C. H. (2014) Modification of PCNA by ISG15 plays a crucial role in termination of error-prone translesion DNA synthesis. *Mol. Cell 54* (4), 626−638.

DOI: 10.1021/acs.biochem.5b00241
Biochemistry XXXX, XXX, XXX−XXX

Chapter 3: Structure of the Sliding Clamp from the Fungal Pathogen Aspergillus fumigatus (AfumPCNA) and Interactions with Human p21

Statement of Authorship

Title of Paper	Structure of the Sliding Clamp from the Fungal Pathogen *Aspergillus fumigatus* (AfumPCNA) and Interactions with Human p21
Publication Status	☐ Published
Publication Details	Marshall, A. C.; Kroker, A. J.; Murray, L. A. M.; Gronthos, K.; Rajapaksha, H.; Wegener, K. L.; Bruning, J. B., Structure of the Sliding Clamp from the Fungal Pathogen Aspergillus fumigatus (AfumPCNA) and Interactions with Human p21. The FEBS journal, 2017.

Principal Author

Name of Principal Author (Candidate)	Alice J Kroker		
Contribution to the Paper	Performed gene cloning, purification guidance, and helped prepare manuscript.		
Overall percentage (%)	30%		
Certification:	This paper reports on original research I conducted during the period of my Higher Degree by Research candidature and is not subject to any obligations or contractual agreements with a third party that would constrain its inclusion in this thesis. I am the co-primary author of this paper.		
Signature		Date	27/2/17

Co-Author Contributions

By signing the Statement of Authorship, each author certifies that:

i. the candidate's stated contribution to the publication is accurate (as detailed above);

ii. permission is granted for the candidate in include the publication in the thesis; and

iii. the sum of all co-author contributions is equal to 100% less the candidate's stated contribution.

Name of Co-Author	Andrew C Marshall		
Contribution to the Paper	Performed protein purification and crystallization, data processing, structure solution and prepared figures and manuscript.		
Signature		Date	13/2/17

Name of Co-Author	Lauren A M Murray		
Contribution to the Paper	Helped purify protein and crystallization trials.		
Signature		Date	22/2/17

Name of Co-Author	Kahlia Gronthos		
Contribution to the Paper	Helped purify protein and crystallization trials.		
Signature		Date	16/2/17

Name of Co-Author	Harinda Rajapaksha		
Contribution to the Paper	Carried out MD simulations.		
Signature		Date	15-02-2017

Name of Co-Author	Kate L Wegener		
Contribution to the Paper	Performed binding studies, and assisted with manuscript preparation.		
Signature		Date	14/2/2017

Name of Co-Author	John B Bruning		
Contribution to the Paper	Conceived and managed project. Helped with data processing, structure solution and preparation of manuscript and figures.		
Signature		Date	13/2/2017

The FEBS Journal

FEBS PRESS science publishing by scientists

Structure of the sliding clamp from the fungal pathogen *Aspergillus fumigatus* (AfumPCNA) and interactions with Human p21

Andrew C. Marshall[1,*], Alice J. Kroker[1,*], Lauren A.M. Murray[1], Kahlia Gronthos[1], Harinda Rajapaksha[2], Kate L. Wegener[1] and John B. Bruning[1]

1 School of Biological Sciences, The University of Adelaide, South Australia, Australia
2 Department of Biochemistry and Genetics, La Trobe Institute for Molecular Life Science, La Trobe University, Bundoora, Australia

Keywords
Aspergillus; p21; PCNA; PIP-box; sliding clamp

Correspondence
J. B. Bruning, School of Biological Sciences, Adelaide, South Australia, Australia
Fax: +61 (08) 8313-4362
Tel: +61 (08) 8313-5218
E-mail: john.bruning@adelaide.edu.au

*These authors contributed equally

(Received 14 November 2016, revised 16 January 2017, accepted 2 February 2017)

doi:10.1111/febs.14035

The fungal pathogen *Aspergillus fumigatus* has been implicated in a drastic increase in life-threatening infections over the past decade. However, compared to other microbial pathogens, little is known about the essential molecular processes of this organism. One such fundamental process is DNA replication. The protein responsible for ensuring processive DNA replication is PCNA (proliferating cell nuclear antigen, also known as the sliding clamp), which clamps the replicative polymerase to DNA. Here we present the first crystal structure of a sliding clamp from a pathogenic fungus (*A. fumigatus*), at 2.6Å. Surprisingly, the structure bears more similarity to the human sliding clamp than other available fungal sliding clamps. Reflecting this, fluorescence polarization experiments demonstrated that AfumPCNA interacts with the PCNA-interacting protein (PIP-box) motif of human p21 with an affinity (K_d) of 3.1 μM. Molecular dynamics simulations were carried out to better understand how AfumPCNA interacts with human p21. These simulations revealed that the PIP-box bound to AfuPCNA forms a secondary structure similar to that observed in the human complex, with a central 3_{10} helix contacting the hydrophobic surface pocket of AfumPCNA as well as a β-strand that forms an antiparallel sheet with the AfumPCNA surface. Differences in the 3_{10} helix interaction with PCNA, attributed to residue Thr131 of AfumPCNA, and a less stable β-strand formation, attributed to residues Gln123 and His125 of AfumPCNA, are likely causes of the over 10-fold lower affinity of the p21 PIP-box for AfumPCNA as compared to hPCNA.

Database
The atomic coordinates and structure factors for the *Aspergillus fumigatus* sliding clamp can be found in the RCSB Protein Data Bank (http://www.rcsb.org) under the accession code 5TUP.

Introduction

In recent decades, an increase in the number of treatment regimens involving immunosuppressant therapies has been associated with a rise in the incidence of invasive nosocomial fungal infections worldwide [1–3]. Aside from transplant failure or cancer relapse, the primary cause of death for immunocompromised patients is infection, and various species of fungi, particularly *Candida* and *Aspergillus* spp., play a major role [4]. The saprophytic filamentous fungus *Aspergillus fumigatus* is abundant in the environment, and the

Abbreviations
Afum, *Aspergillus fumigatus*; IDCL, interdomain connector loop; PCNA, proliferating cell nuclear antigen; PIP, PCNA-interacting protein.

most common cause of invasive fungal infection in immunocompromised patients [5,6]. Typically found feeding on decaying organic matter, it plays a crucial role in the recycling of carbon and nitrogen [7,8]. *Aspergillus fumigatus* spores, called conidia, are ubiquitous and thus inhaled on a daily basis [9]. Conidia are usually cleared efficiently from the lungs by the innate immune system, but in specific cases they may germinate and cause infection [10]. Infection is most often pulmonary, but infections of the bronchi, sinus, and dissemination to the brain and other organs are also common. Susceptibility to invasive infection is closely linked to the immune status of the host; individuals at highest risk are those with hematological malignancies, particularly acute leukemia, and transplant patients [7,11]. Although morbidity and mortality are usually associated with invasive aspergillosis (IA) in immunocompromised patients, an even larger number of patients are affected by chronic or allergic conditions caused by *Aspergillus* spp. [12]. Occurrence of IA in otherwise immunocompetent patients is atypical, but has been reported following influenza [13,14] in ICU patients without hematological malignancy [15] and in otherwise healthy individuals [16,17]. *Aspergillus fumigatus* conidia are small enough to reach the lower airways and are readily internalized by alveolar epithelial cells, where they are able to evade host immune cells and to initiate systemic infection [18]. The low sensitivity of current microbiological and histopathological methods, along with a lack of consistency in surveillance and case definition, has made estimation of the incidence of IA in the past difficult and has probably lead to an underestimation of the true disease burden [19,20]. However, it is generally recognized that the incidence of invasive fungal infections is increasing, with the major contributors shifting from *Candida* spp. to *Aspergillus* spp. [19,21]. Central nervous system aspergillosis is a particularly devastating condition associated with a very poor prognosis and mortality rates of approximately 90% [11,12,17,22,23]. In addition, IA is the most common cause of death due to lung infection in hematopoietic stem cell transplant (HSCT) patients [23]. A multicenter prospective survey of 23 institutions in the US reported an incidence of invasive fungal infections in HSCT patients of 0.9%–13.2%. IA was the most common condition, with *A. fumigatus* by far the most prevalent species implicated. Overall 1-year survival rates for all autologous and allogeneic HSCT patients included in the study were 87% and 64%, respectively, but dropped to 25.4% when including only those who contracted aspergillosis [19]. IA is also common in solid organ transplant recipients, with an associated mortality of approximately 22% [12]. In particular, lung transplant recipients exhibit invasive fungal infections in up to 19% of cases, with the majority of infections caused by *A. fumigatus* [24–26].

Despite the availability and widespread use of antifungals active against *A. fumigatus* for many years, the mortality rate remains unacceptably high. The major drugs approved for the treatment of IA target components of the cell membrane: amphotericin B, and azole antifungals including voriconazole, itraconazole, posaconazole, and more recently, isavuconazole [27]. Amphotericin B is associated with severe side effects, the most notable being severe kidney and liver toxicity, and has been largely superseded by the azole antifungals, although these are also often associated with significant side effects [28,29]. Current aspergillosis management guidelines from the Infectious Diseases Society of America recommend voriconazole for primary therapy in almost all cases, and posaconazole for prophylaxis [12]. The last 15 years or so have seen an alarming increase in the incidence of azole-resistant *A. fumigatus* strains that appear to have originated both in the environment—due to the widespread use of azole antifungals in agriculture—and in the clinic. Azole resistance is a major cause of treatment failure [30–34]. In addition, as the incidence of *Aspergillus* infection increases and species identification methods advance, more related species are added to the list that cause disease. These have differing antifungal susceptibilities and have been associated with negative clinical outcomes, highlighting the need for improved diagnostic protocols and a broader range of antifungal options [6,35]. Expanding our basic knowledge of the essential biological processes of this important fungal pathogen is crucial to further advances in medical treatment, and the development of new antifungal drugs with novel targets. One process that presents as a therapeutic target for many diseases is DNA replication and repair.

Proliferating cell nuclear antigen (PCNA) tethers proteins to DNA in cellular processes including DNA replication, DNA repair, and cell cycle control [36]. It is a member of the sliding clamp family of proteins, found in all three domains of life. Despite a lack of sequence homology between them [37], all sliding clamps share a pseudo sixfold symmetry arising from six structurally similar domains [38,39], and have a high level of structural conservation. In archaea and eukaryotes, the sliding clamp is trimeric [37,39,40]. PCNA subunits from different species are able to interact to form a trimer; the PCNA subunit from *Saccharomyces pombe* is able to interact with both *Drosophila melanogaster* and human PCNA subunits,

suggesting that interactions between PCNA subunits, and important residues in the interaction interface, are evolutionarily conserved [41]. PCNA alone has no intrinsic enzymatic activity but functions by fully encircling DNA and sliding freely. Through this topological interaction it is able to control and coordinate the access of proteins to DNA, particularly at the DNA replication fork. PCNA has been described as a 'tool belt', referring to its ability to interact with numerous and varied proteins [42,43]. These proteins are interchangeable, allowing for the 'belt' to hold different 'tools' depending on its current role within the cell. The majority of proteins that interact with PCNA contain a PCNA-interacting protein (PIP)-box peptide motif [36] which binds a hydrophobic cavity present on each monomer in the trimeric ring and forms an antiparallel β-sheet with the interdomain connector loop (IDCL) of PCNA. This allows for the binding of up to three such proteins to PCNA at one time [44]. This hydrophobic PIP-box-binding pocket is present in all eukaryotic sliding clamps; a comparable pocket is also present in bacterial sliding clamps, although there are significant differences in the pockets and binding peptides between eukaryotes and bacteria [45]. The PIP-box was first defined by Warbrick *et al.*, using a yeast two-hybrid screen followed by alanine scanning to identify key residues involved in the interaction of the tumor-suppressor protein p21 with PCNA, and its ability to inhibit SV40 DNA replication. It has been suggested that drugs based on the PIP-box of p21, either as derivatives or peptide mimetics, could have therapeutic uses in down-regulating DNA replication [41,44]. Small molecules that act as competitive inhibitors of the PCNA–PIP-box interaction have also been identified and proposed as novel anticancer therapeutics [46]. In addition, small molecules [47–49], natural compound derivatives [50], peptides [51], peptide mimetics [45,52], and cyclic peptides [53] that target the function of the bacterial sliding clamp have all been presented as novel antimicrobials. Despite its integral role in cell growth and survival, PCNA has not yet been investigated as a target for novel antifungal drugs.

Here we present the first crystal structure of a sliding clamp from a pathogenic fungus. We have solved the X-ray crystal structure of PCNA from *A. fumigatus* (AfumPCNA) to 2.6Å resolution. The structure reveals a trimeric ring-shaped fold similar to other eukaryotic sliding clamps. Interestingly, the overall structure is more similar to the human sliding clamp than that from *Saccharomyces cerevisiae* (yPCNA). Fluorescence polarization experiments with AfumPCNA and the PIP-box from human p21 demonstrate a K_d of 3 μM, providing evidence that AfumPCNA interacts with proteins at the replication fork though a conserved PIP-box mechanism similar to the human system, rather than the prokaryotic systems which do not employ use of the PIP-box system for protein–protein interactions. We have employed molecular dynamics simulations with AfumPCNA and the human p21 PIP-box to better understand the interactions. This revealed that the secondary structure of the PIP-box motif is similar in its interactions with AfumPCNA as with hPCNA. However, differences in the 3_{10} helix interaction cavity and the IDCL as well as a decreased ability to form a beta-strand conformation are likely to contribute to the lower affinity of p21 for AfumPCNA rather than hPCNA.

Results

Identification of PCNA from *Aspergillus fumigatus*

The *A. fumigatus* protein sequence was identified using the Aspergillus Genome Database and confirmed by means of multiple sequence alignment with PCNA from other species, as shown in Fig. 1. Analysis of the amino acid sequence of PCNA from several different sequences, as shown in Table 1, reveals that PCNA from *A. fumigatus* is most similar to *A. thaliana* (56.9%) and *D. melanogaster* (56.6%), followed very closely by human PCNA (53.9%). It is interesting to note that, in terms of PCNA sequence, the fungus *A. fumigatus* is more closely related to the higher order eukaryotes than to the yeast *S. cerevisiae* (49.6%). Previous studies have shown evolutionary drift of PCNA between the yeast and pathogenic fungi such as AfumPCNA. In eukaryotic species, the N- and C-terminal domains of each subunit are connected via an extended loop (residues 118 to 134) known as the interdomain connector loop (IDCL), which is necessary for interaction with the PIP-box-containing peptides [44]. Evolutionary drift among the PCNA molecules of Fungi is perhaps most notable in the IDCL. Zamir *et al.* [54] compared the IDCL of PCNA from numerous different fungal species and found that variation in just 4 of the 12 IDCL residues analyzed appeared to allow segregation of the different species into two distinct groups, as indicated in Fig. 1. Chimera-based protein–protein binding experiments in which the IDCL of fungal species were interchanged among the PCNA molecules and affinity for PIP-box-containing proteins was measured, demonstrated that

the IDCLs of the two groups of fungi could not be interchanged without significant loss of affinity. IDCL sequences from Group 1 fungal species (including *S. cerevisiae*) were incompatible with IDCL sequences from Group II species (including *A. fumigatus*) suggesting large evolutionary drift among the fungal species. However, to date no structural information has been available to explain these differences.

X-ray crystal structure of PCNA from *Aspergillus fumigatus*

To gain a better understanding of AfumPCNA structure and mechanism, AfumPCNA was purified and crystallized in space group $P2_1$. The AfumPCNA structure was solved to a resolution of 2.6Å by means of molecular replacement. Data processing and

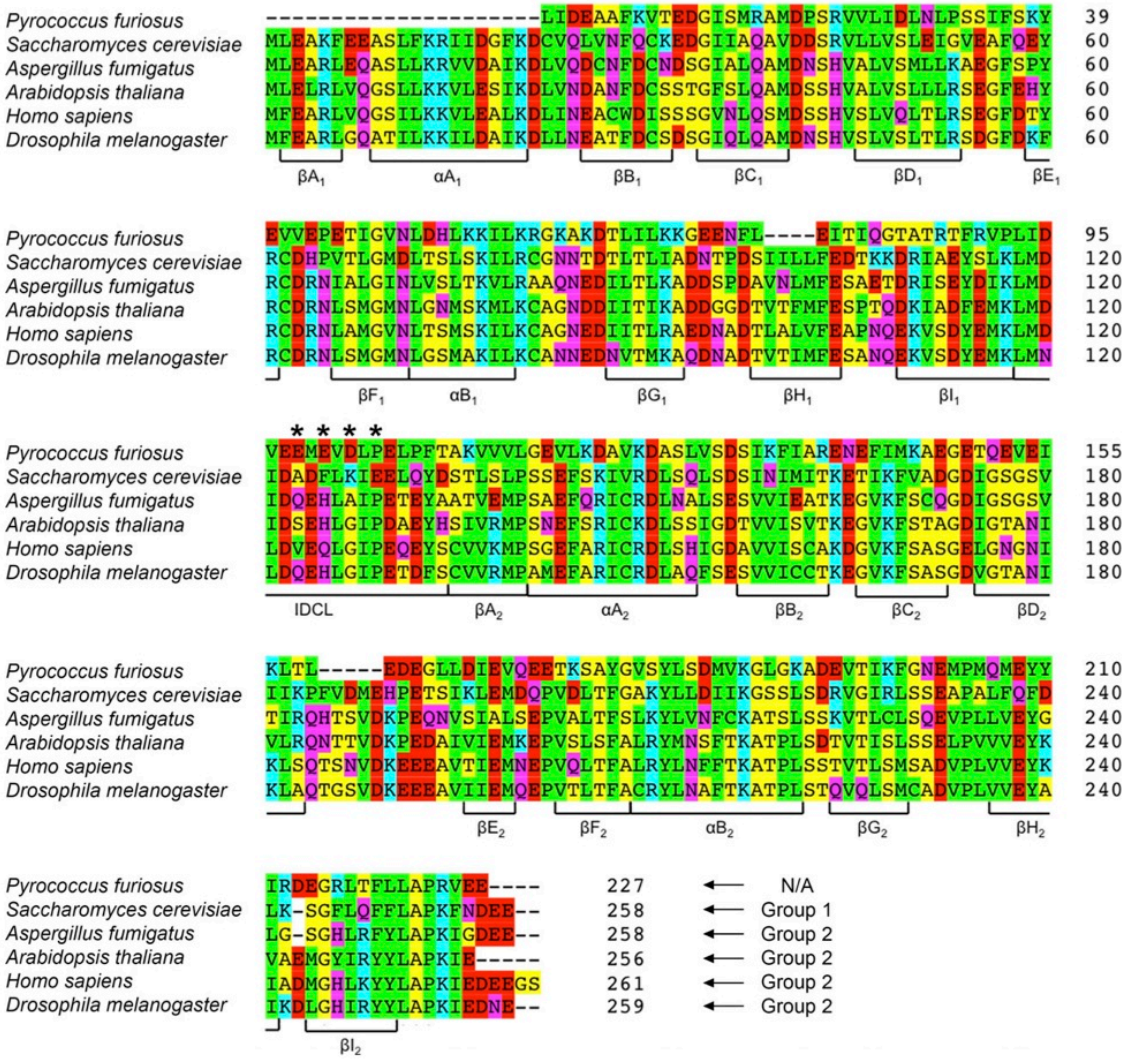

Fig. 1. Sequence alignment of the PCNA protein sequence from six different organisms. Residues are colored according to the following scheme [54]; nonpolar residues are yellow (GAST), polar residues are magenta (NQH), hydrophobic residues are green (CVILPFYMW), negatively charged residues are red (DE), positively charged residues are blue (KR). α-helices and β-sheets are labeled as they were described for the structure of *Saccharomyces cerevisiae* PCNA [37]. The IDCL is labeled as defined by Gulbis *et al.* [44]. The four residues within the IDCL identified by Zamir *et al.* [54] as segregating fungal species into two distinct groups are marked above by asterisks. The IDCL from *Pyrococcus furiosus* does not clearly belong to either group, as indicated.

Table 1. Percent identity (PIM scores) for PCNA amino acid sequence compared between six different organisms.

	Pyrococcus furiosus	*Saccharomyces cerevisiae*	*Aspergillus fumigatus*	*Arabidopsis thaliana*	Human	*Drosophila melanogaster*
P. furiosus	100.00	26.11	23.45	24.34	25.99	25.55
S. cerevisiae	26.11	100.00	49.61	40.00	35.66	36.05
A. fumigatus	23.45	49.61	100.00	56.86	53.88	56.59
A. thaliana	24.34	40.00	56.86	100.00	65.23	62.11
Human	25.99	35.66	53.88	65.23	100.00	71.04
D. melanogaster	25.55	36.05	56.59	62.11	71.04	100.00

Table 2. Data collection and refinement statistics.

	AfumPCNA[a]
Data collection	
Space group	P 2_1
Cell dimensions	
a, *b*, *c* (Å)	56.95, 103.37, 79.2
α, β, γ (°)	90.00, 96.60, 90.00
Resolution (Å)	78.68–2.60 (2.72–2.60)[b]
R_{merge}	0.189 (2.018)
R_{pim}	0.076 (0.837)
CC(1/2)	0.994 (0.330)
$I / \sigma I$	7.2 (1.0)
Completeness (%)	99.5 (96.7)
Redundancy	7.1 (6.6)
Refinement	
Resolution (Å)	44.02–2.602
No. reflections	28 050
R_{work} / R_{free}	0.1970 / 0.2571
No. atoms	
Protein	5634
Water	205
B-factors	
Protein	74
Water	61
RMS deviations	
Bond lengths (Å)	0.004
Bond angles (°)	0.978

[a]Data collected from 1 crystal.
[b]Values in parentheses are for highest-resolution shell.

refinement statistics can be found in Table 2 and a reduced model bias stereo figure of representative electron density can be seen in Fig. 2. The asymmetric unit is composed of three subunits that form a ring-shaped trimer that is representative of DNA sliding clamps from other species (Fig. 3). Subunits of the trimer show high structural similarity, with RMSD values between subunits ranging from 0.89Å to 0.97Å (calculated over 254 Cα atoms) and total surface areas of 12375 Å^2, 12297 Å^2, and 12446 Å^2, giving an average surface area per subunit of 12373 Å^2. Subunits are composed of four α-helices and 18 β-strands arranged into two domains of nearly identical topology, connected by an IDCL (Fig. 3A). Each domain consists of two adjacent α-helices covered on one side by two antiparallel β-sheets of four or five strands each. Each β-sheet is continuous with the β-sheet of the adjacent domain, such that six, nine-stranded β-sheets surround the trimeric ring: three cross the domain interface within each subunit and three cross the interface between each subunit (Fig. 3B). The AfumPCNA trimer therefore has a pseudo sixfold rotational symmetry, with the axis of symmetry running through the center of the ring. The subunits pack to form the trimer leaving a central cavity of approximately 30Å—a diameter which would allow nonspecific interactions with DNA.

Atomic interactions of the AfumPCNA subunit interface

Proliferating cell nuclear antigen oligomerizes via an interface that is conserved among all three subunit–subunit interfaces (Figs 3B and 4). The subunit–subunit interfaces involve the interaction of βI1 and αB1 of the N-terminal domain with βD2 and αA2 of the C-terminal domain. The peripheral β-strands of each domain (βI1 and βD2) form an antiparallel β-sheet such that the β-sheet is continuous across the subunit interface. For the following discussion, we refer to the interface between subunits A and C, unless otherwise specified.

The interface surface area is 687.2 Å^2; similar to the corresponding interfaces of both hPCNA and yPCNA (697.6 Å^2 and 654.1 Å^2, respectively), and involving 11 hydrogen bonds (Fig. 4A) and one salt bridge (Fig. 4B). Eight hydrogen bonds between peptide backbone atoms of residues 109 to 117 (βI1) and 175 to 183 (βD2) have distances ranging from 2.28Å to 3.40Å, and define the antiparallel β-sheet (Fig. 4A). The remaining three hydrogen bonds are weak (distance > 3.6Å) and are between Lys77 (NZ) and Ala153 (O), Thr108 (N) and Gln193 (OE1), and Asp115 (OD2) and Ser177 (OG). Arg110, contained in

βI1, forms a salt bridge with Glu143 from αA2 (Fig. 4B). The core of the interface is hydrophobic, centered around Tyr114, and is composed of αB1 residues Val78 and Ala81, βI1 residues Tyr114 and Ile116, αA2 residues Leu151 and Leu154, and βD2 residues Ile175 and Val180 (Fig. 4B).

The subunit interface is highly conserved among species, with comparisons to hPCNA and yPCNA revealing very similar surface areas and interacting residues. All of the hydrophobic residues at the interface core are conserved in human and yeast PCNA, and each interface involves a similar number of hydrogen bonds. The most conspicuous nonconservative substitution is at position 153 of αA2, which is an alanine, histidine, or glutamine in AfumPCNA, hPCNA, and yPCNA, respectively. However, this substitution for bulkier residues in both hPCNA and yPCNA appears to have very little effect on the conformation of other interface residues, but may contribute to a slightly larger interaction surface. The only other significant nonconservative substitution at the subunit interface is a glutamine residue in AfumPCNA (Gln83), which is glycine in hPCNA. This permits the side chain of Arg146, which points to solvent in AfumPCNA (Fig. 4B), to contact αB1 of the opposing subunit of hPCNA, forming a hydrogen bond with Lys80 (O) (2.97Å). The hPCNA interface includes a salt bridge at the end of the β-strand, involving Lys117 and Glu174, which is absent in both AfumPCNA and yPCNA. Lys117 is conserved in fungal PCNA, but residue 174 is an aspartate residue, which lacks the conformational flexibility required to form an electrostatic interaction with Lys117. The salt bridge between residues 110 and 143 is conserved in AfumPCNA, with the variation that 110 is an arginine rather that a lysine. In yPCNA, Arg110 also forms a salt bridge, but partners with Asp150 rather than Glu143. Interestingly, both Glu143 and Asp150 are conserved and in similar positions in both fungal PCNA structures, suggesting that Arg110 may be able to form a salt bridge with either of these residues. This is confirmed in AfumPCNA upon inspection of the interface between subunits B and C, where indeed an

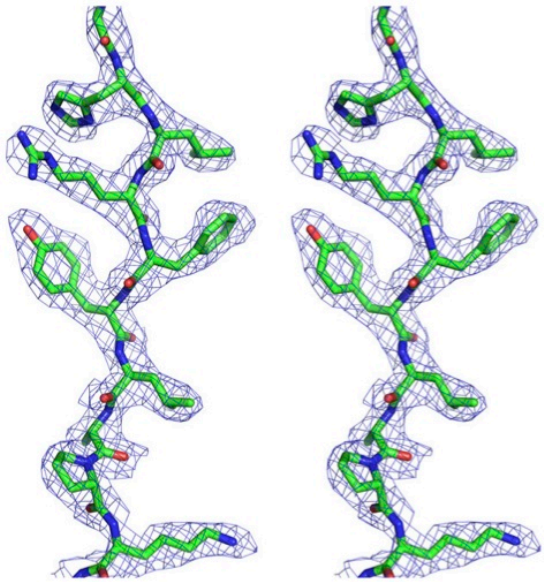

Fig. 2. Representative electron density. Wall-eye stereo image of a reduced model bias feature-enhanced map [68] contoured at 1.5σ encompassing residues Gly244 to Lys253 of AfumPCNA.

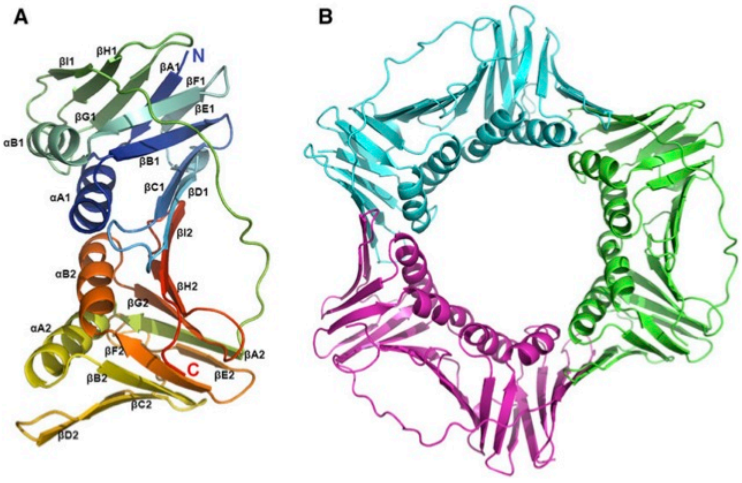

Fig. 3. Structure of the AfumPCNA. Depicted are ribbon diagrams of AfumPCNA. (A) Single subunit of AfumPCNA. (B) AfumPCNA trimer colored by subunit.

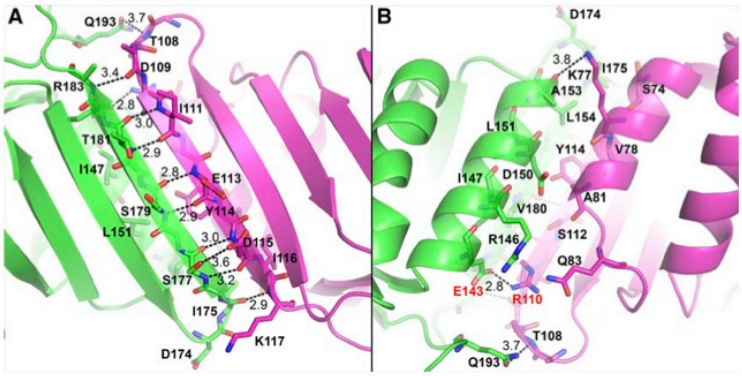

Fig. 4. Subunit–subunit interface of AfumPCNA. AfumPCNA is shown in ribbons with interacting residues shown as sticks. Subunit A is shown in magenta, while subunit B is shown in green. (A) Subunit–subunit interface of the β-sheet region. (B) Subunit–subunit interface of the α-helix region.

Arg110–Asp150 salt bridge is present, rather than the Arg110–Glu143 salt bridge of the interface between subunits A and C. Furthermore, at the remaining interface (A–B), the side chain of Arg110 is disordered in the electron density, consistent with conformational flexibility at this position. In contrast, the shorter side chain of Lys110 of hPCNA precludes it from forming a salt bridge with Asp150, limiting interaction to Glu143.

Comparison of AfumPCNA to the yeast and human PCNA

AfumPCNA shows high overall structural similarity to both the human and yeast PCNA crystal structures (Fig. 5), with average RMSD values across all subunits of 1.51Å and 1.53Å, respectively. Despite this, variation in the sequence of the IDCL results in structural changes that may affect interactions with binding partners. Interestingly, the IDCL of AfumPCNA showed more similarity to the human IDCL rather than the yeast IDCL, implying the AfumPCNA surface may interact with interacting partners by means of a human type PIP-box. The IDCL (residues 118–134) stretches across the outside of seven of the nine strands of the core β-sheet in each subunit (Fig. 6A). It is stabilized by a number of interactions with both backbone atoms and side chains protruding from the underlying sheet, including hydrogen bonds between Met119 (N) and Gly69 (O) (2.94Å), Gln123 (NE2) and Asp29 (OD2) (2.70Å), and Leu126 (O) and Gln38 (NE2) (3.32Å). The hydroxyl group of Tyr133 also forms two separate water-mediated hydrogen bonds with Pro234 (O) and Try249 (OH). In addition, Ile128 packs against hydrophobic residues Leu47 and Tyr249, and Tyr133 sits in a hydrophobic pocket formed by Cys228, Val233, Leu236, and Tyr249.

These interactions are conserved in hPCNA, with the notable exception of Gln123. A valine is present at

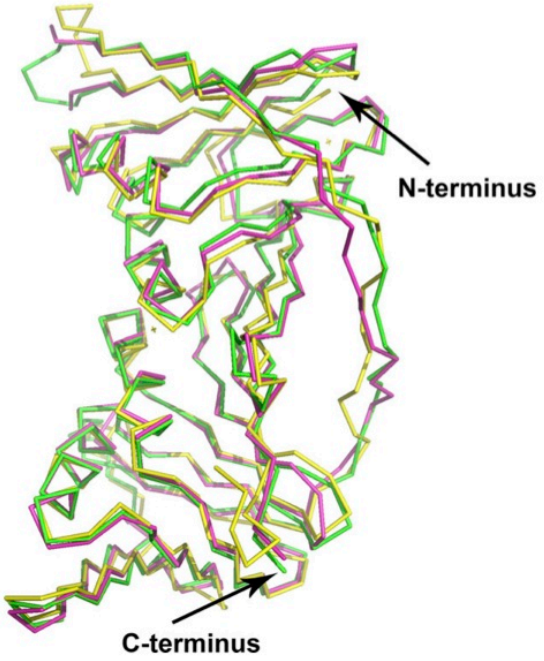

Fig. 5. Superimposition of PCNA subunits from different species. PCNA subunits are depicted in wire format. AfumPCNA is depicted in green (5TUP), hPCNA is depicted in magenta (PDB: 1AXC), and yPCNA is depicted in yellow (PDB: 1PLQ) [37,44].

this position of the IDCL in hPCNA, precluding any hydrogen bonding interaction with Asp29. This aspartate residue has been shown to be involved in binding p21 (and other PIP-box peptides with antiparallel β-strand interaction) [44,55]. Therefore, the sequestering of this hydrogen bond acceptor by Gln123 in AfumPCNA may result in differences in binding specificity and affinity for PIP-box-containing peptides. This difference at position 123 is accompanied by the most evident conformational difference in the IDCL

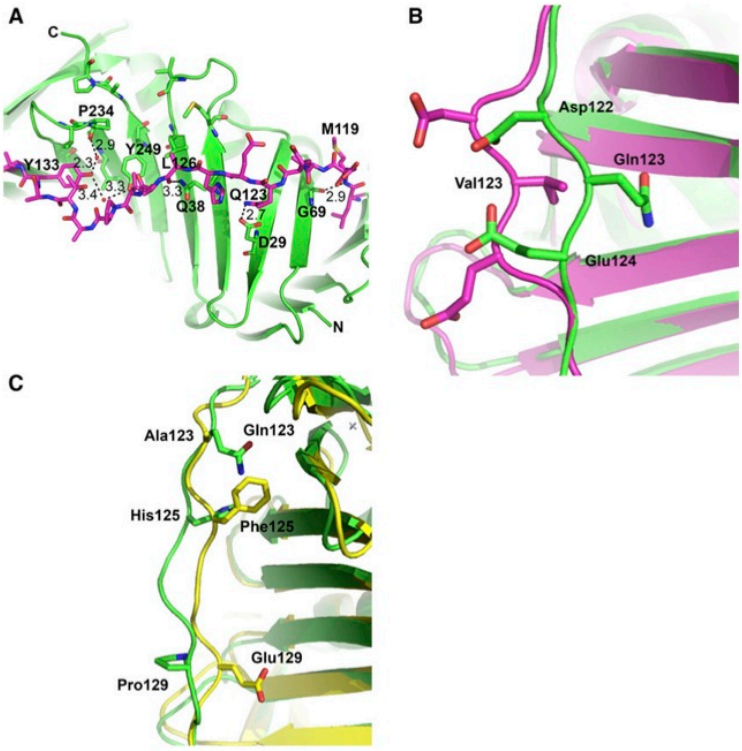

Fig. 6. Details of the AfumPCNA IDCL. (A) Interactions of the AfumPCNA IDCL. AfumPCNA is shown in green ribbons with the IDCL highlighted as magenta sticks. (B) Superimposition of AfumPCNA (green) with unliganded hPCNA (magenta; PDB: 1W60) [56]. (C) Superimposition of AfumPCNA (green) with yPCNA (yellow; PDB: 1PLQ) [37].

between human and AfumPCNA; relative to Val123 of unliganded hPCNA (PDB: 1W60) [56], Gln123(Cα) is shifted 4.14Å toward the surface of PCNA and results in a concomitant shift of adjacent residues Asp122 and Glu124 in the same direction (Fig. 6B).

Inspection of the IDCL from *S. cerevisiae* PCNA (yPCNA) [37] reveals conformational differences with AfumPCNA (Fig. 6C). These differences are due to substitutions at His125 and Pro129, two of the four IDCL residue positions that have been used to separate fungal species into two separate evolutionary families (Fig. 1) [54]. However, this region of the yPCNA structure is involved in a number of crystal contacts, which may also contribute to conformational differences in the IDCL. Interestingly, despite the presence of a hydrophobic residue at position Ala123, similar to hPCNA, the position of the IDCL in this region (122 to 124) is more similar to that of AfumPCNA, which contains a glutamine residue at this position (Gln123), as shown in Fig. 6C. Phe125 of yPCNA participates in hydrophobic interactions that have a similar effect on the position of IDCL residues 122 to 124 as the hydrogen bond between the side chains of Gln123 and Asp29 of AfumPCNA. The side chain of Phe125 packs onto the underlying β-sheet via hydrophobic interaction with Ile36 (Ala36 in AfumPCNA), drawing residues 124 to 127 of the IDCL an average of ~ 1.1Å closer to the underlying β-sheet (Fig. 6C). Phe125 of yPCNA partially occupies the space of Asp29 of both AfumPCNA and hPCNA. This is reflected by the conformation of the side chain of Gln29 of yPCNA, which is shifted ~ 3.8 Å away from the IDCL backbone relative to Asp29 of AfumPCNA, potentially precluding it from acting as a hydrogen-bonding partner for PIP-box-containing peptides. The proline at position 129 in AfumPCNA is Glu129 in yPCNA (Fig. 6C). This substitution induces a different conformation of the IDCL and markedly alters the position of this residue, allowing it to pack ~ 3.7Å closer to the underlying β-sheet, facilitated by an additional weak hydrogen bond between Glu129 (OE1) and Gln247 (NE2) (3.5Å). This increased flexibility also allows Glu130 to occupy the space of Gln131 in hPCNA, which has been shown to form a hydrogen bond with the Tyr151 side chain hydroxyl group of the p21 peptide [44]. AfumPCNA contains a Thr (Thr131) at this position, a considerably shorter side chain which would require extension of PCNA toward the PIP-box for hydrogen bond formation as compared to the human structure.

Proliferating cell nuclear antigen residues (AfumPCNA residue numbers) Met40, Val45, Leu47, Leu126, Ile128, Pro129, Tyr133, Pro234, Tyr249, Ala251, and Pro252 form a hydrophobic pocket that is 'plugged' by the conserved 3_{10} helix of the PIP-box. This interaction has been shown to be essential for high-affinity binding of PIP-box-containing peptides [55]. Strikingly, these residues are 100% conserved between hPCNA and AfumPCNA highlighting the conserved nature of this interaction. Comparison of these with the hydrophobic pocket of yPCNA reveals only minor differences, with the only nonconserved substitution being position 129 in the IDCL, as previously mentioned.

Proliferating cell nuclear antigen residues of the C terminus that have been shown to interact with PIP-box peptides include Ala252, Pro253, and Ile255 of hPCNA and Ala251, Pro252, Lys253, and Phe254 of yPCNA [37,44]. These are conserved in AfumPCNA, suggesting their importance in mediating PCNA–PIP interactions across fungi and mammals. The six C-terminal residues of hPCNA (256 to 261) are disordered in the PCNA:p21-peptide structure. This includes four charged residues which have been suggested to closely associate with the charged residues at the N terminus of the p21 peptide via poorly ordered ionic interactions. The final four residues of AfumPCNA and yPCNA (both 255 to 258) are undefined in the electron density of these structures and include three charged residues, one aspartate and two glutamine residues, suggesting the conservation of this poorly ordered ionic interaction with binding peptides.

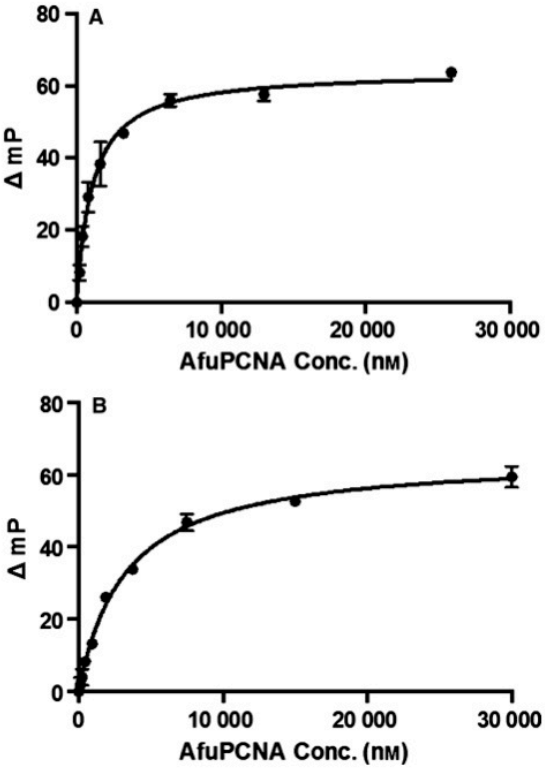

Fig. 7. Fluorescence polarization binding curves. Determination of the binding affinity of AfuPCNA for N-terminally FITC-labeled human p21 peptide in (A) 20 mM Tris with 10% glycerol and (B) PBS, pH 7.4 (full details of buffer conditions are giving in the Materials and methods). Curves represent single experiments, where each data point is the mean of triplicate samples and error bars represent the standard deviation. Each experiment was repeated three times.

AfumPCNA binds p21 peptide with high affinity

To determine if the AfumPCNA interacts with its partners by means of a PIP-box, we determined the affinity of AfumPCNA for a peptide derived from the cyclin-dependent kinase inhibitor protein p21, previously shown to have the highest known affinity for hPCNA [55]. AfumPCNA binding to a canonical human p21 PIP-box motif was determined by incubating FITC-labeled p21 peptide (N-139 GRKRRQTSM TDFYHSKRRLIFS 160-C) with increasing concentrations of AfumPCNA, and measuring the changes in fluorescence polarization. Figure 7 contains the dose–response curves for the fluorescence binding. A K_d value of 3.1 ± 0.1 μM was determined in PBS using similar conditions to Bozza *et al.* [57] (Fig. 7B). These authors determined the affinity of hPCNA to the same peptide in these conditions to be 342 nM. Thus, using similar buffer conditions, the p21 interaction for hPCNA is only 10-fold higher in affinity than the interaction with AfumPCNA. In experiments using Tris buffer (Fig. 7A), the K_d was determined to be 1.0 ± 0.1 μM, indicating that removal of salt strengthens the AfumPCNA/p21 interaction. Electrostatic contacts play a role in hPCNA/p21 complex formation, with salt bridges stabilizing the intermolecular β-sheet (hPCNA Asp29 to p21 Arg154, and hPCNA residues Asp122 and Glu124, to p21 Arg155). These hPCNA residues are conserved in AfumPCNA suggesting the intermolecular electrostatic interactions may be maintained, consistent with the FP data.

Deciphering the interaction of p21 with AfumPCNA by molecular dynamics simulation

Given our finding that AfumPCNA interacts with the human p21 peptide with high affinity, we performed

molecular dynamics simulations to better define the interactions of AfumPCNA with p21 as well as identify the structural basis for the lower affinity interaction with AfumPCNA versus hPCNA. The molecular dynamics simulation was carried out for a total of 50 ns using the AfumPCNA trimer bound to one p21 peptide per subunit. The simulation was stable over the entire time frame as indicated by the RMSD versus time (plotted by secondary structure) depicted in Fig. 8, and the overall structural trajectory is shown in Fig. 9. Two movies of the simulation can be found in the Supporting Information section (Movies S1 and S2).

The molecular dynamics simulation revealed that, although the core binding mode of the p21 peptide to PCNA is largely conserved between human and *A. fumigatus*, a number of differences are present that may contribute to a lower peptide-protein affinity for the *A. fumigatus* protein. The interaction of p21 with AfumPCNA, much like with hPCNA, can be conceptually divided into interactions of the p21 N terminus, 3_{10} helix, and C terminus, the latter of which forms an antiparallel β-sheet with the IDCL of PCNA.

The interaction of the p21 peptide N-terminal residues with the AfumPCNA C terminus was maintained throughout the simulation. Similar to the interactions of p21 with hPCNA, interactions of the N terminus of p21 include a system of hydrogen bonds: a hydrogen bond from p21 Arg143 main chain oxygen atom to Ile255 main chain nitrogen atom and from Gln144 side chain to Ser44 main chain oxygen atom (Fig. 10A). Unlike the p21 interaction with hPCNA, the side chain of Thr145 does not make a hydrogen bond with AfumPCNA and is instead rotated away from the surface of AfumPCNA making no intermolecular contacts by means of the side chain atoms.

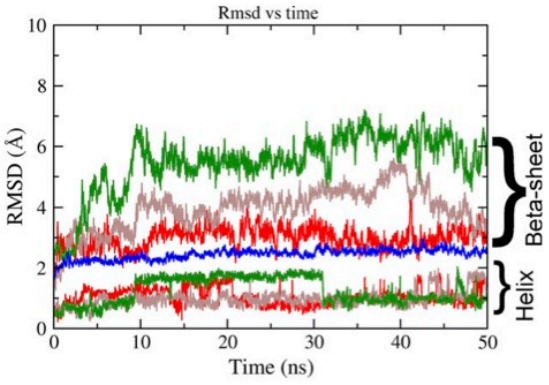

Fig. 8. Molecular dynamics RMSD versus time binned by secondary structure. AfumPCNA is shown as blue, while the p21 peptides are shown in green, red, and brown.

The p21 3_{10} helix that plugs a hydrophobic pocket on PCNA was stable throughout the duration of the simulation, reflecting the high conservation of residues that form the pocket (including residues Met40, Val45, Leu47, Leu126, Ile128, Pro129, Tyr133, Pro234, Tyr249, Ala251, and Pro252). Tyr151 is one of the key residues for high-affinity interaction of p21 with hPCNA [58], due to the side chain hydroxyl proton forming a hydrogen bond to the side chain nitrogen atom of Gln131. This interaction was predicted to be lost in AfumPCNA, due to the substitution of Gln for Thr at this position (Thr131 of AfumPCNA). The simulations showed this held true for two of the three peptide–PCNA interactions, but interestingly, a hydrogen bond between Thr131 (side chain hydroxyl) and p21 peptide Tyr151 (side chain hydroxyl) is present in the remaining peptide interaction, but requires Tyr151 to shift approximately 2.7Å toward the core of the protein. Of the three p21 peptides bound to the PCNA trimer, the peptide which forms the hydrogen bond between Thr131 and Tyr151 also adheres to a well-formed antiparallel β-strand, while the two peptides with unstable β-strand formation are correlated with a loss of hydrogen bonding capacity between these residues (Fig. 10B). From this it can be deduced that at least part of the lower affinity of p21 for AfumPCNA can be attributed to the lessened ability of p21 to hydrogen bond with AfumPCNA residue Thr131, which is intricately linked to the β-strand conformation of the peptide. In addition, AfumPCNA contains a larger and less hydrophobic surface cavity (124 $Å^3$ in hPCNA/p21 versus 235 $Å^3$ in AfumPCNA/p21) capable of promoting interaction with the 3_{10} helix (Fig. 10C,D); both of these effects can partly be attributed to the presence of Thr131 in the AfumPCNA structure rather than Gln131 as seen in the hPCNA structure.

The antiparallel β-sheet formed between the p21 peptide C terminus and residues 121–127 of the AfumPCNA IDCL is maintained throughout the simulation for one of the three peptides, partially maintained for another, but has completely dissociated in the case of the remaining peptide (Figs 9 and 10B). The formation of the β-strand conformation of p21 in the AfumPCNA-bound simulation only occurs with significant rearrangement of the IDCL as compared to the human p21-bound IDCL. The disruption of this interaction is consistent with the observation that Asp123 of the IDCL sequesters the electrostatic interaction to Arg156 in the AfumPCNA crystal structure, precluding the formation of hydrogen bonds to Asp29 from Arg156 of p21 that aid in anchoring the C-terminal half of the peptide to the surface of hPCNA

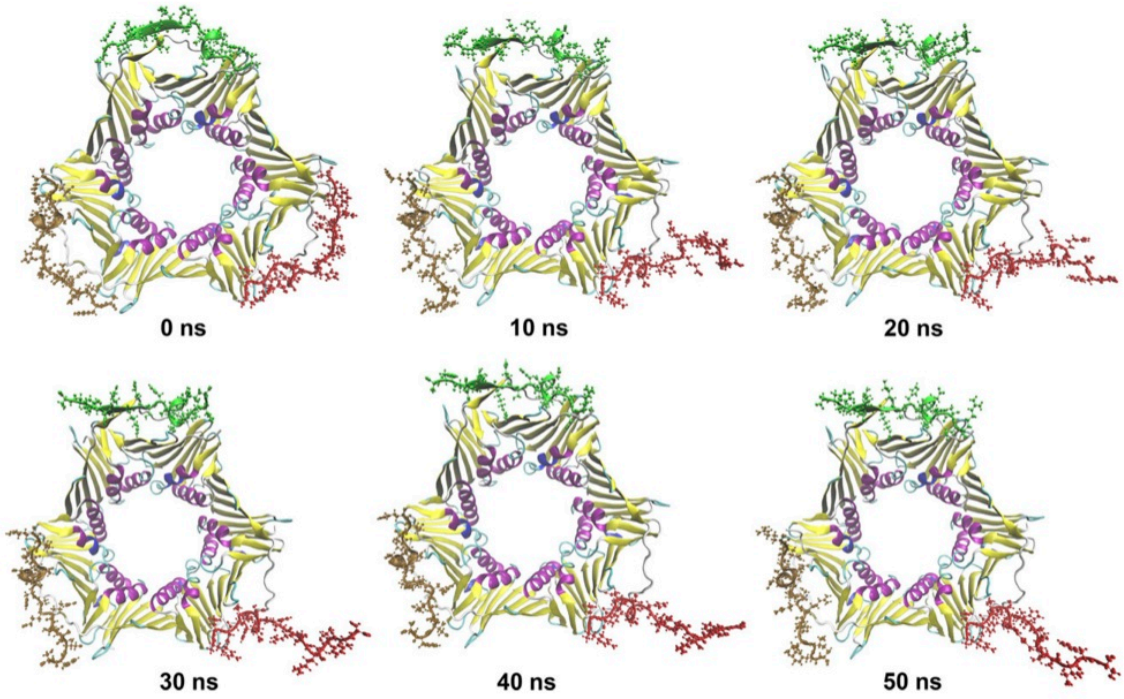

Fig. 9. Molecular dynamics simulation trajectory over time at 10-ns intervals. Displayed is a ribbon diagram of AfumPCNA (colored by secondary structure) with p21 peptides shown as sticks (green, red, and brown).

(Fig. 10E). Furthermore, His125 of AfumPCNA obstructs β-sheet by formation of a favorable side chain hydrogen bond with the His152 side chain of p21, forcing the peptide in a conformation that is too distant from the surface of AfumPCNA to form the tight hydrogen bonds of a β-sheet as seen in the human structure (Fig. 10E).

It is interesting to note that, while the interaction between the central 3_{10}-helical plug and the AfumPCNA hydrophobic pocket is very stable, the polar interactions between the N-terminal and C-terminal peptide residues and the PCNA C terminus and IDCL, respectively, appear to be mutually exclusive. This is shown by the observation that the loss of intermolecular hydrogen bonding at the C-terminal half of the p21 peptide is accompanied by an increase in the number of hydrogen bonds between the N terminus of the peptide and C terminus of AfumPCNA (Fig. 11C). In fact, the only peptide for which the conformation of the peptide's N terminus and 3_{10} helix (residues 143 to 151) is almost identical to that of the hPCNA–p21 peptide structure is the one that has completely lost the β-sheet interaction at the C-terminal end of the peptide. On the other hand, extensive hydrogen bonding involving the C-terminal region of the peptide is accompanied by a decrease in hydrogen bonding at the N terminus of the peptide (Fig. 11A,B). Regarding the peptide for which the β-strand in the C-terminal region of the peptide is well maintained, the 3_{10} helix is forced into a more α-helical conformation by interaction with Thr131; a peptide conformation which favors C-terminal β-strand formation, but disfavors interactions between the N-terminal region and the C terminus of AfumPCNA.

Discussion

Here we present the first crystal structure of PCNA from *A. fumigatus* as well as the first crystal structure of PCNA from a pathogenic fungus. Interestingly, the structure of the AfumPCNA is more structurally related to human PCNA than the previously reported *S. cerevisiae* PCNA. Furthermore, we also demonstrated that AfumPCNA interacts with high affinity with a human PIP-box, implying that PCNA-interacting proteins from the pathogen *A. fumigatus* are likely to interact with AfumPCNA by means of a conserved PIP-box similar to that of the human sequence. Given that p21 interacts with AfumPCNA with 10-fold lower affinity than its human counterpart, we performed

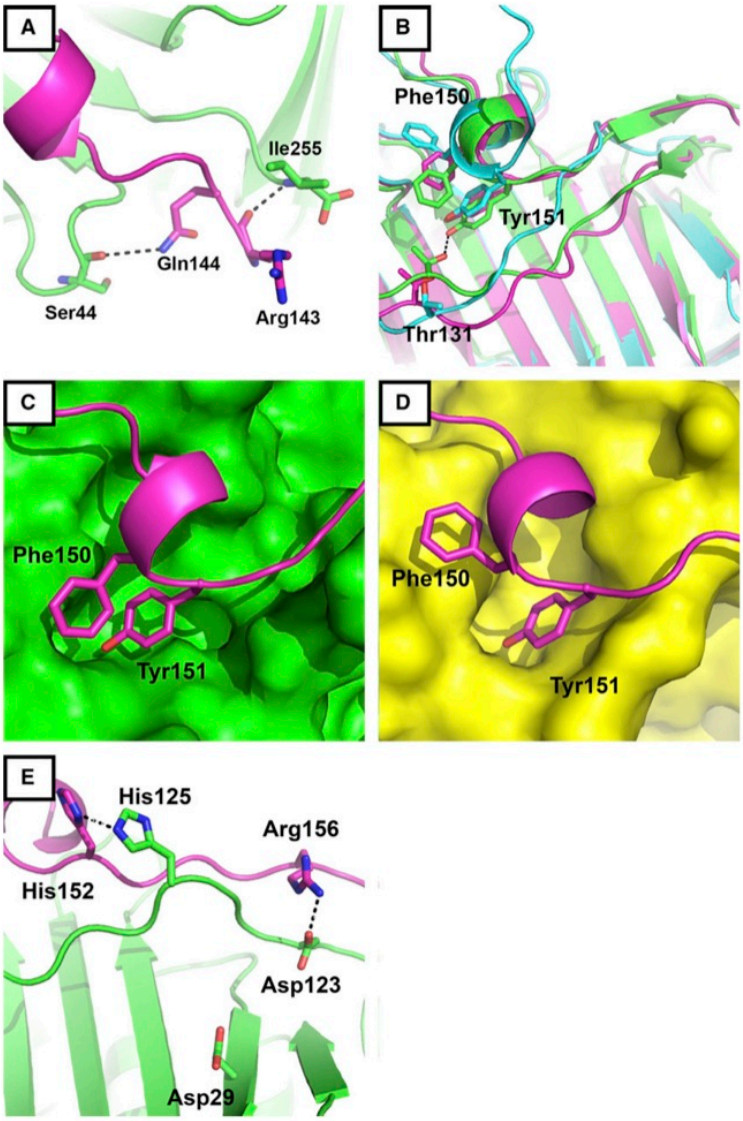

Fig. 10. Interactions of AfumPCNA with the p21 peptide as determined by molecular dynamics. (A) Interactions of the p21 N terminus (magenta) with PCNA (green). (B) Interactions of the conserved Tyr151 of p21 with Thr131 of AfumPCNA. Shown is a superimposition of each PCNA subunit (differentiated by color: cyan, green, and magenta) bound to p21. (C) Surface representation of AfumPCNA (green) bound to p21 (magenta sticks). (D) Surface representation of hPCNA (yellow) [44] bound to p21 (magenta) (PDB: 1AXC). (E) Interactions of the C terminus of p21 (magenta) with AfumPCNA (green).

molecular dynamics simulations to uncover fundamental structural differences in the AfumPCNA surface that can account for these differences in affinity. Our MD revealed differences in the IDCL of AfumPCNA that likely contribute to this difference in affinity, including residues Asp29, His125, Asp123, and Thr131.

Previous studies focusing on human PCNA have suggested that a key factor for determining the affinity of a protein for PCNA is the primary sequence of its PIP-box [55,59]. Therefore, further investigation into native partners of *A. fumigatus* PCNA, with a focus on their PIP-box sequences, could uncover determinants of high-affinity binding. It has also been suggested that, evolutionarily speaking, natural PCNA-interacting proteins are not optimized for high affinity, but rather that affinity is finely tuned to allow for rapid and appropriate exchange of partners to allow the cell to adapt promptly to changing environmental conditions [55,60]. This affords the possibility that artificial PIP-box sequences could be designed that have a greater affinity for PCNA than the highest affinity native PIP-box-containing proteins. Indeed, using the p21 PIP-box sequence to

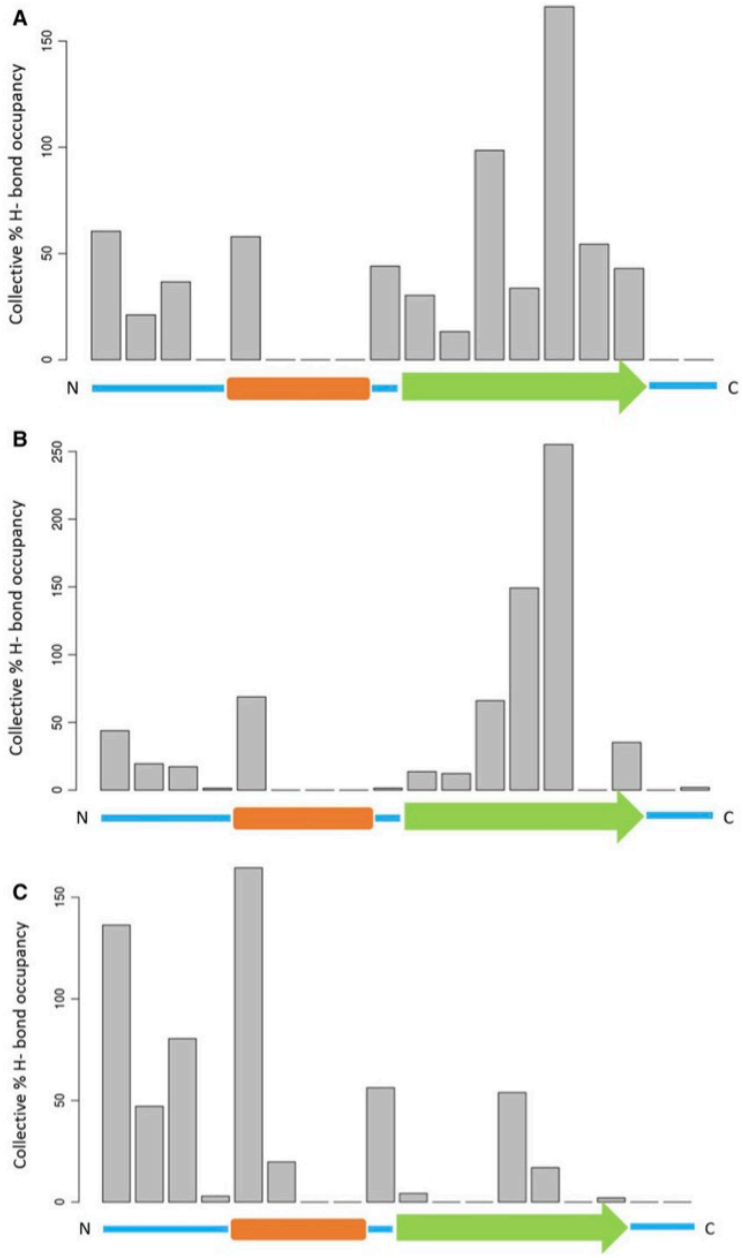

Fig. 11. Frequency of intermolecular hydrogen bonds between residues of the p21 peptide and AfumPCNA during the MD trajectory. 'Collective % H-bond occupancy' (*y*-axis) denotes the proportion of time that a hydrogen bond exists between a specific p21 peptide residue and PCNA over the course of the MD simulation. Note that this value may be > 100% if there are multiple hydrogen bond donors or acceptors implicated in either the peptide residue or PCNA. (A) Hydrogen bonds of subunit A. (B) Hydrogen bonds of subunit B. (C) Hydrogen bonds of subunit C.

guide the design of high-affinity peptide mimetics that target hPCNA for the treatment of cancer is the subject of ongoing investigation. In the same way, we expect that the details of the PCNA–peptide interaction interface presented in the current study will be useful for guiding the synthesis of high-affinity peptides which could, in turn, guide the design of stable, high-affinity peptide mimetics that bind tightly to AfumPCNA, halting DNA replication, thereby preventing fungal cell growth. In addition, the differences between the peptide interaction surfaces of hPCNA and AfumPCNA highlighted here may afford specificity of antifungal peptides toward the fungal PCNA over its human homolog.

Materials and methods

Protein expression and purification

The AfumPCNA coding sequence was PCR amplified from *A. fumigatus* strain af293 cDNA using primers (a) 5′-CCC GGGCATATGTTGGAAGCACGACTAG-3′ and (b) 5′-GG GCCCGGATCCTTACTCCTCATCTCCGATC-3′ and cloned into the pMCSG19 vector using BamHI and NdeI restriction sites. Sequencing revealed that the sequence coding for AfumPCNA included 117 extra nucleotides at the 5′ end when compared to the sequence deposited in the NCBI database (Accession XM_745146) [61] but was identical to the ORF sequence available at www.aspergillusgenome.org (afu1g04900) (accessed 23 May 2016), indicating an error in the original annotation. AfumPCNA was overexpressed in *Escherichia coli* BL21(DE3) shake-flask culture by the addition of 0.5 mM IPTG when the culture reached log-phase, and incubated at 16 °C for approximately 18 h. Cell pellets were resuspended in 20 mM Tris pH 7.5, 20 mM NaCl, 0.5 mM EDTA, 2 mM DTT, and stored at −80 °C until required.

Cells were lysed by high-pressure disruption and insoluble debris was removed by centrifugation before purification of the protein from the crude lysate, as follows. Lysate was loaded onto a 5 mL Unosphere Q column (Bio-Rad, Hercules, CA, USA) and eluted using a linear NaCl gradient (20 to 700 mM). Fractions containing AfumPCNA were pooled and brought up to 1.5M $(NH_4)_2SO_4$ by the dropwise addition of 3 M $(NH_4)_2SO_4$ before incubating overnight at 4 °C with gentle stirring. Precipitate was then cleared by centrifugation; supernatant was loaded onto a 5 mL HiTrap Phenyl FF column (GE) and eluted using a reverse linear salt gradient (1.5 to 0M $(NH_4)_2SO_4$, 20 to 0 mM NaCl). AfumPCNA fractions were pooled and dialyzed with 20 mM Tris pH 7.5, 50 mM NaCl, and 2 mM DTT overnight at 4 °C. Dialyzed protein was concentrated to 10 mL and passed through a HiPrep Sephacryl 26/60 S-300 column (GE) equilibrated in 20 mM Tris pH 7.5, 50 mM NaCl, and 2 mM DTT. AfumPCNA fractions were then pooled and dialyzed against 20 mM Tris pH 7.5, 20 mM NaCl, and 2 mM DTT overnight at 4 °C. Dialyzed protein was loaded onto a 1 mL Enrich Q column (Bio-Rad) and eluted using a linear NaCl gradient (20 to 500 mM). AfumPCNA fractions were pooled and dialyzed with 20 mM Tris pH 7.5, 2 mM DTT, and 10% glycerol overnight at 4 °C, concentrated to approximately 10 mg·mL^{-1} and subjected to crystallization trials immediately.

Crystallization, data collection, and structure determination

Protein crystallization was carried out by vapor diffusion in sitting-drop format at 16 °C. Crystals grew as small plates in 0.2 M KCl, 20% PEG 3350, and diffracted X-rays to 2.6Å using the MX-1 beamline at the Australian Synchrotron [62]. Data were collected at 100 K using 1° oscillations at a wavelength of 0.9537Å. The AfumPCNA data were processed in space group $P2_1$ using iMosflm and solved by molecular replacement using phaserMR [63] with a homology model built using chainsaw [23]. The *Litopenaeus vannamei* PCNA crystal structure (PDB: 4CS5) [64] was used as a template for the homology model. The structure was refined by iterations of manual rebuilding using Coot [65] and refinement using phenix.refine [66]. Groups for TLS parameterization [67] were defined automatically using phenix.refine and used for refinement as this improved refinement statistics. For the final rounds of refinement, NCS restraints were imposed along with optimization of X-ray/stereochemistry weight to improve the stereochemistry of the final model. The final rebuild was performed using a feature-enhanced map (FEM) generated using phenix [68]. The final structure contained 0.66% Ramachandran outliers with 99.34% of the residues contained in the most favored and allowed regions. Coordinates were deposited in the PDB, accession code 5TUP.

P21 peptide binding assay using fluorescence polarization

Fluorescence polarization assays were carried out on a PerkinElmer Victor X5 2030 Multilabel Reader, using 100 nM N-terminally FITC-labeled human P21 peptide (N-139 GRKRRQTSMTDFYHSKRRLIFS 160-C) as the labeled ligand, and increasing concentrations of AfumPCNA (0.2–26 μM). Experiments were performed at room temperature, in either buffer 1: 20 mM Tris (pH 7.5) with 10% glycerol, or buffer 2: phosphate-buffered saline (137 mM NaCl, 2.7 mM KCl, 1.5 mM KH_2PO4, 8.1 mM Na_2HPO_4, pH 7.4). Each buffer also contained 2 mM DTT, 0.01% triton, 1 mM EDTA, and 1xCOMPLETE protease inhibitors.

Data were fit to the following equation:

$$\Delta FP = FP_{max} * (L_T + K_d + R_T) - \sqrt{(L_T + K_d + R_T)^2 - 4L_T R_T} \over 2L_T$$

where ΔFP is the measured change in fluorescence polarization, FP_{max} is the maximum change in polarization of the labeled ligand upon saturation, L_T is the ligand concentration, R_T is the protein concentration, and K_d is the dissociation constant for the interaction. Each experiment consisted of triplicate samples, and experiments were repeated three times to obtain a mean K_d value, and standard deviation.

Molecular dynamics simulations

The p21 peptide was docked onto the AfumPCNA-binding surface of one subunit using the ICMPRO (Molsoft) software

suite [69]. The trimeric complex of AfumPCNA–p21 was constructed using hPCNA as a guide after aligning individual AfumPCNA–p21 complexes with the hPCNA trimer. Molecular dynamics simulation of p21 peptide bound to the AfumPCNA was conducted using NAMD 2.9 [70]. PCNA and peptide complex was parameterized with the CHARMM27 force field [71] and solvated using the solvate plugin of VMD [72]. After neutralization, 150 mM NaCl was added to the solvated system using the autoionize plugin of VMD. Prior to the simulation, the system was equilibrated to NPT ensemble for a period of 2 ns. Then the production simulation was carried out for a period of 50 ns. During the simulation, a 12Å cutoff was used for nonbonded short-range interactions, and long-range electrostatics were treated with the particle-mesh Ewald method [73]. Temperature and pressure were maintained at 310K and 101.3 kPa using Langevin thermostat and the Langevin piston. The time step used was 1 fs. Trajectories were saved at every 20 ps. Data analysis and the visualization of the simulation were carried out by the VISUAL MOLECULAR DYNAMICS package [72].

Acknowledgements

We thank La Trobe University Comprehensive Protein Platform for providing infrastructure and expertise. We thank the beamline scientists of the Australian Synchrotron for help with data collection. The Australian Synchrotron CAP8221 in part funded this work.

Author contributions

AJK performed gene cloning, purification guidance, and helped prepare manuscript. ACM performed protein purification and crystallization, data processing, structure solution, and prepared figures and manuscript. KG and LM helped purify protein and crystallization trials. KLW performed binding studies, and assisted with manuscript preparation. HR carried out MD simulations. JBB conceived and managed project, and helped with data processing, structure solution, and preparation of manuscript and figures.

References

1 Bitar D, Lortholary O, Le Strat Y, Nicolau J, Coignard B, Tattevin P, Che D & Dromer F (2014) Population-based analysis of invasive fungal infections, France, 2001-2010. *Emerg Infect Dis* **20**, 1149–1155.

2 McNeil MM, Nash SL, Hajjeh RA, Phelan MA, Conn LA, Plikaytis BD & Warnock DW (2001) Trends in mortality due to invasive mycotic diseases in the United States, 1980-1997. *Clin Infect Dis* **33**, 641–647.

3 Yoon HJ, Choi HY, Kim YK, Song YJ & Ki M (2014) Prevalence of fungal infections using National Health Insurance data from 2009-2013, South Korea. *Epidemiol Health* **36**, e2014017.

4 Steinbach WJ (2013) Are we there yet? Recent progress in the molecular diagnosis and novel antifungal targeting of *Aspergillus fumigatus* and invasive aspergillosis. *PLoS Pathog* **9**, e1003642.

5 Ben-Ami R, Lewis RE & Kontoyiannis DP (2010) Enemy of the (immunosuppressed) state: an update on the pathogenesis of *Aspergillus fumigatus* infection. *Br J Haematol* **150**, 406–417.

6 Sugui JA, Kwon-Chung KJ, Juvvadi PR, Latge JP & Steinbach WJ (2015) *Aspergillus fumigatus* and related species. *Cold Spring Harb Perspect Med* **5**, a019786.

7 Latge JP (1999) *Aspergillus fumigatus* and aspergillosis. *Clin Microbiol Rev* **12**, 310–350.

8 Mullins J, Harvey R & Seaton A (1976) Sources and incidence of airborne *Aspergillus fumigatus* (Fres). *Clin Allergy* **6**, 209–217.

9 Hospenthal DR, Kwon-Chung KJ & Bennett JE (1998) Concentrations of airborne Aspergillus compared to the incidence of invasive aspergillosis: lack of correlation. *Med Mycol* **36**, 165–168.

10 McCormick A, Loeffler J & Ebel F (2010) *Aspergillus fumigatus*: contours of an opportunistic human pathogen. *Cell Microbiol* **12**, 1535–1543.

11 Gallien S, Fournier S, Porcher R, Bottero J, Ribaud P, Sulahian A, Socie G & Molina JM (2008) Therapeutic outcome and prognostic factors of invasive aspergillosis in an infectious disease department: a review of 34 cases. *Infection* **36**, 533–538.

12 Patterson TF, Thompson GR 3rd, Denning DW, Fishman JA, Hadley S, Herbrecht R, Kontoyiannis DP, Marr KA, Morrison VA, Nguyen MH *et al.* (2016) Practice guidelines for the diagnosis and management of Aspergillosis: 2016 Update by the Infectious Diseases Society of America. *Clin Infect Dis* **63**, e1–60.

13 Abad A, Fernandez-Molina JV, Bikandi J, Ramirez A, Margareto J, Sendino J, Hernando FL, Ponton J, Garaizar J & Rementeria A (2010) What makes *Aspergillus fumigatus* a successful pathogen? Genes and molecules involved in invasive aspergillosis *Revista iberoamericana de micologia* **27**, 155–182.

14 Wauters J, Baar I, Meersseman P, Meersseman W, Dams K, De Paep R, Lagrou K, Wilmer A, Jorens P & Hermans G (2012) Invasive pulmonary aspergillosis is a frequent complication of critically ill H1N1 patients: a retrospective study. *Intensive Care Med* **38**, 1761–1768.

15 Meersseman W, Vandecasteele SJ, Wilmer A, Verbeken E, Peetermans WE & Van Wijngaerden E (2004) Invasive aspergillosis in critically ill patients without malignancy. *Am J Respir Crit Care Med* **170**, 621–625.

16 Chen CH, Ho C, Liu HC, Tsung TT & Hung TT (2011) Spontaneous empyema necessitatis caused by

Aspergillus fumigatus in an immunocompetent patient. *JRSM Short Rep* **2**, 25.
17 Siddiqui K, Douglas M, Carey M & Benamer H (2008) A case of invasive aspergillosis in a patient with no identifiable immunodeficiencies. *Libyan J Med* **3**, 49–51.
18 Escobar N, Ordonez SR, Wosten HA, Haas PJ, de Cock H & Haagsman HP (2016) Hide, keep quiet, and keep low: properties that make *Aspergillus fumigatus* a successful lung pathogen. *Front Microbiol* **7**, 438.
19 Kontoyiannis DP, Marr KA, Park BJ, Alexander BD, Anaissie EJ, Walsh TJ, Ito J, Andes DR, Baddley JW, Brown JM *et al.* (2010) Prospective surveillance for invasive fungal infections in hematopoietic stem cell transplant recipients, 2001–2006: overview of the Transplant-Associated Infection Surveillance Network (TRANSNET) Database. *Clin Infect Dis* **50**, 1091–1100.
20 Warnock DW (2007) Trends in the epidemiology of invasive fungal infections. *Nihon Ishinkin Gakkai zasshi* **48**, 1–12.
21 Groll AH, Shah PM, Mentzel C, Schneider M, Just-Nuebling G & Huebner K (1996) Trends in the postmortem epidemiology of invasive fungal infections at a university hospital. *J Infect* **33**, 23–32.
22 Lin SJ, Schranz J & Teutsch SM (2001) Aspergillosis case-fatality rate: systematic review of the literature. *Clin Infect Dis* **32**, 358–366.
23 Walsh TJ, Anaissie EJ, Denning DW, Herbrecht R, Kontoyiannis DP, Marr KA, Morrison VA, Segal BH, Steinbach WJ, Stevens DA *et al.* (2008) Treatment of aspergillosis: clinical practice guidelines of the Infectious Diseases Society of America. *Clin Infect Dis* **46**, 327–360.
24 Arthurs SK, Eid AJ, Deziel PJ, Marshall WF, Cassivi SD, Walker RC & Razonable RR (2010) The impact of invasive fungal diseases on survival after lung transplantation. *Clin Transplant* **24**, 341–348.
25 Doligalski CT, Benedict K, Cleveland AA, Park B, Derado G, Pappas PG, Baddley JW, Zaas DW, Harris MT & Alexander BD (2014) Epidemiology of invasive mold infections in lung transplant recipients. *Am J Transplant* **14**, 1328–1333.
26 Neofytos D, Fishman JA, Horn D, Anaissie E, Chang CH, Olyaei A, Pfaller M, Steinbach WJ, Webster KM & Marr KA (2010) Epidemiology and outcome of invasive fungal infections in solid organ transplant recipients. *Transplant Infect Dis* **12**, 220–229.
27 Hadrich I, Makni F, Neji S, Abbes S, Cheikhrouhou F, Trabelsi H, Sellami H & Ayadi A (2012) Invasive aspergillosis: resistance to antifungal drugs. *Mycopathologia* **174**, 131–141.
28 Chowdhry R & Marshall WL (2008) Antifungal therapies in the intensive care unit. *J Intensive Care Med* **23**, 151–158.
29 Kim A, Nicolau DP & Kuti JL (2011) Hospital costs and outcomes among intravenous antifungal therapies for patients with invasive aspergillosis in the United States. *Mycoses* **54**, e301–e312.
30 Albataineh MT, Sutton DA, Fothergill AW & Wiederhold NP (2016) Update from the Laboratory: clinical identification and susceptibility testing of fungi and trends in antifungal resistance. *Infect Dis Clin North Am* **30**, 13–35.
31 Lelièvre L, Groh M, Angebault C, Maherault AC, Didier E & Bougnoux ME (2013) Azole resistant *Aspergillus fumigatus*: an emerging problem. *Médecine et Maladies Infectieuses* **43**, 139–145.
32 van der Linden JW, Snelders E, Kampinga GA, Rijnders BJ, Mattsson E, Debets-Ossenkopp YJ, Kuijper EJ, Van Tiel FH, Melchers WJ & Verweij PE (2011) Clinical implications of azole resistance in *Aspergillus fumigatus*, The Netherlands, 2007–2009. *Emerg Infect Dis* **17**, 1846–1854.
33 Vermeulen E, Lagrou K & Verweij PE (2013) Azole resistance in *Aspergillus fumigatus*: a growing public health concern. *Curr Opin Infect Dis* **26**, 493–500.
34 Verweij PE, Chowdhary A, Melchers WJ & Meis JF (2016) Azole resistance in *Aspergillus fumigatus*: can we retain the clinical use of mold-active antifungal azoles? *Clin Infect Dis* **62**, 362–368.
35 Lamoth F (2016) *Aspergillus fumigatus*-related species in clinical practice. *Front Microbiol* **7**, 683.
36 Moldovan GL, Pfander B & Jentsch S (2007) PCNA, the maestro of the replication fork. *Cell* **129**, 665–679.
37 Krishna TS, Kong XP, Gary S, Burgers PM & Kuriyan J (1994) Crystal structure of the eukaryotic DNA polymerase processivity factor PCNA. *Cell* **79**, 1233–1243.
38 Maga G & Hubscher U (2003) Proliferating cell nuclear antigen (PCNA): a dancer with many partners. *J Cell Sci* **116**, 3051–3060.
39 Matsumiya S, Ishino Y & Morikawa K (2001) Crystal structure of an archaeal DNA sliding clamp: proliferating cell nuclear antigen from *Pyrococcus furiosus*. *Protein Sci* **10**, 17–23.
40 Shamoo Y & Steitz TA (1999) Building a replisome from interacting pieces: sliding clamp complexed to a peptide from DNA polymerase and a polymerase editing complex. *Cell* **99**, 155–166.
41 Warbrick E, Lane DP, Glover DM & Cox LS (1995) A small peptide inhibitor of DNA replication defines the site of interaction between the cyclin-dependent kinase inhibitor p21WAF1 and proliferating cell nuclear antigen. *Current Biol* **5**, 275–282.
42 De Biasio A & Blanco FJ (2013) Proliferating cell nuclear antigen structure and interactions: too many partners for one dancer? *Advances Protein Chem Struct Biol* **91**, 1–36.
43 Freudenthal BD, Gakhar L, Ramaswamy S & Washington MT (2010) Structure of monoubiquitinated PCNA and implications for translesion synthesis and

DNA polymerase exchange. *Nat Struct Mol Biol* **17**, 479–484.
44 Gulbis JM, Kelman Z, Hurwitz J, O'Donnell M & Kuriyan J (1996) Structure of the C-terminal region of p21(WAF1/CIP1) complexed with human PCNA. *Cell* **87**, 297–306.
45 Wolff P, Olieric V, Briand JP, Chaloin O, Dejaegere A, Dumas P, Ennifar E, Guichard G, Wagner J & Burnouf DY (2011) Structure-based design of short peptide ligands binding onto the *E. coli* processivity ring. *J Med Chem* **54**, 4627–4637.
46 Punchihewa C, Inoue A, Hishiki A, Fujikawa Y, Connelly M, Evison B, Shao Y, Heath R, Kuraoka I, Rodrigues P *et al.* (2012) Identification of small molecule proliferating cell nuclear antigen (PCNA) inhibitor that disrupts interactions with PIP-box proteins and inhibits DNA replication. *J Biol Chem* **287**, 14289–14300.
47 Georgescu RE, Yurieva O, Kim SS, Kuriyan J, Kong XP & O'Donnell M (2008) Structure of a small-molecule inhibitor of a DNA polymerase sliding clamp. *Proc Natl Acad Sci USA* **105**, 11116–11121.
48 Yin Z, Wang Y, Whittell LR, Jergic S, Liu M, Harry E, Dixon NE, Kelso MJ, Beck JL & Oakley AJ (2014) DNA replication is the target for the antibacterial effects of nonsteroidal anti-inflammatory drugs. *Chem Biol* **21**, 481–487.
49 Yin Z, Whittell LR, Wang Y, Jergic S, Liu M, Harry EJ, Dixon NE, Beck JL, Kelso MJ & Oakley AJ (2014) Discovery of lead compounds targeting the bacterial sliding clamp using a fragment-based approach. *J Med Chem* **57**, 2799–2806.
50 Kling A, Lukat P, Almeida DV, Bauer A, Fontaine E, Sordello S, Zaburannyi N, Herrmann J, Wenzel SC, Konig C *et al.* (2015) Antibiotics. Targeting DnaN for tuberculosis therapy using novel griselimycins. *Science (New York, NY)* **348**, 1106–1112.
51 Wolff P, Amal I, Olieric V, Chaloin O, Gygli G, Ennifar E, Lorber B, Guichard G, Wagner J, Dejaegere A *et al.* (2014) Differential modes of peptide binding onto replicative sliding clamps from various bacterial origins. *J Med Chem* **57**, 7565–7576.
52 Wijffels G, Johnson WM, Oakley AJ, Turner K, Epa VC, Briscoe SJ, Polley M, Liepa AJ, Hofmann A, Buchardt J *et al.* (2011) Binding inhibitors of the bacterial sliding clamp by design. *J Med Chem* **54**, 4831–4838.
53 Kjelstrup S, Hansen PM, Thomsen LE, Hansen PR & Lobner-Olesen A (2013) Cyclic peptide inhibitors of the beta-sliding clamp in *Staphylococcus aureus*. *PLoS One* **8**, e72273.
54 Zamir L, Zaretsky M, Fridman Y, Ner-Gaon H, Rubin E & Aharoni A (2012) Tight coevolution of proliferating cell nuclear antigen (PCNA)-partner interaction networks in fungi leads to interspecies network incompatibility. *Proc Natl Acad Sci USA* **109**, E406–E414.
55 Bruning JB & Shamoo Y (2004) Structural and thermodynamic analysis of human PCNA with peptides derived from DNA polymerase-delta p66 subunit and flap endonuclease-1. *Structure* **12**, 2209–2219.
56 Kontopidis G, Wu SY, Zheleva DI, Taylor P, McInnes C, Lane DP, Fischer PM & Walkinshaw MD (2005) Structural and biochemical studies of human proliferating cell nuclear antigen complexes provide a rationale for cyclin association and inhibitor design. *Proc Natl Acad Sci USA* **102**, 1871–1876.
57 Bozza WP, Yang K, Wang J & Zhuang Z (2012) Developing peptide-based multivalent antagonists of proliferating cell nuclear antigen and a fluorescence-based PCNA binding assay. *Anal Biochem* **427**, 69–78.
58 Kroker AJ & Bruning JB (2015) p21 exploits residue Tyr151 as a tether for high-affinity PCNA binding. *Biochemistry* **54**, 3483–3493.
59 De Biasio A, Campos-Olivas R, Sanchez R, Lopez-Alonso JP, Pantoja-Uceda D, Merino N, Villate M, Martin-Garcia JM, Castillo F, Luque I *et al.* (2012) Proliferating cell nuclear antigen (PCNA) interactions in solution studied by NMR. *PLoS One* **7**, e48390.
60 Fridman Y, Gur E, Fleishman SJ & Aharoni A (2013) Computational protein design suggests that human PCNA-partner interactions are not optimized for affinity. *Proteins* **81**, 341–348.
61 Nierman WC, Pain A, Anderson MJ, Wortman JR, Kim HS, Arroyo J, Berriman M, Abe K, Archer DB, Bermejo C *et al.* (2005) Genomic sequence of the pathogenic and allergenic filamentous fungus *Aspergillus fumigatus*. *Nature* **438**, 1151–1156.
62 McPhillips TM, McPhillips SE, Chiu HJ, Cohen AE, Deacon AM, Ellis PJ, Garman E, Gonzalez A, Sauter NK, Phizackerley RP *et al.* (2002) Blu-Ice and the Distributed Control System: software for data acquisition and instrument control at macromolecular crystallography beamlines. *J Synchrotron Radiat* **9**, 401–406.
63 McCoy AJ, Grosse-Kunstleve RW, Adams PD, Winn MD, Storoni LC & Read RJ (2007) Phaser crystallographic software. *J Appl Crystallogr* **40**, 658–674.
64 Carrasco-Miranda JS, Lopez-Zavala AA, Arvizu-Flores AA, Garcia-Orozco KD, Stojanoff V, Rudino-Pinera E, Brieba LG & Sotelo-Mundo RR (2014) Crystal structure of the shrimp proliferating cell nuclear antigen: structural complementarity with WSSV DNA polymerase PIP-box. *PLoS One* **9**, e94369.
65 Emsley P & Cowtan K (2004) Coot: model-building tools for molecular graphics. *Acta Crystallogr D Biol Crystallogr* **60**, 2126–2132.
66 Afonine PV, Grosse-Kunstleve RW, Echols N, Headd JJ, Moriarty NW, Mustyakimov M, Terwilliger TC,

Urzhumtsev A, Zwart PH & Adams PD (2012) Towards automated crystallographic structure refinement with phenix.refine. *Acta Crystallogr D Biol Crystallogr* **68**, 352–367.
67 Winn MD, Isupov MN & Murshudov GN (2001) Use of TLS parameters to model anisotropic displacements in macromolecular refinement. *Acta Crystallogr D Biol Crystallogr* **57**, 122–133.
68 Afonine PV, Moriarty NW, Mustyakimov M, Sobolev OV, Terwilliger TC, Turk D, Urzhumtsev A & Adams PD (2015) FEM: feature-enhanced map. *Acta Crystallogr D Biol Crystallogr* **71**, 646–666.
69 Abagyan R & Totrov M (1994) Biased probability Monte Carlo conformational searches and electrostatic calculations for peptides and proteins. *J Mol Biol* **235**, 983–1002.
70 Phillips JC, Braun R, Wang W, Gumbart J, Tajkhorshid E, Villa E, Chipot C, Skeel RD, Kale L & Schulten K (2005) Scalable molecular dynamics with NAMD. *J Comput Chem* **26**, 1781–1802.
71 MacKerell AD, Bashford D, Bellott M, Dunbrack RL, Evanseck JD, Field MJ, Fischer S, Gao J, Guo H, Ha S *et al.* (1998) All-atom empirical potential for molecular modeling and dynamics studies of proteins. *J Phys Chem B* **102**, 3586–3616.
72 Humphrey W, Dalke A & Schulten K (1996) VMD: visual molecular dynamics. *J Mol Graph* **14** , 27–28.
73 Darden TA & Pedersen LG (1993) Molecular modeling: an experimental tool. *Environ Health Perspect* **101**, 410–412.

Supporting information

Additional Supporting Information may be found online in the supporting information tab for this article:

Movie S1. 50 ns molecular dynamics simulation of AfumPCNA with p21 PIP-box with camera view adjacent to PIP-box-binding surface.

Movie S2. 50 ns molecular dynamics simulation of AfumPCNA with p21 PIP-box with camera view adjacent to central DNA cavity.

Conclusion

Sliding clamps are structurally highly conserved and are involved in interactions that are key for the control of DNA replication and cell cycle control. The research presented in this thesis provides further insight into how the PIP-box protein packs into the PIP-box binding pocket of PCNA, and how p21 is able to bind tighter and with higher binding affinity. The research and methodology that was performed here can be extended to investigate which other residues within the PIP-box sequence are responsible for the tighter packing and higher binding affinity of p21 for PCNA. This would lead into the design of a peptide mimetic to include these identified residues and potential modifications to increase binding affinity. Such a peptide mimetic would be tested *in vivo* to investigate its ability to inhibit biological PCNA-PIP-box interactions, and the resulting impact on DNA replication, DNA repair and cell growth. The long term aim is to identify modifications of all residues within the PIP-box and surrounding sequence that result in the highest possible affinity binder to PCNA, and incorporate these structures into a compound, potentially a peptide mimetic, that would also be chemically suitable as a drug.

The research presented in this thesis also showed that the conservation of the sliding clamp structure extends to the fungus *A. fumigatus*, and that the mechanism of binding to interacting partners through a PIP-box-like peptide motif is also conserved. The question remains of whether it is plausible to exploit the differences between human and *A. fumigatus* PCNA, to inhibit *A. fumigatus* PCNA without adverse effects on the human PCNA. To answer this question will require further research. The 10-fold difference in affinity for a p21 peptide between human and *A. fumigatus* PCNA that was shown in the research herein suggests that there are likely to be differences in residue-specific interactions that could be exploited in the design of an *A. fumigatus* PCNA-specific inhibitor.

Future directions for research in this field would include the continued study and design of peptide mimetics using the knowledge about the p21 PIP-box to develop a high-affinity PCNA binder. This could be used to both stop cell growth and increase the effectiveness of current chemotherapeutic and antifungal drugs. Continued research of the PIP-box interactions between PCNA and interacting partners could also contribute to increasing the understanding of the

relationship of structure to the affinity and function of an interaction and offering opportunities to manipulate this, such as through rational drug design. It would also address some of the key questions in the DNA replication field that continue to be asked related to the replisome and cell cycle control.

Appendix: Review of the Structural and Dynamic Mechanisms of PPARγ Partial Agonism

During the course of my postgraduate study there was the opportunity for me to also contribute to a review on the structural biology of another group of proteins, the peroxisome proliferator activated receptors (PPARs). The following paper reviews the current knowledge about the structure of PPARγ and its ligands, and how different interactions within the same binding pocket lead to differences in function.

While PPARs have a very different function and significance within the cell to PCNA, interactions of similar ligands within the same ligand binding pocket lead to different transcriptional and cellular outcomes because of differences in structural and dynamic mechanism, much like the interactions seen between PCNA and PIP-box proteins. Further understanding of the intricacies of different interactions between proteins and their ligands or binding partners can lead us closer to the rational design of drugs that either inhibit or mimic the interaction of proteins on a broader scale.

Statement of Authorship

Title of Paper	Review of the Structural and Dynamic Mechanisms of PPAR□ Partial Agonism
Publication Status	☐ Published
Publication Details	Kroker, A. J.; Bruning, J. B., Review of the Structural and Dynamic Mechanisms of PPARgamma Partial Agonism. PPAR research, 2015. 2015: p. 816856.

Principal Author

Name of Principal Author (Candidate)	Alice J Kroker
Contribution to the Paper	Review of literature and manuscript preparation.
Overall percentage (%)	80%
Certification:	This paper reports on original research I conducted during the period of my Higher Degree by Research candidature and is not subject to any obligations or contractual agreements with a third party that would constrain its inclusion in this thesis. I am the primary author of this paper.
Signature	Date 27/2/17

Co-Author Contributions

By signing the Statement of Authorship, each author certifies that:

i. the candidate's stated contribution to the publication is accurate (as detailed above);

ii. permission is granted for the candidate in include the publication in the thesis; and

iii. the sum of all co-author contributions is equal to 100% less the candidate's stated contribution.

Name of Co-Author	John B Bruning
Contribution to the Paper	Involved in manuscript and figure preparation.
Signature	Date 13/2/2017

Hindawi Publishing Corporation
PPAR Research
Volume 2015, Article ID 816856, 15 pages
http://dx.doi.org/10.1155/2015/816856

Review Article

Review of the Structural and Dynamic Mechanisms of PPARγ Partial Agonism

Alice J. Kroker and John B. Bruning

School of Biological Sciences, The University of Adelaide, Adelaide, SA 5005, Australia

Correspondence should be addressed to John B. Bruning; john.bruning@adelaide.edu.au

Received 26 June 2015; Accepted 19 August 2015

Academic Editor: Richard P. Phipps

PPARγ (peroxisome proliferator activated receptor γ) is a ligand activated transcription factor of the nuclear receptor superfamily that controls the expression of a variety of genes involved in fatty acid metabolism, adipogenesis, and insulin sensitivity. While endogenous ligands of PPARγ include fatty acids and eicosanoids, synthetic full agonists of the receptor, including members of the thiazolidinedione (TZD) class, have been widely prescribed for the treatment of type II diabetes mellitus (T2DM). Unfortunately, the use of full agonists has been hampered by harsh side effects with some removed from the market in many countries. In contrast, partial agonists of PPARγ have been shown to retain favourable insulin sensitizing effects while exhibiting little to no side effects and thus represent a new potential class of therapeutics for the treatment of T2DM. Partial agonists have been found to not only display differences in transcriptional and cellular outcomes, but also act through distinct structural and dynamic mechanisms within the ligand binding cavity compared to full agonists.

1. Introduction

PPARs (peroxisome proliferator activated receptors) are members of the nuclear receptor superfamily, acting as ligand inducible transcription factors. There are three different, highly homologous subtypes of PPAR: PPARα, PPARδ (also referred to as PPARβ), and PPARγ, each encoded by different genes and with different tissue expression and ligand selectivity [1]. PPARα is most highly expressed in hepatocytes, cardiomyocytes, enterocytes, and kidney proximal tubule cells [2]. PPARδ is expressed nearly ubiquitously and generally found in higher concentrations while PPARγ is most strongly expressed in adipose tissue and the immune system [2]. All PPARs have roles in fat and carbohydrate metabolism and homeostasis, as well as cell proliferation and differentiation, inflammation, vascular biology, and cancer [1]. The name and association with peroxisome proliferation come from the initial identification of PPARα in rodents; however, PPARs have no function in peroxisome proliferation in humans [3]. PPARs are an example of a nuclear receptor that forms an obligate heterodimer with RXR (Retinoid X Receptor) [4]. Of the three subtypes PPARγ is the most well studied. There are two different isoforms of PPARγ as a result of different promoters and alternative splicing: PPARγ2 contains an extra 30 amino acids at the N-terminus in comparison to PPARγ1 [5]. PPARγ1 has a wide tissue expression pattern (white and brown adipose tissue, cardiac muscle, and liver tissue), while PPARγ2 expression is exclusive to adipose tissue [6].

Hundreds of genes are under the control of PPARγ, with many involved in energy, carbohydrate, and lipid metabolism. PPARγ also acts as a modulator of inflammation and fluid homeostasis (reviewed in [7]). It has been described as a master regulator of adipogenesis, being necessary and sufficient for adipocyte formation [8]. Representative genes under the control of PPARγ are located in Table 1. Genes regulated by PPARγ are differentially regulated not only by agonist binding but also by phosphorylation of the ligand binding domain of PPARγ [9–11].

The mechanism of action of PPARγ is initiated by ligand binding which induces a conformational change in the receptor. This leads to the dissociation of any corepressor complexes (such as those with histone deacetylase activity)

Table 1: Selected genes under transcriptional control of PPARγ.

Gene set	Gene product	Function
Regulated by PPARγ phosphorylation	*Cyp2f2*	Cytochrome P-450
	RarreS2	Retinoic acid responder 2 (adipokine)
	Selenbp1	Selenium binding protein 1
	Car3	Carbonic anhydrase 3
	Peg10	Retrotransposon-derived protein PEG10 (cell proliferation/apoptosis)
	Cidec	Cell death-inducing DFFA-like effector c (lipid droplet formation and apoptosis in adipocytes)
	Cd24a	Heat stable antigen 24 (glycoprotein expressed on B cells/granulocytes)
	Acyl	Acyl carrier protein
	Nr1d2	Rev-erb β (nuclear receptor subfamily 1, group D, member 2)
	Ddx17	DEAD box helicase 17
	Aplp2	Amyloid-like protein 2 (glucose/insulin homeostasis)
	Nr3c1	Glucocorticoid receptor
	Rybp	RING1 and YY1-binding protein (transcriptional regulation)
	Txnip	Thioredoxin-interacting protein
	Nr1d1	Rev-erb α (nuclear receptor subfamily 1, group D, member 1)
	Adiponectin	Adipokine
	Adipsin	Adipokine
Regulated by PPARγ agonists	*aP2*	Adipocyte protein 2 (fatty acid carrier protein)
	Lpl	Lipoprotein lipase
	Cycs	Cytochrome c
	Ppcs	Phosphopantothenate cysteine ligase (coenzyme A biosynthesis)
	Fdx1	Adrenal ferredoxin
	Fgfrl1	Fibroblast growth factor receptor-like 1
	Idh3a	Isocitrate dehydrogenase
	Abhd1	Abhydrolase
	Nadk	NAD+ kinase
	Arhgap5	Rho GTPase activating protein 5
	Pdk4	Pyruvate dehydrogenase lipoamide kinase isozyme 4
	Las1l	Ribosomal biogenesis protein
	Cib2	Calcium and integrin binding family member
	Fmr1	Fragile X mental retardation 1
	Pim3	Serine/threonine-protein kinase (it inhibits ERK1/2)
	Hsdl2	Hydroxysteroid dehydrogenase like 2 (short chain dehydrogenase family)
	Phospho1	Phosphatase expressed in bone and cartilage
	Plin1	Perilipin 1 (lipolysis regulation)
	Plin2	Adipose differentiation-related protein (lipolysis regulation)
	Lass4	Ceramide synthesis
	C/EBPα	Leucine zipper family transcription factor
	Glut4	Insulin-dependent glucose transporter
	PPARγ	PPARγ regulates its own expression
	Fasn	Fatty acid synthase
	CD36	Fatty acid translocase
	Fatp-1	Insulin sensitive fatty acid transporter
	Fatp-4	Fatty acid transport protein/very long chain fatty acyl-CoA synthetase
	Pepck	Phosphoenolpyruvate carboxykinase
	Gk	Glycerol kinase

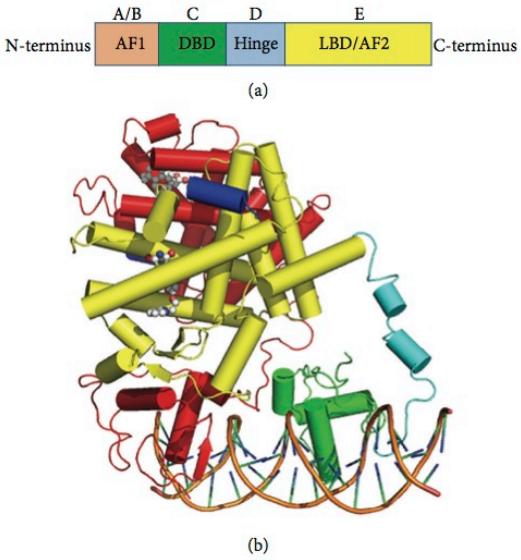

FIGURE 1: PPARγ domain organization. (a) Primary structure of PPARγ. (b) Crystal structure of the intact PPARγ-RXR heterodimer bound to PPRE DNA with agonist ligands retinoic acid and full agonist rosiglitazone. Proteins and DNA are shown as ribbons while ligands are shown as spheres. RXR is coloured red, the PPARγ ligand binding domain is coloured yellow, the PPARγ DNA binding domain is coloured green, the PPARγ hinge is coloured cyan, and the NCOA2 coactivator peptide is coloured blue. PDB: 3DZY [14].

and the recruitment of coactivators [12]. When the PPAR-RXR heterodimer is not bound to a ligand it forms a complex with corepressor proteins including NCoR (nuclear receptor corepressor 1) and SMRT (silencing mediator of retinoic acid and thyroid hormone receptor). These function to block PPAR activated transcription, keeping basal levels of PPAR-mediated transcription minimal. Upon full or partial agonist binding, corepressors dissociate from the PPAR-RXR complex, allowing for the recruitment of coactivators. These coactivators can then perform different functions to promote transcription, including altering chromatin structure and recruiting transcriptional machinery to the target gene promoter. Coactivators of PPARγ include CBP (CREB binding protein), MED1 (Mediator 1; also known as PBP/TRAP220/DRIP205), SRC1 (steroid receptor coactivator 1), SRC2, SRC3, and PGC1α (peroxisome proliferator activated receptor gamma coactivator 1 α) [13].

2. PPARγ Domain Structure

PPARγ, similar to other nuclear receptors, has a conserved domain structure consisting of 5 domains named A–E from N- to C-terminus (Figure 1(a)) [14]. The N-terminal regulatory domain, consisting of domains A and B, contains the intrinsically disordered activation function 1 (AF1) which is involved in ligand-independent coregulator binding [15, 16]. This region is poorly conserved, differing greatly between different nuclear receptors. The C domain functions as the DNA binding domain and is the most conserved region among nuclear receptors, with respect to primary and tertiary structure. Two highly conserved zinc fingers are involved in the recognition of specific DNA half-sites termed peroxisome proliferator response elements (PPRE) [17]. These half-sites are either direct or indirect repeats, separated by a spacer of between 1 and 5 base pairs. Each zinc finger contains 4 cysteine residues allowing for the coordination to a zinc ion. The presence of zinc fingers distinguishes nuclear receptors from other DNA binding proteins. DNA binding allows for either the activation and recruitment of DNA transcription machinery or the repression of transcription. The DNA binding domain is also involved in nuclear receptor dimerization, in a DNA-dependent, cooperative manner. All members of the nuclear receptor superfamily bind to DNA either as a heterodimer or homodimer; DNA binding occurs as a heterodimer with RXR in the case of the PPARs. Each DNA binding domain subunit binds to a separate DNA half-site. The poorly conserved D domain functions as a flexible hinge allowing for rotation between the DNA binding domain and the ligand binding domain, as well as containing a nuclear localisation signal. The ligand binding domain (E domain) is the largest domain in PPARγ and is the second most conserved domain among nuclear receptors after the DNA binding domain. Within the nuclear receptor family the secondary structure within the ligand binding domain is more conserved than the primary amino acid sequence. There are four main functions of the ligand binding domain: a second dimerization interface, the ligand binding pocket, a coregulator binding surface, and activation function 2 (AF2). Ligand binding stabilizes the structure of the ligand binding domain and facilities the interaction with coregulator molecules to remodel chromatin and recruit transcriptional machinery, resulting in gene expression [18]. Whilst the ligand binding domain is highly conserved, differences within the ligand binding pocket, such as size and amino acid composition, confer ligand specificity. The size of the ligand binding pocket differs between classic receptors, true orphan receptors, and adopted orphan receptors. PPAR is an example of an adopted orphan receptor and has a larger ligand binding pocket compared to the classic receptors [19]. Upon stabilization in the active, ligand-bound position AF2 acts as a binding site for coregulator proteins.

3. Retinoid X Receptor

Many nonsteroid nuclear receptors, including retinoic acid receptor, vitamin D3 receptor, thyroid receptor, PPAR, liver X receptor, and farnesoid X receptor, heterodimerise with the RXR [20]. RXR is activated by the ligand 9-cis-retinoic acid, as well as synthetic agonists referred to as retinoids [21]. Within a heterodimerised complex RXR can have two different roles. It can form a nonpermissive complex with the receptors of retinoic acid receptor, thyroid receptor, and vitamin D3 receptor where ligand binding to both receptors in the heterodimer is necessary for activation of transcription. RXR can also form a permissive complex with PPAR, liver

X receptor, and farnesoid X receptor, where ligand binding to only one receptor of the heterodimer is sufficient for transcriptional activity.

4. Endogenous Ligands of PPARγ

All three PPAR subtypes were discovered prior to the discovery of their activating ligands. Given the promiscuous nature of the ligand binding pocket, identification of all endogenous PPARγ ligands is still an active area of research. To date, the known endogenous ligands often show low affinity and limited subtype selectivity. It is a remarkable observation that the number and mode of interaction of synthetic agonists of PPARγ have been much more readily defined in comparison to endogenous ligands. Many of the endogenous ligands identified thus far are dietary metabolites. By far the largest class discovered to date include oxidized low-density lipoprotein metabolites [22]. This encompasses a wide variety of mono- and polyunsaturated fatty acids which have been shown to interact with PPARγ. Fatty acid metabolites derived from arachidonic acid and linoleic and linolenic acids include agonists such as 5-oxo-15-(S)-HETE and 5-oxo-ETE which have been shown to be agonists of PPARγ and only of moderate affinity. Most long chain fatty acids have been shown to have limited affinity for PPARγ and very long chain fatty acids have been shown to have little to no affinity for PPARγ. The essential eicosanoids such as 8-(S)-hydroxyeicosatetraenoic acid (8-HETE) and 15-deoxy-D12,14-prostaglandin J_2 (15d-PGJ_2) have also been identified as endogenous ligands of PPARγ [23]. Interestingly, 5-hydroxytryptamine (5-HT, also known as serotonin) was shown to be a high affinity agonist for PPARγ; the physiological importance of this discovery is still being studied [24]. In short, within the cell PPARγ may be activated by a large number of moderate affinity dietary metabolites or by a few key high affinity agonists which are still to be discovered.

5. Thiazolidinediones (TZDs) and T2DM

T2DM is a complex disease characterized by insulin resistance, leading to pancreatic islet and β-cell dysfunction, hyperglycemia, dyslipidemia, and inflammation [25]. T2DM accounts for 90% of all diabetes cases with causative factors thought to be environmental, namely poor diet and lack of exercise, and the disease is often coincident with obesity. Patients require more insulin for proper glucose and metabolic homeostasis, either through increased endogenous production or direct peptide injection, but this in turn leads to disruption of normal pancreatic function and β-islet cell dysfunction. Patients also have an increased risk of cardiovascular issues, with cardiovascular disease being the main cause of death. PPARγ activation by full agonists has been seen to improve insulin sensitivity and glucose control, as well as lowering the levels of circulating fatty acids and other markers of cardiovascular disease [26, 27]. For this reason, the potent PPARγ activators of the TZD class have been used in the treatment of T2DM as insulin sensitizers. TZDs are named after their characteristic thiazolidinedione head group. They act as insulin sensitizers in the skeletal muscles and liver as well as promoting adipogenesis of insulin-sensitive adipocytes. As a monotherapy TZDs produce a 1–1.5% reduction in HbA1c which is boosted several more percent when coadministered with other medications [28], signifying its long term benefit to blood glucose levels.

TZDs are used as potent insulin sensitizers in T2DM patients because of their high affinity for PPARγ. Troglitazone (Rezulin) was the first TZD introduced in early 1997 but was quickly removed from the market in the US and Europe in late 1997 and 2000, respectively, because of liver toxicity unrelated to receptor activation [29]. Rosiglitazone (Avandia) was first approved in 1999 but was withdrawn in Europe and access was restricted in the US because of a connection to congestive heart failure; in 2013 these restrictions were lifted after further consideration of the data [30]. Pioglitazone (Actos) was also released in 1999 but restricted later because of possible side effects including increased bladder cancer risk [31]. Despite restrictions, pioglitazone is still largely prescribed and $250 million worth was sold in 2014, although year after year sales are decreasing because of concerns over possible side effects. The TZD rivoglitazone (Daiichi Sankyo) is currently undergoing clinical trials. It is proposed that the full agonist activity of TZDs is responsible for the range of side effects associated with these drugs such as rosiglitazone. These side effects include anemia, hemodilution, edema, weight gain, adipogenesis, renal fluid retention, loss of bone mineral density (leading to potential bone fracture), cardiomegaly, and increased incidence of other cardiovascular events [32]. The exact cause of congestive heart failure is not fully understood but is thought to be related to renal sodium retention. Likewise, edema and increased plasma volume are thought to be caused by an increase of tubular transporters and a decrease of glomerular filtration rates in the kidney [33]. While the expressions of certain renal transporters such as aquaporin 3 (AQP3) are under the transcriptional control of PPARγ, the specific causative mechanisms of these side effects are still being researched.

6. Partial Agonists as Selective PPARγ Modulators (SPPARMs) for Treatment of T2DM

Much effort has been invested in separating the insulin sensitizing effects of PPARγ agonists from the transcriptional activation of genes which result in untoward side effects. This has been achieved through use of partial agonists which by definition only partially activate transcriptional output of any given gene in comparison to a full agonist. It is important to note that partial agonists retain high affinity to the receptor; PPARγ partial agonists operate through different structural and mechanistic methods than full agonists rather than simply exhibiting lowered transcriptional output due to suboptimal potency and/or affinity. Partial agonists of PPARγ have lessened side effects compared to full agonists and have been coined as SPPARMs [34, 35]. Treatment with SPPARMs in animal models shows very limited signs of edema, congestive heart failure, and bone mineral density

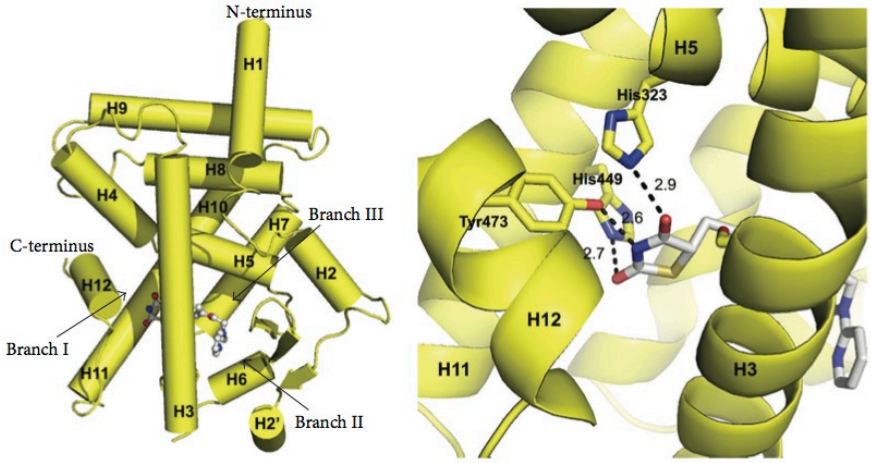

FIGURE 2: Interaction mode of full agonist rosiglitazone. The PPARγ ligand binding domain is shown in yellow and rosiglitazone is shown in white sticks coloured by element. (a) Ribbons diagram of the PPARγ ligand binding domain bound to rosiglitazone. The branches of the ligand binding pocket have been labelled with Roman numerals. (b) Hydrogen bond network of the rosiglitazone TZD head group with AF2 residues. PDB: 4EMA [49].

problems compared to full agonist treatment, whilst still retaining insulin sensitizing effects. While the amelioration of these side effects with partial agonists in comparison to full agonists has been connected to a decrease in upregulation of many genes thought to be responsible for the unfavourable side effects, the exact mechanism of the insulin sensitizing effects is still being studied.

The partial agonists reported to date are generally not of the TZD class and none have FDA approval; however, several PPARγ partial agonists are currently in clinical trials. The most well-known and perhaps most promising example is INT131 (previously AMG-131), which has progressed through Phase II clinical trials [36]. Angiotensin II receptor agonist Telmisartan, which is normally prescribed for hypertension, has also been observed to have PPARγ partial agonist effects, despite not being marketed as such [37]. Other PPARγ partial agonists that have advanced to or through Phase II clinical trials include MCC-555, DRF-2593, Metaglidasen, and Halofenate [38–40]. Partial agonists that have not made it through preclinical trials include nTZDpa, BVT.13, GW0072, and MRL24 [34, 41, 42]. Very few if any partial agonists have failed in clinical trials with several having not been tested in the latter stages of clinical trials yet. Partial agonists of PPARγ can show a wide spectrum of transcriptional activation in comparison to rosiglitazone; for example, BVT.13 is more of an intermediate agonist with a transcriptional output 80% that of rosiglitazone (in a PPRE transcriptional reporter assay), while partial agonists such as MRL24 have a transcriptional output approximately 20% that of rosiglitazone. Partial agonists have shown insulin sensitizing effects, while not demonstrating fatty acid storage in adipocyte cell models such as 3T3-L1 cells. Furthermore, those that have been tested in *ob/ob* mice and Zucker fatty rats showed no increase in weight as well as lower blood glucose and insulin levels [43]. Interestingly, partial agonists generally display a differential coactivator recruitment pattern compared to full agonists such as rosiglitazone. This often includes a decreased level of p300, CBP, and DRIP205/TRAP220 recruitment [44, 45]. A limited number of PPARγ partial agonist crystal structures are available and those displaying high potency (>10 μM EC_{50} in transcriptional assay) can be viewed in Table 2. Whilst these initial crystal structures have been informative, much remains to be discovered and the precise atomic and mechanistic properties of partial agonists remain elusive.

7. Structure of PPARγ

The first X-ray crystal structure of PPARγ included only the ligand binding domain and was solved by Nolte et al., in 1998 [19]. The ligand binding domain consists of 13 α-helices, labelled H1–H12 and H2′, as well as one β-sheet region. Ribbons diagram of the structure can be seen in Figure 2(a). The ligand binding domain is approximately 32 kDa and is composed of 270 amino acids. The ligand binding pocket is located in the centre of the ligand binding domain (its size is approximately 1200 $Å^3$) and has been described as a large Y- or T-shaped cavity with three branches, each branch having different properties and binding preferences. Branch I, consisting of H3, H5, H11, and H12, is of hydrophilic character and is the interaction site for the acidic head group of ligands such as rosiglitazone. In comparison, branch II, which is surrounded by H2′, H3, H6, and H7 as well as the β-sheet region, is of hydrophobic character, while branch III, surrounded by the β-sheet, H2, H3, and H5, has both hydrophobic and hydrophilic regions. The large ligand

Table 2: Crystal structures of PPARγ partial agonists.

Ligand	Ligand type	PDB	Reference	Transactivation
PA-082	Isoquinoline	2FVJ	[62]	EC_{50} = 260 nM 40% efficacy
Compound 2: 3-fluoro-*N*-[1-(4-fluorophenyl)-3-(2-thienyl)-1*H*-pyrazol-5-yl]benzenesulfonamide	Sulfonamide	2G0G	[58]	IC_{50} = 512 nM 31% efficacy
Compound 1: *N*-[1-(4-fluorophenyl)-3-(2-thienyl)-1*H*-pyrazol-5-yl]-3,5-bis(trifluoro-methyl)benzenesulfonamide	Sulfonamide	2G0H	[58]	IC_{50} = 22.7 nM 50% efficacy
(S)-1 (LT127): 2-(4-2-[1,3-benzoxazol-2-yl(heptyl)amino]ethyl-phenoxy)-2-methyl-butanoic acid	Misc. acid (ureidofibrate derivative)	2I4Z 2I4P	[63]	EC_{50} = 593 nM 50.4% efficacy
SPPARγM2	Indole	2P4Y	[50]	EC_{50} = 3 nM 18% efficacy
2t	Acetamide	2POB	[64]	EC_{50} = 6.0 μM IC_{50} = 5.6 μM 54% efficacy
MRL-24	Indole	2Q5P	[47]	45% efficacy
nTZDpa	Indole	2Q5S	[47]	~20% efficacy
SR145	Indole	2Q61	[47]	~20% efficacy
SR147	Indole	2Q6R	[47]	~20% efficacy
BVT.13	Misc. acid	2Q6S	[47]	~20% efficacy
Amorfrutin 1	Misc. acid	2YFE	[65]	EC_{50} = 458 nM 39% efficacy
Cerco-A	(−)-Cercosporamide derivative	3B1M	[54]	EC_{50} = 3.5 nM 27% efficacy
(R)-1: (2S)-2-(biphenyl-4-yloxy)-3-phenylpropanoic acid	Misc. acid	3D6D	[66]	EC_{50} = 5.93 μM 24% efficacy
INT131	Sulfonamide	3FUR	[60]	EC_{50} = 4 nM 30% efficacy
T2384	Sulfonamide	3K8S	[67]	EC_{50} = 560 nM 25% efficacy
Compound 23	(−)-Cercosporamide derivative	3LMP	[55]	EC_{50} = 180 nM 47% efficacy
TCBPA	Bisphenol	3OSI	[68]	IC_{50} = 6.0 μM 37% efficacy
TBBPA	Bisphenol	3OSW	[68]	IC_{50} = 70 nM 37% efficacy
2l: (S)-3-(5-(2-(1H-tetrazol-5-yl)phenyl)-2,3-dihydro-1H-inden-1-yl)-2-ethyl-5-isobutyl-7-methyl-3H-imidazo[4,5-b]pyridine	Misc. pyridine	3R8A	[69]	EC_{50} = 212 nM 31% efficacy
Compound 13	Benzimidazole	3S9S	[52]	pEC_{50} = 7.4 75% activation
GQ-16	Thiazolidine	3T03	[61]	k_i = 160 nM 30% efficacy
Compound 17	(−)-Cercosporamide derivative	3V9T	[57]	EC_{50} = 240 nM 22% efficacy
Compound 21	(−)-Cercosporamide derivative	3V9V	[57]	EC_{50} = 130 nM 79% efficacy
Telmisartan	Benzimidazole	3VN2	[53]	EC_{50} = 4.5 μM 25–30% efficacy

Table 2: Continued.

Ligand	Ligand type	PDB	Reference	Transactivation
(R)-7j: (R)-2-benzyl-3-(4-propoxy-3-((4-(pyrimidin-2-yl)benzamido)methyl)phenyl)propanoic acid	Misc. acid	3VSO	[70]	EC_{50} = 34.6 nM 65% efficacy
Amorfrutin 2	Misc. acid	4A4V	[71]	EC_{50} = 1.2 μM 30% efficacy
Amorfrutin B	Misc. acid	4A4W	[71]	EC_{50} = 50 nM 20% efficacy
Compound 15	(−)-Cercosporamide derivative	4F9M	[56]	EC_{50} = 12 nM 64% efficacy
12b: imidazo[4,5-c]pyridin-4-one derivative	Misc. pyridine	4HEE	[72]	EC_{50} = 292 nM 25% efficacy
GW0072	Thiazolidine	4PRG	[41]	IC_{50} = 110 nM 15–20% efficacy

binding pocket in PPARγ allows for the promiscuous binding of many ligands with lower affinity. The AF2 surface is formed by H12, H3, H4, and H5 and forms a hydrophobic binding cleft on the surface of PPARγ to which the LXXL motif of coactivators binds.

While no true full-length crystal structure of PPARγ exists, the "intact" form of the receptor which includes domains C–E (the DNA binding domain, hinge, and ligand binding domain) in complex with RXR and bound to a PPRE DNA fragment was solved in 2008 by Chandra et al. [14]. Ribbons diagram of this nearly full-length PPARγ-RXR heterodimer on DNA can be viewed in Figure 1(b). This was the first multidomain crystal structure of any nuclear receptor. The structure showed that the PPAR/RXR ligand binding domains dimerize in exactly the same manner as previous crystal structures of the ligand binding domains alone had indicated. This was the first view of a PPARγ DNA binding domain, showing a zinc finger that closely resembled that of other nuclear receptor DNA binding domains. The hinge region was composed of coils largely lacking secondary structure consistent with its role to allow for movement of the two domains (ligand binding domain and DNA binding domain) about each other. Surprisingly, not much contact surface was observed between the RXR and PPAR DNA binding domains. The PPAR ligand binding domain near the β-sheet, proximal loops, and small helices (H2 and H2′) contacts the RXR DNA binding domain (rather than the ligand binding domain surface near the AF2) allowing for speculation of how signals may be transmitted from the ligand binding domain to the DNA binding domain and vice versa. One unanswered question is how partial agonist signals are relayed through coactivators to promote less transactivation.

8. Structural Dynamics of PPARγ and Stabilization of H12

The first experimental structural dynamics of the PPARγ ligand binding domain were reported by NMR methods [46]. While NMR has not been used to produce an atomic level structure of PPARγ, defining 3D HNCO spectra have been used to monitor levels of protein dynamics in the receptor. Few peaks were able to be measured for the apo receptor indicating that the ligand binding domain is in very high molecular motion when not bound to ligand. The converse was shown upon addition of rosiglitazone, indicating that this model full agonist was able to greatly stabilize the mobility of the receptor. These results were confirmed by hydrogen-deuterium exchange (HDX) which showed that rosiglitazone strongly and selectively stabilizes H12 and H3 [47]. Initial hypotheses postulated that full agonists work by stabilizing the AF2 surface through H12, allowing less of an entropic penalty for coactivator binding and thus full transcriptional output. Likewise, it was postulated that partial agonists only partially stabilize the AF2 through H12 generating more of an entropic penalty to coactivator binding and thus allowing less of a transcriptional output. This was in agreement with the common philosophy that activating ligands, particularly full agonists, reposition H12 according to the "mousetrap model", whereby movement of H12 following ligand binding traps the ligand within the ligand binding pocket [48]. Despite these nice models involving H12, the importance of the stabilization of H12 for coregulator binding and transactivation may not be completely straightforward. HDX showed that, surprisingly, partial agonists show no stabilization of H12, including BVT.13 which has a transactivation output nearly 80% of that of rosiglitazone [47]. Instead, partial agonists were shown to preferentially stabilize other regions of the ligand binding domain, especially the β-sheet region. The connection between the dynamic stabilization signature of partial agonists, coactivator recruitment, and insulin sensitizing effects is still an important question in the field being researched.

9. Structure of Full Agonist TZDs

Rosiglitazone forms a near horseshoe conformation centred about H3 [19, 49]. The central benzene ring of rosiglitazone

is poised directly behind H3 making hydrophobic contacts and the TZD head is located in the pocket near the AF2. Full agonists of the TZD type have been observed to form an extensive hydrogen bond network between the TZD head group and the PPARγ ligand binding domain. The hydrogen bond network between rosiglitazone and PPARγ can be seen in Figure 2(b). In particular, intermolecular hydrogen bonds extend from the TZD head group of rosiglitazone to side chains of PPARγ residues H323 (2.9 Å), H449 (2.7 Å), and Y473 (2.6 Å) allowing for stabilization of the AF2 surface. Rosiglitazone also extends to other regions of the binding pocket, occupying branches II and III of the pocket and increasing binding affinity and efficacy. Rosiglitazone also makes hydrophobic and van der Waals contacts with residues of H3, H5, H6, H7, and the β-sheet.

10. Indoles

Indoles have been used as a scaffold in the development of PPARγ partial agonists and were among some of the first partial agonists to be developed. The indole-based partial agonists for which there are crystal structures include nTZDpa (and derivatives SR147 and SR145), SPPARγM2, and MRL24 [47, 50]. Figure 3 shows the structural details of these three indole-based PAPRγ partial agonists. These three scaffolds lie between H3 and the β-sheet region, filling branches II and III of the ligand binding pocket, with no contact at all with H12. The indole moiety in all three structures lies proximal to H3 making hydrophobic contacts and van der Waals contacts with residues of H3 such as Cys285 and Arg288. All three compounds use an acid group to form hydrogen bonds with the β-sheet region, particularly the amine of the backbone of residue Ser342 (2.6–3.3 Å). These compounds also significantly stabilize the β-sheet through contacts with Ile341. All three compounds also make hydrophobic contacts with Leu330 and/or Leu333 of H5. Interestingly, nTZDpa is different from MRL24 and SPPARγM2 in that it extends more deeply into branch III of the ligand binding pocket to make a *pi-pi* interaction with Phe264 as well as hydrophobic interactions with the side chains of Ile281 and Met348. While all three compounds were halogen substituted, the scaffolds were permissive as to where the halogens could be substituted and there was no specific halogen binding site in common for the compounds.

Some indole-based compounds can inhibit the cytochrome P450s leading to off-target effects [51]. This was shown to be circumvented by incorporating an additional nitrogen atom into the scaffold in the form of 7-azaindoles; cytochrome P450 inhibition is not seen with 7-azaindole scaffolds [51]. Unfortunately, several of the 7-azaindoles have poor pharmacokinetic characteristics leading to reduced *in vivo* efficacy. Finally, some indole-based PPARγ agonists have been shown to have PPARα transactivation activity, limiting their use as subtype selective inhibitors.

11. Benzimidazoles

Given the success of indole scaffolds, benzimidazole scaffolds were an obvious choice for further design of PPARγ partial agonists as benzimidazole is an indole ring set substituted with one more nitrogen atom in the small ring. Two crystal structures available for this class include Compound 13 and Telmisartan [52, 53]. The structural details of both of these compounds can be seen in Figure 4. Both compounds form a horseshoe shaped conformation similar to that of rosiglitazone. The Telmisartan ligand contains 2 benzimidazole groups: a central benzimidazole group that binds near H3 and a secondary benzimidazole group that binds deep within branch I pocket with contact to H3. In both structures a benzimidazole ring is centred against H3, placing the compound packing more into branch I pocket than branches II and III pockets. Although both compounds are partial agonists, both compounds extend into branch I of the ligand binding pocket, which contains H12 and the AF2 residues. While neither makes a hydrogen bond network as extensive as rosiglitazone, both compounds do engage in hydrogen bonding to AF2 residues. Compound 13 hydrogen bonds with side chains of Ser289 (2.8 Å) of H3 and Tyr327 (3.0 Å) of H5. Telmisartan hydrogen bonds to the side chain of H12 residue Tyr473 (3.1 Å), which, based on the distance, is weaker than the similar contact in rosiglitazone (2.6 Å). Both compounds also make hydrophobic contacts with Leu469 of H12. Interestingly, both compounds also make use of residues Phe363 and Phe282 which are much lower in branch I pocket than any of the contact residues of rosiglitazone. Telmisartan makes an extensive *pi-pi* interaction with Phe363 through use of the secondary benzimidazole group. Hydrophobic contacts are made by both compounds with H3 to residues such as Cys285. While both compounds extend to branch III of the ligand binding pocket, there is only minimal contact with the β-sheet region and neither forms electrostatic interactions. This is despite Telmisartan, for example, bearing an acidic group that is located between H3 and the β-sheet.

Telmisartan is an attractive PPARγ partial agonist given the fact that it is already FDA approved; new derivatives are likely to be made in the future. Its primary pharmaceutical application is as an angiotensin II type 1 receptor blocker (ARB), used to lower blood pressure and treat cardiovascular disease. Of the small handful of ARBs capable of also acting as SPPARMs Telmisartan has the strongest ability to induce PPARγ activity.

12. (−)-Cerocosporamides

(−)-Cercosporamide is a natural product derived from the fungi *Cercosporidium henningsii*. Multiple cercosporamides have been found to have partial agonist activity with PPARγ. Several crystal structures for cercosporamide derivatives bound to PPARγ exist including Cerco-A and Compounds 23, 17, 21, and 15 [54–57]. The cercosporamides for which there are crystal structures available show less chemical diversity than those of the other classes described in this review. All of the compounds of this class share a core, 3-ring system referred to as a dibenzofuran. From the dibenzofuran extends a carboxamide group allowing for the substitution of larger groups. For example, Cerco-A is a derivative of (−)-cercosporamide that bears the dibenzofuran ring system

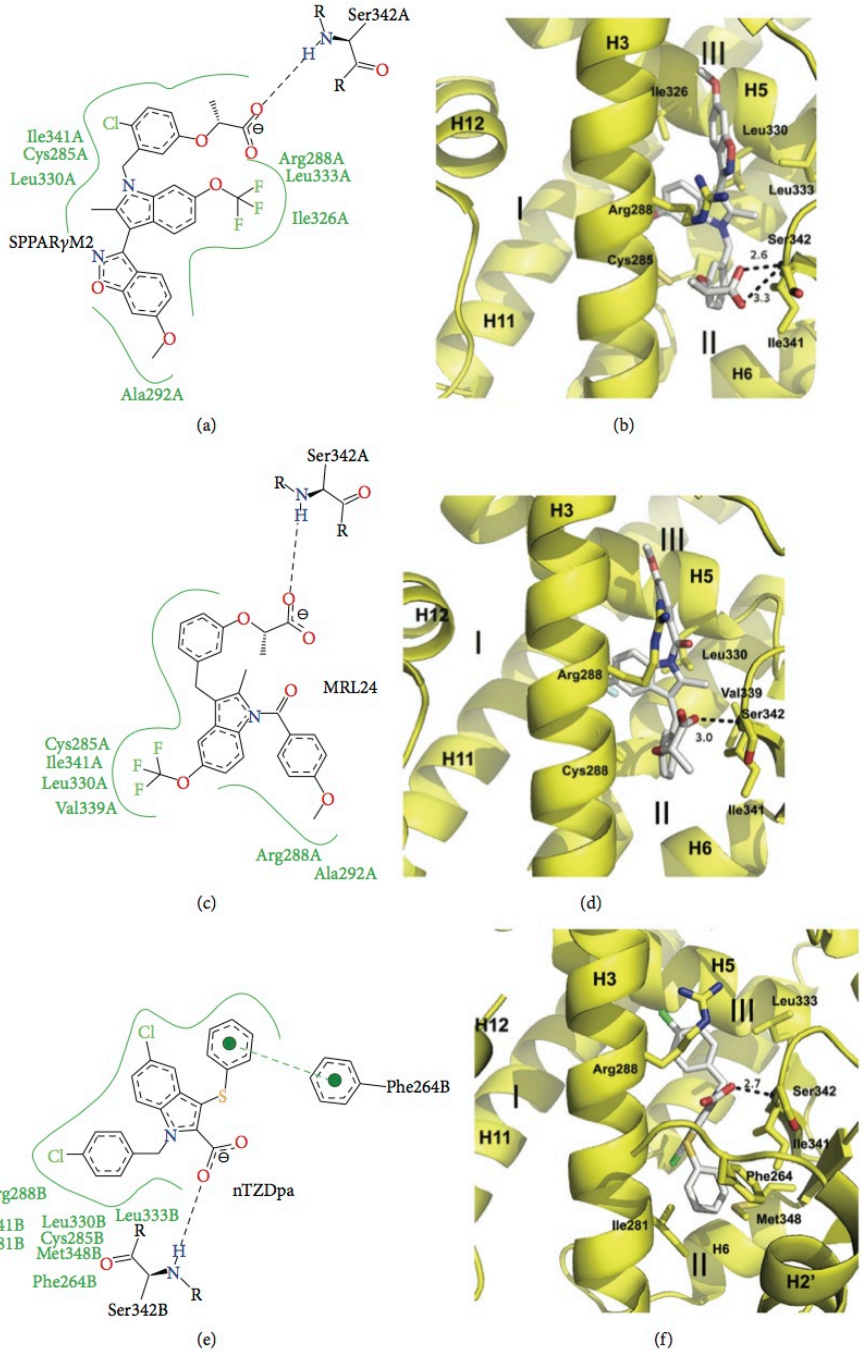

FIGURE 3: Crystal structures of indole containing PPARγ partial agonists. (a) Poseview map of SPPARγM2. (b) Crystal structure of SPPARγM2 bound to the PPARγ ligand binding domain. PDB: 2P4Y [50]. (c) Poseview map of MRL24. (d) Crystal structure of MRL24 bound to the PPARγ ligand binding domain. PDB: 2Q5P [47]. (e) Poseview map of nTZDpa. (f) Crystal structure of nTZDpa bound to the PPARγ ligand binding domain. PDB: 2Q5S [47]. The branches of the ligand binding pocket have been labelled with Roman numerals.

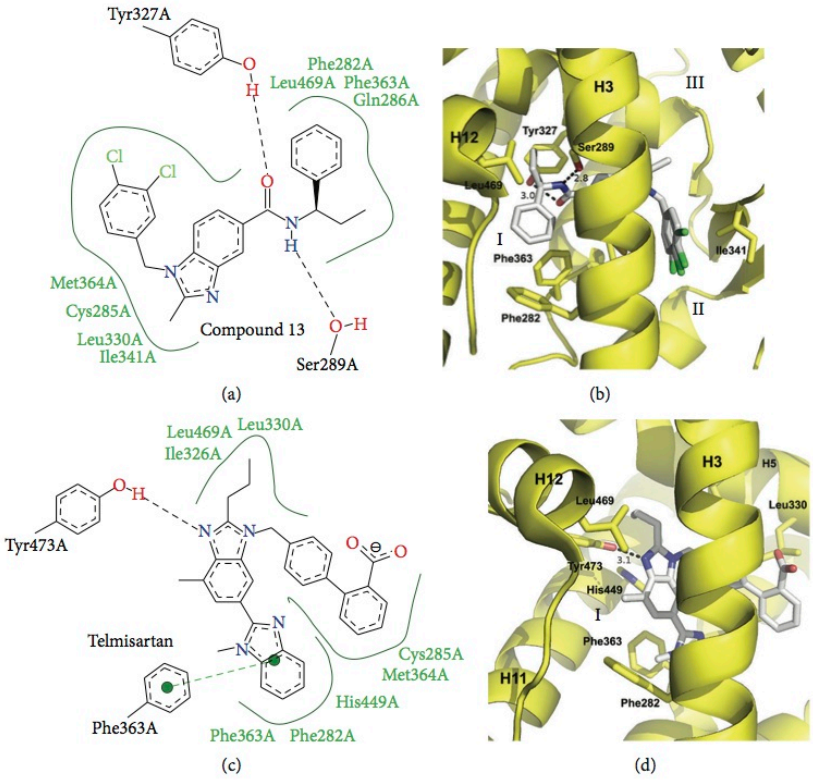

FIGURE 4: Crystal structures of benzimidazole containing PPARγ partial agonists. (a) Poseview map of Compound 13. (b) Crystal structure of Compound 13 bound to the PPARγ ligand binding domain. PDB: 3S9S [52]. (c) Poseview map of Telmisartan. (d) Crystal structure of Telmisartan bound to the PPARγ ligand binding domain. PDB: 3VN2 [53]. The branches of the ligand binding pocket have been labelled with Roman numerals.

with naphthalene substitutions. The structural details of Compound 23 can be seen in Figure 5 as a representative of the group. Compound 23 binds in branch II pocket with the dibenzofuran moiety packed between H3 and the β-sheet. The rings extend further out of the pocket towards the bulk solvent allowing for an electrostatic interaction with Arg280 (2.6 Å) that is not often seen with other partial agonists. Contacts of Compound 23 with the β-sheet are very minimal. A naphthalene group extending from the carboxamide linker allows for hydrophobic interactions with Leu330 and Met334 of H5. Compound 23 does not extend into branch I AF2 pocket but other cercosporamide compounds have been modified to introduce substitutions at the naphthalene C3 position to create this extension and allow interaction with H12.

13. Sulfonamides

Sulfonamide compounds are a diverse set of PPARγ partial agonists that share a sulfonamide linker. Crystal structures for these partial agonists include INT131, T2384, Compound 1, and Compound 2 [58–60]. Structural details for INT131 and Compound 2 can be seen in Figure 6. Sulfonamides lie primarily at the juncture of branches I, II, and III, proximal to H3. They do not form interactions with H12 residues or electrostatic interactions with the β-sheet; however, INT131 does engage in two hydrogen bonds with Tyr327 (2.7 and 3.1 Å). Both INT131 and Compound 2 form *pi-pi* interactions with Phe363 of H7. Other hydrophobic interactions include Met364 of H3, Leu330 of H5, and Ile341 of the β-sheet which interacts with INT131. As with many other PPARγ partial agonists, this class of compounds often is substituted with halogens but these substitutions are often compound specific with no common halogen binding site among them. Given the fact that INT131 has progressed through stage II clinical trials and is highly potent, this class of compounds is likely to be more widely studied in the future.

14. Thiazolidines

Given the success of thiazolidinedione compounds such as rosiglitazone, effort has been made into finding analogues which use similar or related chemistry. Two such compounds, GW0072 and GQ-16, are partial agonists of PPARγ. Whilst

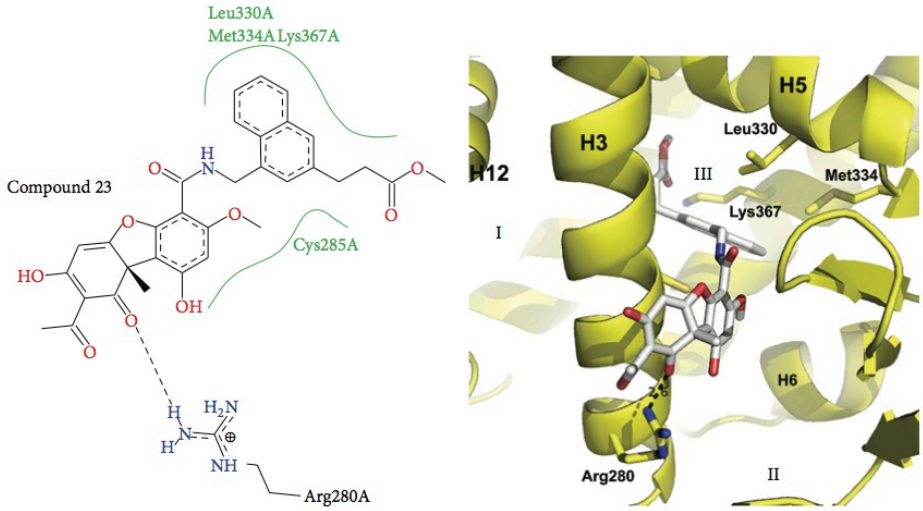

Figure 5: Crystal structure of a representative cercosporamide PPARγ partial agonist. (a) Poseview map of Compound 23. (b) Crystal structure of Compound 23 bound to the PPARγ ligand binding domain. PDB: 3LMP [55]. The branches of the ligand binding pocket have been labelled with Roman numerals.

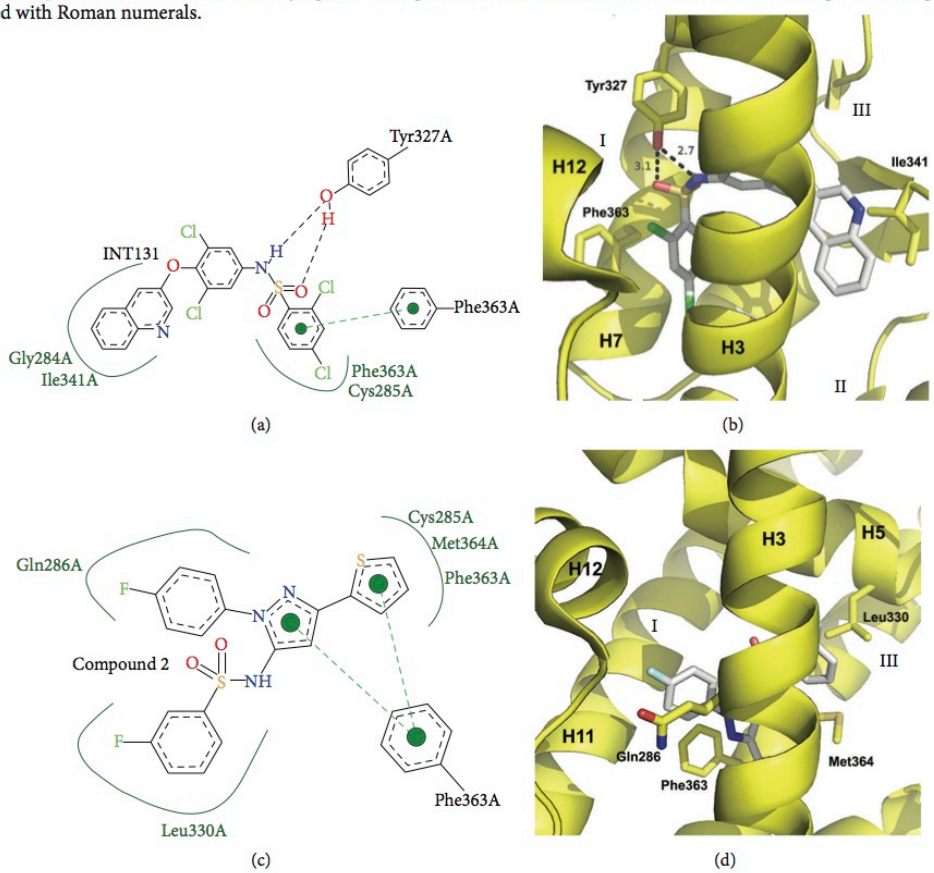

Figure 6: Crystal structures of sulfonamide containing PPARγ partial agonists. (a) Poseview map of INT131. (b) Crystal structure of INT131 bound to the PPARγ ligand binding domain. PDB: 3FUR [60]. (c) Poseview map of Compound 2. (d) Crystal structure of Compound 2 bound to the PPARγ ligand binding domain. PDB: 2G0G [58]. The branches of the ligand binding pocket have been labelled with Roman numerals.

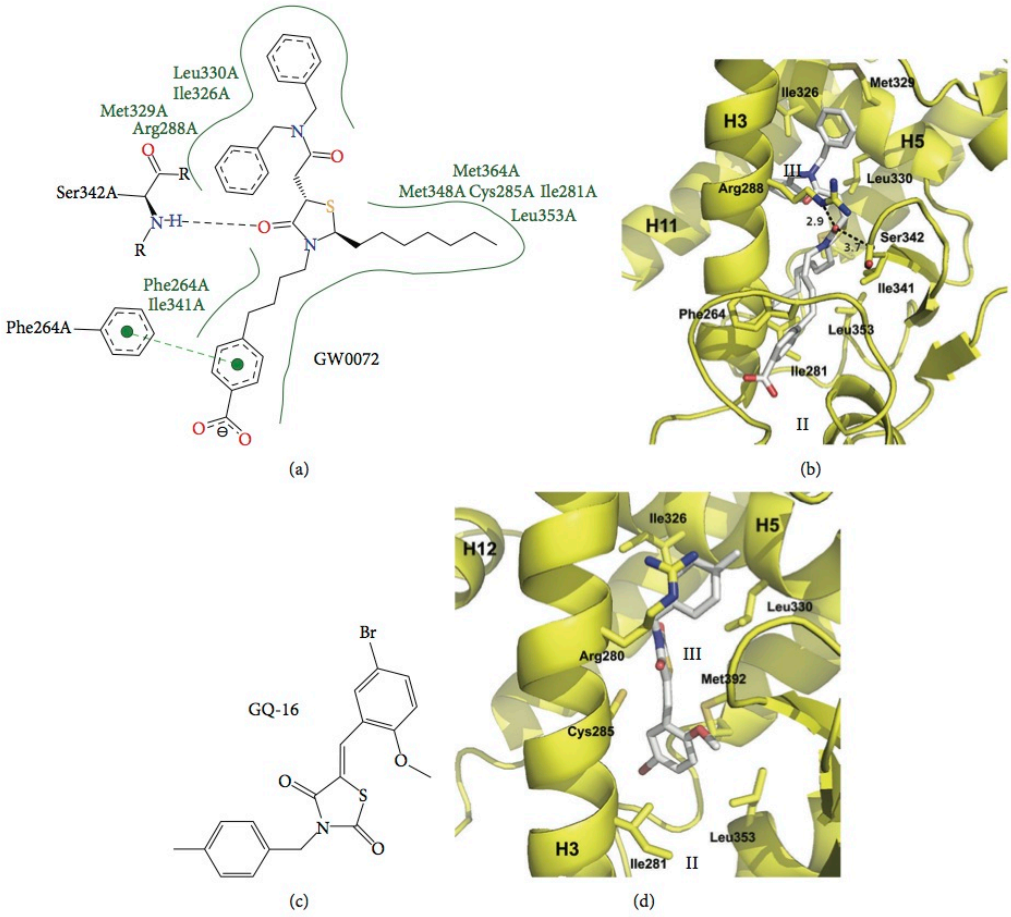

FIGURE 7: Crystal structures of thiazolidine containing PPARγ partial agonists. (a) Poseview map of GW0072. (b) Crystal structure of GW0072 bound to the PPARγ ligand binding domain. PDB: 4PRG [41]. (c) Chemical diagram of GQ-16. (d) Crystal structure of GQ-16 bound to the PPARγ ligand binding domain. PDB: 3T03 [49]. The branches of the ligand binding pocket have been labelled with Roman numerals.

GQ-16 can be classed as a thiazolidinedione, GW0072 is a thiazolidine as it lacks one of the two carbonyl groups necessary to be classified as a thiazolidinedione [41, 61]. Partial agonist TZDs are very chemically diverse but usually make use of the TZD as a central moiety to which other substituents are attached. This is in contrast to the full agonist TZDs which generally use the TZD groups as terminal moieties. Crystal structures are available for both GQ-16 and GW0072 and their interactions with PPARγ can be seen in Figure 7. Both GQ-16 and GW0072 make no interactions in AF2 branch I portion of the ligand binding pocket but instead lie between H3 and the β-sheet, extending from branch II to branch III of the ligand binding pocket. GW0072 is nearly twice the size of most other PPARγ partial agonists whereas GQ-16 is more near the size of other partial agonists such as nTZDpa that occupy this portion of the ligand binding pocket. GW0072 stabilizes the β-sheet and H3 of PPARγ through electrostatic interactions from its TZD oxygen atom to the side chain of Arg288 and the backbone amine of Ser342. Both compounds make numerous hydrophobic and van der Waals contacts with side chains of residues from H3 and H5 (such as Ile281, Leu330, Ile326, and Cys285) and H2′ (Leu353).

15. Common Structural Mechanisms among PPARγ Partial Agonists

While there is a clear need for more structural data to better define the mechanism of PPARγ partial agonists, the crystal structures available thus far have allowed for the identification of some initial trends among partial agonists. By far, most partial agonists do not occupy branch I of the ligand binding pocket and thus do not make any contacts with AF2

residues. Instead, most partial agonists occupy branches II and III portions of the ligand binding pocket between H3 and the β-sheet. While some partial agonists do occupy branch I, none of them form as energetically strong electrostatic interactions with all three of the residues that stabilize the AF2 (His323, Tyr473, and His449) as rosiglitazone does. Instead, the partial agonists identified thus far that occupy branch I only hydrogen-bond with one of the AF2 residues and often display a longer interaction distance implying a weaker interaction or, alternatively, these compounds make electrostatic interactions with other residues in the proximity such as Tyr327 or Ser289. Partial agonists which extend into branch I of the ligand binding pocket often can make use of limited hydrophobic interactions with H12 such as with Leu469. All partial agonists interact with H3 and most have a scaffold which is centred around H3. Nearly every partial agonist interacts in a hydrophobic manner with Cys285 of H3 and most interact with Arg288 using either electrostatic interactions or hydrophobic/van der Waals interactions. Additionally, most partial agonists stabilize the β-sheet. This is most often accomplished through hydrogen bonding from an acidic group to the backbone amine of Ser342. However, partial agonists that lack an acidic group can also stabilize the β-sheet by means of hydrophobic interactions especially with the side chain of Ile341. Finally, some partial agonists implement fairly unique interactions on edges of the ligand binding pocket, including *pi-pi* interactions with Phe282 of H3, Phe264 of the loop adjoining H2′, and Phe363 of H7.

Several biological questions relating to the downstream events of partial agonist binding still remain. How do compounds such as BVT.13 which do not occupy branch I of the ligand binding pocket or stabilize the AF2 residues still afford an 80% transcriptional output as compared to rosiglitazone? Why do partial agonists induce differential coactivator recruitment profiles as compared to full agonists? Are there secondary coactivator binding sites outside of the AF2 on the ligand binding domain? How do all partial agonists block phosphorylation of the receptor at Ser273? While the intact crystal structure of the PPARγ-RXR heterodimer on DNA gives some initial clues as the β-sheet region and phosphorylation site are poised near the DNA binding domain, more expansive structural studies will need to be carried out to answer these questions.

Conflict of Interests

The authors declare that there is no conflict of interests regarding the publication of this paper.

References

[1] P. Tontonoz and B. M. Spiegelman, "Fat and beyond: the diverse biology of PPARγ," *Annual Review of Biochemistry*, vol. 77, pp. 289–312, 2008.

[2] O. Braissant, F. Foufelle, C. Scotto, M. Dauça, and W. Wahli, "Differential expression of peroxisome proliferator-activated receptors (PPARs): tissue distribution of PPAR-alpha, -beta, and -gamma in the adult rat," *Endocrinology*, vol. 137, no. 1, pp. 354–366, 1996.

[3] I. Issemann and S. Green, "Activation of a member of the steroid hormone receptor superfamily by peroxisome proliferators," *Nature*, vol. 347, no. 6294, pp. 645–650, 1990.

[4] K. L. Gearing, M. Göttlicher, M. Teboul, E. Widmark, and J.-Å. Gustafsson, "Interaction of the peroxisome-proliferator-activated receptor and retinoid X receptor," *Proceedings of the National Academy of Sciences of the United States of America*, vol. 90, no. 4, pp. 1440–1444, 1993.

[5] P. Tontonoz, E. Hu, and B. M. Spiegelman, "Stimulation of adipogenesis in fibroblasts by PPARγ2, a lipid-activated transcription factor," *Cell*, vol. 79, no. 7, pp. 1147–1156, 1994.

[6] R. Saladin, L. Fajas, S. Dana, Y. D. Halvorsen, J. Auwerx, and M. Briggs, "Differential regulation of peroxisome proliferator activated receptor γ1 (PPARγ1) and PPARγ2 messenger RNA expression in the early stages of adipogenesis," *Cell Growth & Differentiation*, vol. 10, no. 1, pp. 43–48, 1999.

[7] D. B. Savage, "PPARγ as a metabolic regulator: insights from genomics and pharmacology," *Expert Reviews in Molecular Medicine*, vol. 7, no. 1, pp. 1–6, 2005.

[8] E. D. Rosen, P. Sarraf, A. E. Troy et al., "PPAR gamma is required for the differentiation of adipose tissue in vivo and in vitro," *Molecular Cell*, vol. 4, no. 4, pp. 611–617, 1999.

[9] A. S. Banks, F. E. McAllister, J. P. G. Camporez et al., "An ERK/Cdk5 axis controls the diabetogenic actions of PPARgamma," *Nature*, vol. 517, no. 7534, pp. 391–395, 2015.

[10] J. H. Choi, A. S. Banks, J. L. Estall et al., "Anti-diabetic drugs inhibit obesity-linked phosphorylation of PPARγ by Cdk5," *Nature*, vol. 466, no. 7305, pp. 451–456, 2010.

[11] J. H. Choi, A. S. Banks, T. M. Kamenecka et al., "Antidiabetic actions of a non-agonist PPARγ ligand blocking Cdk5-mediated phosphorylation," *Nature*, vol. 477, no. 7365, pp. 477–481, 2011.

[12] V. Zoete, A. Grosdidier, and O. Michielin, "Peroxisome proliferator-activated receptor structures: ligand specificity, molecular switch and interactions with regulators," *Biochimica et Biophysica Acta—Molecular and Cell Biology of Lipids*, vol. 1771, no. 8, pp. 915–925, 2007.

[13] L. Mouchiroud, L. J. Eichner, R. J. Shaw, and J. Auwerx, "Transcriptional coregulators: fine-tuning metabolism," *Cell Metabolism*, vol. 20, no. 1, pp. 26–40, 2014.

[14] V. Chandra, P. Huang, Y. Hamuro et al., "Structure of the intact PPAR-γ-RXR-α nuclear receptor complex on DNA," *Nature*, vol. 456, no. 7220, pp. 350–356, 2008.

[15] S. Hummasti and P. Tontonoz, "The peroxisome proliferator-activated receptor N-terminal domain controls isotype-selective gene expression and adipogenesis," *Molecular Endocrinology*, vol. 20, no. 6, pp. 1261–1275, 2006.

[16] A. Bugge and S. Mandrup, "Molecular mechanisms and genome-wide aspects of PPAR subtype specific transactivation," *PPAR Research*, vol. 2010, Article ID 169506, 12 pages, 2010.

[17] A. IJpenberg, E. Jeannin, W. Wahli, and B. Desvergne, "Polarity and specific sequence requirements of peroxisome proliferator-activated receptor (PPAR)/retinoid X receptor heterodimer binding to DNA. A functional analysis of the malic enzyme gene PPAR response element," *The Journal of Biological Chemistry*, vol. 272, no. 32, pp. 20108–20117, 2010.

[18] C. Helsen and F. Claessens, "Looking at nuclear receptors from a new angle," *Molecular and Cellular Endocrinology*, vol. 382, no. 1, pp. 97–106, 2014.

[19] R. T. Nolte, G. B. Wisely, S. Westin et al., "Ligand binding and co-activator assembly of the peroxisome proliferator-activated receptor-γ," *Nature*, vol. 395, no. 6698, pp. 137–143, 1998.

[20] F. Gilardi and B. Desvergne, "RXRs: collegial partners," *Sub-Cellular Biochemistry*, vol. 70, pp. 75–102, 2014.

[21] N. S. C. Eager, A. Rowe, and P. M. Brickell, "A member of the chicken RXR family of nuclear receptors activates transcription in response to retinoic acid," *FEBS Letters*, vol. 292, no. 1-2, pp. 103–106, 1991.

[22] M. Schupp and M. A. Lazar, "Endogenous ligands for nuclear receptors: digging deeper," *The Journal of Biological Chemistry*, vol. 285, no. 52, pp. 40409–40415, 2010.

[23] B. M. Forman, P. Tontonoz, J. Chen, R. P. Brun, B. M. Spiegelman, and R. M. Evans, "15-deoxy-$\Delta^{12,14}$-prostaglandin J_2 is a ligand for the adipocyte determination factor PPARγ," *Cell*, vol. 83, no. 5, pp. 803–812, 1995.

[24] T. Waku, T. Shiraki, T. Oyama, K. Maebara, R. Nakamori, and K. Morikawa, "The nuclear receptor PPARγ individually responds to serotonin-and fatty acid-metabolites," *EMBO Journal*, vol. 29, no. 19, pp. 3395–3407, 2010.

[25] G. C. Mannino and G. Sesti, "Individualized therapy for type 2 diabetes: clinical implications of pharmacogenetic data," *Molecular Diagnosis and Therapy*, vol. 16, no. 5, pp. 285–302, 2012.

[26] C. Day, "Thiazolidinediones: a new class of antidiabetic drugs," *Diabetic Medicine*, vol. 16, no. 3, pp. 179–192, 1999.

[27] S. L. Pearson, M. A. Cawthorne, J. C. Clapham et al., "The thiazolidinedione insulin sensitiser, BRL 49653, increases the expression of PPAR-γ and aP2 in adipose tissue of high-fat-fed rats," *Biochemical and Biophysical Research Communications*, vol. 229, no. 3, pp. 752–757, 1996.

[28] L. S. Phillips, G. Grunberger, E. Miller, R. Patwardhan, E. B. Rappaport, and A. Salzman, "Once- and twice-daily dosing with rosiglitazone improves glycemic control in patients with type 2 diabetes," *Diabetes Care*, vol. 24, no. 2, pp. 308–315, 2001.

[29] T. Ikeda, "Drug-induced idiosyncratic hepatotoxicity: prevention strategy developed after the troglitazone case," *Drug Metabolism and Pharmacokinetics*, vol. 26, no. 1, pp. 60–70, 2011.

[30] N. S. B. Rawson, "Review of the quality of observational studies of the association between rosiglitazone and acute myocardial infarction," *Journal of Population Therapeutics and Clinical Pharmacology*, vol. 21, no. 2, pp. e214–e232, 2014.

[31] R. E. J. Ryder, "Pioglitazone has a dubious bladder cancer risk but an undoubted cardiovascular benefit," *Diabetic Medicine*, vol. 32, no. 3, pp. 305–313, 2015.

[32] S. Horita, M. Nakamura, N. Satoh, M. Suzuki, and G. Seki, "Thiazolidinediones and edema: recent advances in the pathogenesis of thiazolidinediones-induced renal sodium retention," *PPAR Research*, vol. 2015, Article ID 646423, 7 pages, 2015.

[33] Y. Endo, M. Suzuki, H. Yamada et al., "Thiazolidinediones enhance sodium-coupled bicarbonate absorption from renal proximal tubules via PPARγ-dependent nongenomic signaling," *Cell Metabolism*, vol. 13, no. 5, pp. 550–561, 2011.

[34] J. P. Berger, A. E. Petro, K. L. Macnaul et al., "Distinct properties and advantages of a novel peroxisome proliferator-activated protein [gamma] selective modulator," *Molecular Endocrinology*, vol. 17, no. 4, pp. 662–676, 2003.

[35] S. M. Rangwala and M. A. Lazar, "The dawn of the SPPARMs?" *Science's STKE*, vol. 2002, no. 121, p. pe9, 2002.

[36] A. M. DePaoli, L. S. Higgins, R. R. Henry, C. Mantzoros, and F. L. Dunn, "Can a selective PPARγ modulator improve glycemic control in patients with type 2 diabetes with fewer side effects compared with pioglitazone?" *Diabetes Care*, vol. 37, no. 7, pp. 1918–1923, 2014.

[37] H. Kakuta, E. Kurosaki, T. Niimi et al., "Distinct properties of telmisartan on agonistic activities for peroxisome proliferator-activated receptor γ among clinically used angiotensin II receptor blockers: drug-target interaction analyses," *Journal of Pharmacology and Experimental Therapeutics*, vol. 349, no. 4, pp. 10–20, 2014.

[38] A. Laghezza, R. Montanari, A. Lavecchia et al., "On the metabolically active form of metaglidasen: improved synthesis and investigation of its peculiar activity on peroxisome proliferator-activated receptors and skeletal muscles," *ChemMedChem*, vol. 10, no. 3, pp. 555–565, 2015.

[39] R. Agrawal, P. Jain, and S. N. Dikshit, "Balaglitazone: a second generation peroxisome proliferator-activated receptor (PPAR) gamma (γ) agonist," *Mini-Reviews in Medicinal Chemistry*, vol. 12, no. 2, pp. 87–97, 2012.

[40] O. P. Lazarenko, S. O. Rzonca, L. J. Suva, and B. Lecka-Czernik, "Netoglitazone is a PPAR-gamma ligand with selective effects on bone and fat," *Bone*, vol. 38, no. 1, pp. 74–84, 2006.

[41] J. L. Oberfield, J. L. Collins, C. P. Holmes et al., "A peroxisome proliferator-activated receptor gamma ligand inhibits adipocyte differentiation," *Proceedings of the National Academy of Sciences of the United States of America*, vol. 96, no. 11, pp. 6102–6106, 1999.

[42] T. Östberg, S. Svensson, G. Selén et al., "A new class of peroxisome proliferator-activated receptor agonists with a novel binding epitope shows antidiabetic effects," *Journal of Biological Chemistry*, vol. 279, no. 39, pp. 41124–41130, 2004.

[43] F. Zhang, B. E. Lavan, and F. M. Gregoire, "Selective modulators of PPAR-γ activity: molecular aspects related to obesity and side-effects," *PPAR Research*, vol. 2007, Article ID 32696, 7 pages, 2007.

[44] L. S. Higgins and C. S. Mantzoros, "The development of INT131 as a selective PPARgamma modulator: approach to a safer insulin sensitizer," *PPAR Research*, vol. 2008, Article ID 936906, 9 pages, 2008.

[45] T. Allen, F. Zhang, S. A. Moodie et al., "Halofenate is a selective peroxisome proliferator-activated receptor gamma modulator with antidiabetic activity," *Diabetes*, vol. 55, no. 9, pp. 2523–2533, 2006.

[46] B. A. Johnson, E. M. Wilson, Y. Li, D. E. Moller, R. G. Smith, and G. Zhou, "Ligand-induced stabilization of PPARγ monitored by NMR spectroscopy: implications for nuclear receptor activation," *Journal of Molecular Biology*, vol. 298, no. 2, pp. 187–194, 2000.

[47] J. B. Bruning, M. J. Chalmers, S. Prasad et al., "Partial agonists activate PPARγ using a helix 12 independent mechanism," *Structure*, vol. 15, no. 10, pp. 1258–1271, 2007.

[48] J.-P. Renaud, N. Rochel, M. Ruff et al., "Crystal structure of the RAR-γ ligand-binding domain bound to all-trans retinoic acid," *Nature*, vol. 378, no. 6558, pp. 681–689, 1995.

[49] M. V. Liberato, A. S. Nascimento, S. D. Ayers et al., "Medium chain fatty acids are selective peroxisome proliferator activated receptor (PPAR) γ activators and Pan-PPAR partial agonists," *PLoS ONE*, vol. 7, no. 5, Article ID e36297, 2012.

[50] M. Einstein, T. E. Akiyama, G. A. Castriota et al., "The differential interactions of peroxisome proliferator-activated receptor γ ligands with Tyr473 is a physical basis for their unique biological activities," *Molecular Pharmacology*, vol. 73, no. 1, pp. 62–74, 2008.

[51] S. D. Debenham, A. Chan, F. W. Lau et al., "Highly functionalized 7-azaindoles as selective PPAR gamma modulators,"

Bioorganic & Medicinal Chemistry Letters, vol. 18, no. 17, pp. 4798–4801, 2008.

[52] M. Sime, A. C. Allan, P. Chapman et al., "Discovery of GSK1997132B a novel centrally penetrant benzimidazole PPARgamma partial agonist," *Bioorganic and Medicinal Chemistry Letters*, vol. 21, no. 18, pp. 5568–5572, 2011.

[53] Y. Amano, T. Yamaguchi, K. Ohno et al., "Structural basis for telmisartan-mediated partial activation of PPAR gamma," *Hypertension Research*, vol. 35, no. 7, pp. 715–719, 2012.

[54] K. Wakabayashi, S. Hayashi, Y. Matsui et al., "Pharmacology and in vitro profiling of a novel peroxisome proliferator-activated receptor γ ligand, cerco-A," *Biological and Pharmaceutical Bulletin*, vol. 34, no. 7, pp. 1094–1104, 2011.

[55] A. Furukawa, T. Arita, S. Satoh et al., "Discovery of a novel selective PPARγ modulator from (-)-cercosporamide derivatives," *Bioorganic and Medicinal Chemistry Letters*, vol. 20, no. 7, pp. 2095–2098, 2010.

[56] A. Furukawa, T. Arita, T. Fukuzaki et al., "Synthesis and biological evaluation of novel (−)-cercosporamide derivatives as potent selective PPARγ modulators," *European Journal of Medicinal Chemistry*, vol. 54, pp. 522–533, 2012.

[57] A. Furukawa, T. Arita, T. Fukuzaki et al., "Substituents at the naphthalene C3 position of (−)-cercosporamide derivatives significantly affect the maximal efficacy as PPARγ partial agonists," *Bioorganic & Medicinal Chemistry Letters*, vol. 22, no. 3, pp. 1348–1351, 2012.

[58] I.-L. Lu, C.-F. Huang, Y.-H. Peng et al., "Structure-based drug design of a novel family of PPARγ partial agonists: virtual screening, X-ray crystallography, and in vitro/in vivo biological activities," *Journal of Medicinal Chemistry*, vol. 49, no. 9, pp. 2703–2712, 2006.

[59] Y. Li, J. Zhang, F. J. Schopfer et al., "Molecular recognition of nitrated fatty acids by PPARγ," *Nature Structural & Molecular Biology*, vol. 15, no. 8, pp. 865–867, 2008.

[60] A. Motani, Z. Wang, J. Weiszmann et al., "INT131: a selective modulator of PPARγ," *Journal of Molecular Biology*, vol. 386, no. 5, pp. 1301–1311, 2009.

[61] A. A. Amato, S. Rajagopalan, J. Z. Lin et al., "GQ-16, a novel peroxisome proliferator-activated receptor γ (PPARγ) ligand, promotes insulin sensitization without weight gain," *The Journal of Biological Chemistry*, vol. 287, no. 33, pp. 28169–28179, 2012.

[62] E. Burgermeister, A. Schnoebelen, A. Flament et al., "A novel partial agonist of peroxisome proliferator-activated receptor-gamma (PPARgamma) recruits PPARgamma-coactivator-lalpha, prevents triglyceride accumulation, and potentiates insulin signaling in vitro," *Molecular Endocrinology*, vol. 20, no. 4, pp. 809–830, 2006.

[63] G. Pochetti, C. Godio, N. Mitro et al., "Insights into the mechanism of partial agonism: crystal structures of the peroxisome proliferator-activated receptor γ ligand-binding domain in the complex with two enantiomeric ligands," *Journal of Biological Chemistry*, vol. 282, no. 23, pp. 17314–17324, 2007.

[64] R. P. Trump, J. E. Cobb, B. G. Shearer et al., "Co-crystal structure guided array synthesis of PPARgamma inverse agonists," *Bioorganic & Medicinal Chemistry Letters*, vol. 17, no. 14, pp. 3916–3920, 2007.

[65] C. Weidner, J. C. de Groot, A. Prasad et al., "Amorfrutins are potent antidiabetic dietary natural products," *Proceedings of the National Academy of Sciences of the United States of America*, vol. 109, no. 19, pp. 7257–7262, 2012.

[66] R. Montanari, F. Saccoccia, E. Scotti et al., "Crystal structure of the peroxisome proliferator-activated receptor γ (PPARγ) ligand binding domain complexed with a novel partial agonist: a new region of the hydrophobic pocket could be exploited for drug design," *Journal of Medicinal Chemistry*, vol. 51, no. 24, pp. 7768–7776, 2008.

[67] Y. Li, Z. Wang, N. Furukawa et al., "T2384, a novel antidiabetic agent with unique peroxisome proliferator-activated receptor γ binding properties," *The Journal of Biological Chemistry*, vol. 283, no. 14, pp. 9168–9176, 2008.

[68] A. Riu, M. Grimaldi, A. le Maire et al., "Peroxisome proliferator-activated receptor γ is a target for halogenated analogs of bisphenol A," *Environmental Health Perspectives*, vol. 119, no. 9, pp. 1227–1232, 2011.

[69] A. Casimiro-Garcia, G. F. Filzen, D. Flynn et al., "Discovery of a series of imidazo[4,5-b]pyridines with dual activity at angiotensin II type 1 receptor and peroxisome proliferator-activated receptor-gamma," *Journal of Medicinal Chemistry*, vol. 54, no. 12, pp. 4219–4233, 2011.

[70] M. Ohashi, T. Oyama, E. W. Putranto et al., "Design and synthesis of a series of α-benzyl phenylpropanoic acid-type peroxisome proliferator-activated receptor (PPAR) gamma partial agonists with improved aqueous solubility," *Bioorganic & Medicinal Chemistry*, vol. 21, no. 8, pp. 2319–2332, 2013.

[71] J. C. de Groot, C. Weidner, J. Krausze et al., "Structural characterization of amorfrutins bound to the peroxisome proliferator-activated receptor γ," *Journal of Medicinal Chemistry*, vol. 56, no. 4, pp. 1535–1543, 2013.

[72] A. Casimiro-Garcia, R. J. Heemstra, C. F. Bigge et al., "Design, synthesis, and evaluation of imidazo[4,5-c]pyridin-4-one derivatives with dual activity at angiotensin II type 1 receptor and peroxisome proliferator-activated receptor-gamma," *Bioorganic and Medicinal Chemistry Letters*, vol. 23, no. 3, pp. 767–772, 2013.

References

Abbas, T & Dutta, A 2009, 'p21 in cancer: intricate networks and multiple activities', *Nat Rev Cancer*, vol. 9, no. 6, Jun, pp. 400-414.

Actis, M, Inoue, A, Evison, B, Perry, S, Punchihewa, C & Fujii, N 2013, 'Small molecule inhibitors of PCNA/PIP-box interaction suppress translesion DNA synthesis', *Bioorg Med Chem*, Jan 22.

Baple, EL, Chambers, H, Cross, HE, Fawcett, H, Nakazawa, Y, Chioza, BA, Harlalka, GV, Mansour, S, Sreekantan-Nair, A, Patton, MA, Muggenthaler, M, Rich, P, Wagner, K, Coblentz, R, Stein, CK, Last, JI, Taylor, AM, Jackson, AP, Ogi, T, Lehmann, AR, Green, CM & Crosby, AH 2014, 'Hypomorphic PCNA mutation underlies a human DNA repair disorder', *J Clin Invest*, Jun 9.

Bechtel, PE, Hickey, RJ, Schnaper, L, Sekowski, JW, Long, BJ, Freund, R, Liu, N, Rodriguez-Valenzuela, C & Malkas, LH 1998, 'A unique form of proliferating cell nuclear antigen is present in malignant breast cells', *Cancer Res*, vol. 58, no. 15, Aug 1, pp. 3264-3269.

Bravo, R, Fey, SJ, Bellatin, J, Larsen, PM, Arevalo, J & Celis, JE 1981, 'Identification of a nuclear and of a cytoplasmic polypeptide whose relative proportions are sensitive to changes in the rate of cell proliferation', *Exp Cell Res*, vol. 136, no. 2, Dec, pp. 311-319.

Bruning, JB & Shamoo, Y 2004, 'Structural and thermodynamic analysis of human PCNA with peptides derived from DNA polymerase-delta p66 subunit and flap endonuclease-1', *Structure*, vol. 12, no. 12, Dec, pp. 2209-2219.

Bubeck, D, Reijns, MA, Graham, SC, Astell, KR, Jones, EY & Jackson, AP 2011, 'PCNA directs type 2 RNase H activity on DNA replication and repair substrates', *Nucleic Acids Res*, vol. 39, no. 9, May, pp. 3652-3666.

Cayrol, C, Knibiehler, M & Ducommun, B 1998, 'p21 binding to PCNA causes G1 and G2 cell cycle arrest in p53-deficient cells', *Oncogene*, vol. 16, no. 3, Jan 22, pp. 311-320.

Chia, N, Cann, I & Olsen, GJ 2010, 'Evolution of DNA replication protein complexes in eukaryotes and Archaea', *PLoS One*, vol. 5, no. 6, p. e10866.

De Biasio, A & Blanco, FJ 2013, 'Proliferating cell nuclear antigen structure and interactions: too many partners for one dancer?', *Adv Protein Chem Struct Biol*, vol. 91, pp. 1-36.

De Biasio, A, Campos-Olivas, R, Sanchez, R, Lopez-Alonso, JP, Pantoja-Uceda, D, Merino, N, Villate, M, Martin-Garcia, JM, Castillo, F, Luque, I & Blanco, FJ 2012, 'Proliferating cell nuclear antigen (PCNA) interactions in solution studied by NMR', *PLoS One*, vol. 7, no. 11, p. e48390.

De Biasio, A, de Opakua, AI, Mortuza, GB, Molina, R, Cordeiro, TN, Castillo, F, Villate, M, Merino, N, Delgado, S, Gil-Carton, D, Luque, I, Diercks, T, Bernado, P, Montoya, G & Blanco, FJ 2015, 'Structure of p15(PAF)-PCNA complex and implications for clamp sliding during DNA replication and repair', *Nat Commun*, vol. 6, p. 6439.

De March, M, Merino, N, Barrera-Vilarmau, S, Crehuet, R, Onesti, S, Blanco, FJ & De Biasio, A 2017, 'Structural basis of human PCNA sliding on DNA', *Nat Commun*, vol. 8, Jan 10, p. 13935.

Dieckman, LM, Freudenthal, BD & Washington, MT 2012, 'PCNA Structure and Function: Insights from Structures of PCNA Complexes and Post-translationally Modified PCNA', *Subcell Biochem*, vol. 62, pp. 281-299.

Dillehay, KL, Lu, S & Dong, Z 2014, 'Anti-tumor effects of a novel small molecule targeting PCNA chromatin association in prostate cancer', *Mol Cancer Ther*, Sep 24, pp. 2817-2826.

Duffy, CM, Hilbert, BJ & Kelch, BA 2015, 'A Disease-Causing Variant in PCNA Disrupts a Promiscuous Protein Binding Site', *J Mol Biol*, Dec 11.

Freudenthal, BD, Gakhar, L, Ramaswamy, S & Washington, MT 2010, 'Structure of monoubiquitinated PCNA and implications for translesion synthesis and DNA polymerase exchange', *Nat Struct Mol Biol*, vol. 17, no. 4, Apr, pp. 479-484.

Fridman, Y, Gur, E, Fleishman, SJ & Aharoni, A 2013, 'Computational protein design suggests that human PCNA-partner interactions are not optimized for affinity', *Proteins*, vol. 81, no. 2, Feb, pp. 341-348.

Gilljam, KM, Feyzi, E, Aas, PA, Sousa, MM, Muller, R, Vagbo, CB, Catterall, TC, Liabakk, NB, Slupphaug, G, Drablos, F, Krokan, HE & Otterlei, M 2009, 'Identification of a novel, widespread, and functionally important PCNA-binding motif', *J Cell Biol*, vol. 186, no. 5, Sep 7, pp. 645-654.

Gu, L, Smith, S, Li, C, Hickey, RJ, Stark, JM, Fields, GB, Lang, WH, Sandoval, JA & Malkas, LH 2014, 'A PCNA-Derived Cell Permeable Peptide Selectively Inhibits Neuroblastoma Cell Growth', *PLoS One*, vol. 9, no. 4, p. e94773.

Gulbis, JM, Kelman, Z, Hurwitz, J, O'Donnell, M & Kuriyan, J 1996, 'Structure of the C-terminal region of p21(WAF1/CIP1) complexed with human PCNA', *Cell*, vol. 87, no. 2, Oct 18, pp. 297-306.

Hanahan, D & Weinberg, RA 2000, 'The hallmarks of cancer', *Cell*, vol. 100, no. 1, Jan 7, pp. 57-70.

—— 2011, 'Hallmarks of cancer: the next generation', *Cell*, vol. 144, no. 5, Mar 4, pp. 646-674.

Hishiki, A, Hashimoto, H, Hanafusa, T, Kamei, K, Ohashi, E, Shimizu, T, Ohmori, H & Sato, M 2009, 'Structural basis for novel interactions between human translesion synthesis polymerases and proliferating cell nuclear antigen', *J Biol Chem*, vol. 284, no. 16, Apr 17, pp. 10552-10560.

Hoelz, DJ, Arnold, RJ, Dobrolecki, LE, Abdel-Aziz, W, Loehrer, AP, Novotny, MV, Schnaper, L, Hickey, RJ & Malkas, LH 2006, 'The discovery of labile methyl esters on proliferating cell nuclear antigen by MS/MS', *Proteomics*, vol. 6, no. 17, Sep, pp. 4808-4816.

Hoffmann, S, Smedegaard, S, Nakamura, K, Mortuza, GB, Raschle, M, Ibanez de Opakua, A, Oka, Y, Feng, Y, Blanco, FJ, Mann, M, Montoya, G, Groth, A, Bekker-Jensen, S & Mailand, N 2016, 'TRAIP is a PCNA-binding ubiquitin ligase that protects genome stability after replication stress', *J Cell Biol*, vol. 212, no. 1, Jan 4, pp. 63-75.

Inoue, A, Kikuchi, S, Hishiki, A, Shao, Y, Heath, R, Evison, BJ, Actis, M, Canman, CE, Hashimoto, H & Fujii, N 2014, 'A Small Molecule Inhibitor of Monoubiquitinated Proliferating Cell Nuclear Antigen (PCNA) Inhibits Repair of Interstrand DNA Cross-link, Enhances DNA Double Strand Break, and Sensitizes Cancer Cells to Cisplatin', *J Biol Chem*, vol. 289, no. 10, Mar 7, pp. 7109-7120.

Jeruzalmi, D, O'Donnell, M & Kuriyan, J 2002, 'Clamp loaders and sliding clamps', *Curr Opin Struct Biol*, vol. 12, no. 2, Apr, pp. 217-224.

Jonsson, ZO, Hindges, R & Hubscher, U 1998, 'Regulation of DNA replication and repair proteins through interaction with the front side of proliferating cell nuclear antigen', *EMBO J*, vol. 17, no. 8, Apr 15, pp. 2412-2425.

Kong, XP, Onrust, R, O'Donnell, M & Kuriyan, J 1992, 'Three-dimensional structure of the beta subunit of E. coli DNA polymerase III holoenzyme: a sliding DNA clamp', *Cell*, vol. 69, no. 3, pp. 425-437.

Kontopidis, G, Wu, SY, Zheleva, DI, Taylor, P, McInnes, C, Lane, DP, Fischer, PM & Walkinshaw, MD 2005, 'Structural and biochemical studies of human proliferating cell nuclear antigen complexes provide a rationale for cyclin association and inhibitor design', *Proc Natl Acad Sci U S A*, vol. 102, no. 6, Feb 8, pp. 1871-1876.

Krishna, TS, Kong, XP, Gary, S, Burgers, PM & Kuriyan, J 1994, 'Crystal structure of the eukaryotic DNA polymerase processivity factor PCNA', *Cell*, vol. 79, no. 7, Dec 30, pp. 1233-1243.

Kroker, AJ & Bruning, JB 2015, 'p21 Exploits Residue Tyr151 as a Tether for High-Affinity PCNA Binding', *Biochemistry*, May 27.

Lingeman, RG, Hickey, RJ & Malkas, LH 2014, 'Expression of a novel peptide derived from PCNA damages DNA and reverses cisplatin resistance', *Cancer Chemother Pharmacol*, Sep 5.

Maga, G & Hubscher, U 2003, 'Proliferating cell nuclear antigen (PCNA): a dancer with many partners', *J Cell Sci*, vol. 116, no. Pt 15, Aug 1, pp. 3051-3060.

Malkas, LH, Herbert, BS, Abdel-Aziz, W, Dobrolecki, LE, Liu, Y, Agarwal, B, Hoelz, D, Badve, S, Schnaper, L, Arnold, RJ, Mechref, Y, Novotny, MV, Loehrer, P, Goulet, RJ & Hickey, RJ 2006, 'A cancer-associated PCNA expressed in breast cancer has implications as a potential biomarker', *Proc Natl Acad Sci U S A*, vol. 103, no. 51, Dec 19, pp. 19472-19477.

Massodi, I, Bidwell, GL, 3rd & Raucher, D 2005, 'Evaluation of cell penetrating peptides fused to elastin-like polypeptide for drug delivery', *J Control Release*, vol. 108, no. 2-3, Nov 28, pp. 396-408.

Matsumiya, S, Ishino, Y & Morikawa, K 2001, 'Crystal structure of an archaeal DNA sliding clamp: proliferating cell nuclear antigen from Pyrococcus furiosus', *Protein Sci*, vol. 10, no. 1, Jan, pp. 17-23.

Miyachi, K, Fritzler, MJ & Tan, EM 1978, 'Autoantibody to a nuclear antigen in proliferating cells', *J Immunol*, vol. 121, no. 6, Dec, pp. 2228-2234.

Moldovan, GL, Pfander, B & Jentsch, S 2007, 'PCNA, the maestro of the replication fork', *Cell*, vol. 129, no. 4, May 18, pp. 665-679.

Naryzhny, SN & Lee, H 2007, 'Characterization of proliferating cell nuclear antigen (PCNA) isoforms in normal and cancer cells: there is no cancer-associated form of PCNA', *FEBS Lett*, vol. 581, no. 25, Oct 16, pp. 4917-4920.

O'Donnell, M, Kuriyan, J, Kong, XP, Stukenberg, PT & Onrust, R 1992, 'The sliding clamp of DNA polymerase III holoenzyme encircles DNA', *Mol Biol Cell*, vol. 3, no. 9, Sep, pp. 953-957.

Punchihewa, C, Inoue, A, Hishiki, A, Fujikawa, Y, Connelly, M, Evison, B, Shao, Y, Heath, R, Kuraoka, I, Rodrigues, P, Hashimoto, H, Kawanishi, M, Sato, M, Yagi, T & Fujii, N 2012, 'Identification of small molecule proliferating cell nuclear antigen (PCNA) inhibitor that disrupts interactions with PIP-box proteins and inhibits DNA replication', *J Biol Chem*, vol. 287, no. 17, Apr 20, pp. 14289-14300.

Sakurai, S, Kitano, K, Yamaguchi, H, Hamada, K, Okada, K, Fukuda, K, Uchida, M, Ohtsuka, E, Morioka, H & Hakoshima, T 2005, 'Structural basis for recruitment of human flap endonuclease 1 to PCNA', *EMBO J*, vol. 24, no. 4, Feb 23, pp. 683-693.

Schafer, KA 1998, 'The cell cycle: a review', *Vet Pathol*, vol. 35, no. 6, Nov, pp. 461-478.

Schorpp, K, Rothenaigner, I, Maier, J, Traenkle, B, Rothbauer, U & Hadian, K 2016, 'A Multiplexed High-Content Screening Approach Using the Chromobody Technology to Identify Cell Cycle Modulators in Living Cells', *J Biomol Screen*, Apr 4.

Shamoo, Y & Steitz, TA 1999, 'Building a replisome from interacting pieces: sliding clamp complexed to a peptide from DNA polymerase and a polymerase editing complex', *Cell*, vol. 99, no. 2, Oct 15, pp. 155-166.

Stoimenov, I & Helleday, T 2009, 'PCNA on the crossroad of cancer', *Biochem Soc Trans*, vol. 37, no. Pt 3, Jun, pp. 605-613.

Strzalka, W, Oyama, T, Tori, K & Morikawa, K 2009, 'Crystal structures of the Arabidopsis thaliana proliferating cell nuclear antigen 1 and 2 proteins complexed with the human p21 C-terminal segment', *Protein Sci*, vol. 18, no. 5, May, pp. 1072-1080.

Tan, Z, Wortman, M, Dillehay, KL, Seibel, WL, Evelyn, CR, Smith, SJ, Malkas, LH, Zheng, Y, Lu, S & Dong, Z 2012, 'Small-molecule targeting of proliferating cell nuclear antigen chromatin association inhibits tumor cell growth', *Mol Pharmacol*, vol. 81, no. 6, Jun, pp. 811-819.

Wang, SC 2014, 'PCNA: a silent housekeeper or a potential therapeutic target?', *Trends Pharmacol Sci*, Mar 18.

Wang, Y, Xu, M & Jiang, T 2016, 'Crystal structure of human PCNA in complex with the PIP box of DVC1', *Biochem Biophys Res Commun*, Apr 12.

Warbrick, E 1998, 'PCNA binding through a conserved motif', *Bioessays*, vol. 20, no. 3, Mar, pp. 195-199.

Warbrick, E, Lane, DP, Glover, DM & Cox, LS 1995, 'A small peptide inhibitor of DNA replication defines the site of interaction between the cyclin-dependent kinase inhibitor p21WAF1 and proliferating cell nuclear antigen', *Curr Biol*, vol. 5, no. 3, Mar 1, pp. 275-282.

Wilson, RH, Biasutto, AJ, Wang, L, Fischer, R, Baple, EL, Crosby, AH, Mancini, EJ & Green, CM 2017, 'PCNA dependent cellular activities tolerate dramatic perturbations in PCNA client interactions', *DNA Repair (Amst)*, vol. 50, Feb, pp. 22-35.

Wolff, P, Olieric, V, Briand, JP, Chaloin, O, Dejaegere, A, Dumas, P, Ennifar, E, Guichard, G, Wagner, J & Burnouf, DY 2011, 'Structure-based design of short peptide ligands binding onto the E. coli processivity ring', *J Med Chem*, vol. 54, no. 13, Jul 14, pp. 4627-4637.

Yin, Z, Kelso, MJ, Beck, JL & Oakley, AJ 2013, 'Structural and thermodynamic dissection of linear motif recognition by the E. coli sliding clamp', *J Med Chem*, vol. 56, no. 21, Nov 14, pp. 8665-8673.

Yin, Z, Wang, Y, Whittell, LR, Jergic, S, Liu, M, Harry, E, Dixon, NE, Kelso, MJ, Beck, JL & Oakley, AJ 2014, 'DNA Replication Is the Target for the Antibacterial Effects of Nonsteroidal Anti-Inflammatory Drugs', *Chem Biol*, Mar 12.

Yin, Z, Whittell, LR, Wang, Y, Jergic, S, Liu, M, Harry, EJ, Dixon, NE, Beck, JL, Kelso, MJ & Oakley, AJ 2014, 'Discovery of lead compounds targeting the bacterial sliding clamp using a fragment-based approach', *J Med Chem*, vol. 57, no. 6, Mar 27, pp. 2799-2806.

Yin, Z, Whittell, LR, Wang, Y, Jergic, S, Ma, C, Lewis, PJ, Dixon, NE, Beck, JL, Kelso, MJ & Oakley, AJ 2015, 'Bacterial Sliding Clamp Inhibitors that Mimic the Sequential Binding Mechanism of Endogenous Linear Motifs', *J Med Chem*, vol. 58, no. 11, Jun 11, pp. 4693-4702.

Zhang, Z, Zhang, S, Lin, SH, Wang, X, Wu, L, Lee, EY & Lee, MY 2012, 'Structure of monoubiquitinated PCNA: implications for DNA polymerase switching and Okazaki fragment maturation', *Cell Cycle*, vol. 11, no. 11, Jun 1, pp. 2128-2136.

Zhao, H, Lo, YH, Ma, L, Waltz, SE, Gray, JK, Hung, MC & Wang, SC 2011, 'Targeting tyrosine phosphorylation of PCNA inhibits prostate cancer growth', *Mol Cancer Ther*, vol. 10, no. 1, Jan, pp. 29-36.

Zheleva, DI, Zhelev, NZ, Fischer, PM, Duff, SV, Warbrick, E, Blake, DG & Lane, DP 2000, 'A quantitative study of the in vitro binding of the C-terminal domain of p21 to PCNA: affinity, stoichiometry, and thermodynamics', *Biochemistry*, vol. 39, no. 25, Jun 27, pp. 7388-7397.